République Algérienne Démocratique et Populaire
Ministère de l'Enseignement Supérieur et de la Recherche Scientifique

Université Echahid Hamma Lakhdar - El Oued
Faculté de Sciences Exactes
Département de Chimie

Thèse en vue de l'obtention du diplôme de doctorat en chimie
Spécialité : Pharmacochimie des substances actives d'intérêt biologique
SUJET DE LA THESE:

Synthèse, caractérisation, étude de l'activité antimutagène et antioxydante et détermination des paramètres de liaison de quelques ferrocénylnitrobenzènes et ferrocénylbenzonitriles avec les radicaux $O_2^{-\cdot}$ et DPPH$^{\cdot}$

Présentée Par : Hacen Benamara

Soutenue le : 26/01/2022

Devant le jury composé de :

Mr. LANEZ Touhami,	Professeur,	Université de El Oued,	Rapporteur
M. Khelef Abdelhamid,	Professeur,	Université de El Oued,	Président
Mme. MEDILA Ifriqiya,	MCA,	Université de El Oued,	Examinatrice
Mr. BECHKI Lazhar,	Professeur,	Université de Ouargla,	Examinateur
Mr. Lahrach Mokhtar,	Professeur,	Université de Djelfa,	Examinateur
Mr. Saidi Mokhtar,	Professeur,	Université de Ouargla,	Examinateur

Année universitaire 2022/2021

People's Democratic Republic of Algeria

Minestry of Higher Education and Research Scientist

University of El Oued

Faculty of Exact Sciences

Department of Chemistry

Thesis with a view to obtaining the doctoral degree in chemistry

Specialty: Pharmacochemistry of active substances of biological interest

SUBJECT OF THE THESIS:

Synthesis, characterization, anticancer and antioxidant activity evaluation and determination the binding parameters of some ferrocenyl nitrobenzenes and ferrocenyl benzonitriles with radicals $O_2^{-\cdot}$ and DPPH

Presented by: Benamara Hacen

Graduated 26/01/2022

In front of the jury

Mr. LANEZ Touhami,	Professor,	Université de El Oued,	Rapporter
M. Khelef Abdelhamid,	Professor,	Université de El Oued,	President
Mme. MEDILA Ifriqya,	MCA,	Université de El Oued,	Examiner
Mr. BECHKI Lazhar,	Professor,	Université de Ouargla,	Examiner
Mr. Lahrach Mokhtar,	Professor,	Université de Djelfa,	Examiner
Mr. Saidi Mokhtar,	Professor,	Université de Ouargla,	Examiner

2022/2021

الإهداء

أهدي ثمرة جهدي هذا...

إلى ملاكي في الحياة .. إلى معنى الحب والحنان.. إلى بسمة الحياة وسر الوجود إلى من كان دعاؤها سر نجاحي وحنانها بلسم جراحي إلى أغلى الأحباب...أمي الحبيبة

إلى من كلله الله بالهيبة والوقار.. إلى من أحمل اسمه بكل افتخار.. أرجو من الله أن يمد في عمره ليرى ثمار جهوده قد أينعت وحان وقت قطافها بعد طول رجاء وانتظار، والذي ستبقى كلماته نجوما أهتدي بها اليوم وفي الغد وإلى الأبد ...أبي العزيز

إلى من شاركوني الدمعة والابتسامة.. إلى من كانوا متكئا أستند عليه وخير معين ألجأ إليه.. إلى من لم يبخلوا عني بالنصح والتوجيه إخوتي وأخواتي **حنان.. زمزم.. وداد.. رياض.. عادل.. نذير.. نريمان**

إلى من تذوقت معهم أجمل اللحظات وإلى من ساروا معي في هذا الدرب الطويل إلى رفقاء الدرب.. **د. شعيب فطحيزة التجاني و د.عبد اللطيف قدادره.. د.محمد كركوبي.. عبد الحق زيتون.. طارق لبيهي.. صلاح سالمي.. آدم بن شنه**

إلى زملاء المخبر.. د.**الحفناوي العانز.. د.مسعود مرغني.. د.علي خنوفه.. د.رابح مشانه.. د.عائشة عدايكه .. د.نجيبه زغب .. د. إيمان قديري.**

حسن بن عماره

شكر وعرفان

الحمد والشكر لله الذي لا معبود سواه، الذي رزقني العقل وحسن التوكل عليه سبحانه وتعالى وألهمني الصبر ووفقني إلى إتمام هذا العمل المتواضع، والصلاة السلام على نبيه محمد وآله وصحبه وسلم...

تم إنجاز هذا العمل بفضل الله وعونه في مخبر تثمين وترقية الموارد الصحراوية تحت إشراف أستاذي الفاضل الأستاذ الدكتور العانز التهامي، فجزاه الله عني الخير كله وله مني جزيل الشكر والتقدير والاحترام على مجهوداته ونصائحه القيمة وتوجيهاته السديدة التي كانت عونا لي في إتمام هذا العمل.

وقبل أن أمضي قدما.. أقدم أسمى عبارات الشكر والإمتنان إلى كل الطاقم الإداري لكلية علوم الدقيقة الذين كان منهم كل الحرص والمتابعة في سبيل إنجاز وإتمام هذه الأطروحة.

كما أشكر أعضاء لجنة المناقشة لقبولهم مناقشة هذا العمل بداية برئيسها الأستاذ الدكتور عبد الحميد خلف وكذلك كل من الأستاذة الدكاترة بشكي لزهر، لحرش مختار، وسعيدي مختار و مديلة إفريقيا.

وكذلك أتوجه بالشكر إلى مهندسي مخبر تثمين وترقية الموارد الصحراوية.. السيد على طليبه والسيد الصادق الناني لما قدماه من نصائح ومساعده طيلة هذا العمل فالشكر لهما وجزاهما الله خير الجزاء

كما أتوجه بالشكر أيضا إلى السيدة الفاضلة الدكتورة فطحيزة التجاني منى من كلية اللغات لما قدمته من نصائح بيداغوجية لكتابة هذه المذكرة.

حسن بن عماره

Abstract

The main goal of this work is the preparation of potentially biologically active compounds and evaluating their antioxidant and anticancer activities. In this context, a series of 2, 3, and 4-benzonitrilferrocene were prepared by the coupling reaction between ferrocene and the diazonium salts of the corresponding cyanoaniline. Cyclic voltammetry and electronic spectroscopy techniques were used to characterize and evaluate the antioxidant and anticancer potencies of the ligands ferrocenyl nitrobenzenes (NPF) and ferrocenyl benzonitriles (FBN). Moreover, CV method has been concerned for studying the behaviours of both series with the targets in free and bound form for determining which form (NPF / FBN) or (NPF^+ / FBN^+) are more active through the redox equilibrium process with DNA and BSA by calculation the K_{ox}/K_{red} values. The voltammetric response of the studied compounds before and after the increasing addition of DNA and BSA shows that all the electrochemical reactions are kinetically controlled by the diffusion step and showed that diffusion coefficients values of the compounds NPF and FBN are higher than that of the ligand-DNA and ligand-BSA complexes, which can be summarized in the order $D_{ligand} > D_{complex}$. Furthermore, the magnitude and the sign of ΔG for all the studied compounds confirm the spontaneity of the reaction via non-covalent bonds. All obtained k_b values are much greater than 1 which confirm the formation of the adducts ligand-DNA and ligand-BSA. The obtained data of the electrochemical and spectroscopic assays of the ligands NPF and FBN also allowed the determination of their binding affinities towards $O_2^{-\cdot}$ and DPPH· which were by electrostatic forces through a spontaneous reaction. In order to validate the obtained experimental results and visualize the ligand-receptor interactions, molecular docking study was carried out between the optimized structures of the ligands NPF and FBN with the treated crystal structures of DNA and BSA using AutoDock 4.2 software. The docking results showed high compatibility between the studied ligands and the target binding pockets of either DNA or BSA. Finally, ligands NFP and FBN represent strong candidates as antioxidant and anticancer agents.

Keywords:

Benzonitrilferrocene, Diazotization reaction, DNA, BSA, binding parameters.

الملخص

الهدف الرئيس من هذا العمل هو تحضير مركبات ذات فعالية بيولوجية وتقييم فعاليتها المضادة للأكسدة والطفرات. في هذا السياق ، تم تحضير سلسلة من مركبات بنزونيتريل فيروسان بإستعمال تفاعل ديازنيوم وبعد ذلك نقوم بدمجه مع الفيروسان. وكذلك استخدمت كل من تقنية الفولطامتري الحلقي وتقنية مطيافية الأشعة فوق البنفسجية المرئية لتشخيص وتثمين الفعالية المضادة للأكسدة والطفرات للمركبات ferrocenyl nitrobenzenes (FBN) وferrocenyl benzonitriles (NPF) . أيضا، تقنية الفلطامتري الحلقي استخدمت لدراسة سلوكيات المركبات المدروسة في شكلها المرتبط وغير المرتبط مع كل من DNA و BSA من أجل تحديد أي الأشكال (NPF / FBN) أو (NPF^+/ FBN^+) أكثر نشاطًا خلال توازن الأكسدة والاختزال مع DNA و BSA وذلك عن طريق حساب قيم K_{ox} / K_{red}. بينت دراسة السلوك الفلطامتري للمركبات المدروسة قبل وبعد الإضافة المتزايدة لـ DNA و BSA أن قيم معاملات الانتشار للمركبات المدروسة اكبر من تلك الخاصة بـ ligand-DNA و ligand-BSA وهذا يعزى إلى الفرق الكبير في الوزن الجزيئي بالنسبة لكل من المركبات المدروسة والمعقدات (هذا العامل الأخير يؤثر بشكل مباشر على سرعة الإنتشار) ، كما يمكن تلخيص قيم معاملات الإنتشار على النحو التالي $D_{ligand} > D_{comple}$. علاوة على ذلك ، فإن حجم وإشارة ΔG لجميع المركبات المدروسة يؤكدان على تلقائية التفاعل و كان بواسطة روابط غير تساهمية. جميع قيم K_b التي تم الحصول عليها أكبر بكثير من 1 وهذا ما يؤكد كذلك على تشكيل معقدات ligand-DNA و ligand-BSA. كما سمحت البيانات التي تم الحصول عليها للاختبارات الكهروكيميائية والطيفية لمركبات NPF و FBN بتحديد مقدار ألفة ترابطها مع $O_2^{-\cdot}$ و DPPH والتي كانت كذلك بواسطة قوى إلكتروستاتسكية من خلال تفاعل تلقائي. من أجل التحقق من صحة النتائج التجريبية التي تم الحصول عليها و توضيح الروابط الناشئة بين المركبات المدروسة وكل من BSA وDNA ، أجريت دراسة الالتحام الجزيئي بين الهياكل المحسّنة لـ NPF و FBN مع الهياكل البلورية المعالجة لـ DNA و BSA باستخدام برنامج AutoDock 4.2. أظهرت نتائج الالتحام توافقًا عاليًا بين المركبات المدروسة وجيوب الربط المستهدفة لكل من DNA و BSA. أخيرًا، المركبات NFP و FBN مرشحة بقوة لاستعمالها كأدوية فعاله مضادة للأكسدة والطفرات.

الكلمات المفتاحية:

بنزونيتريل فيروسان، نتروفينيل فيروسان،DNA، BSA ، معاملات الإرتباط.

Résumé

L'objectif principal de ce travail est la préparation de composés potentiellement biologiquement actifs et l'évaluation de leurs activités antioxydants et anticancéreuses. Dans ce contexte, une série de 2, 3 et 4-benzonitrilferrocène ont été préparés par la réaction de couplage entre le ferrocène et les sels de diazonium de la cyanoaniline correspondante. Des techniques de voltamétrie cyclique et de spectroscopie électronique ont été utilisées pour caractériser et évaluer les pouvoirs antioxydant et anticancéreux des ligands ferrocényl nitrobenzènes (NPF) et ferrocényl benzonitriles (FBN). De plus, la méthode CV s'est intéressée à l'étude des comportements des deux séries avec les cibles sous forme libre et liée pour déterminer quelle forme (NPF / FBN) ou (NPF^+ / FBN^+) est la plus active à travers le processus d'équilibre redox avec l'ADN et la BSA par calculer les valeurs Kox/Kred. La réponse voltamétrique des composés étudiés avant et après l'ajout croissant d'ADN et de BSA montre que toutes les réactions électrochimiques sont contrôlées cinétiquement par l'étape de diffusion et a montré que les valeurs des coefficients de diffusion des composés NPF et FBN sont supérieures à celle de ligand-ADN et ligand-BSA complexes, qui peuvent être résumés dans l'ordre $D_{ligand} > D_{complex}$. De plus, l'amplitude et le signe de ΔG pour tous les composés étudiés confirment la spontanéité de la réaction via des forces non covalentes. Toutes les valeurs de kb obtenues sont bien supérieures à 1 ce qui confirme la formation des adduits ligand-ADN et ligand-BSA. Les données obtenues des dosages électrochimiques et spectroscopiques des ligands NPF et FBN ont également permis de déterminer leurs affinités de liaison envers $O_2^{-\cdot}$ et $DPPH^{\cdot}$ qui étaient par des forces électrostatiques par une réaction spontanée. Afin de valider les résultats expérimentaux obtenus et de visualiser les interactions ligand-récepteur, une étude d'amarrage moléculaire a été réalisée entre les structures optimisées des ligands NPF et FBN avec les structures cristallines traitées d'ADN et de BSA à l'aide du logiciel AutoDock 4.2. Les résultats d'amarrage ont montré une compatibilité élevée entre les ligands étudiés et les poches de liaison ciblent de l'ADN ou de la BSA. Enfin, les ligands NFP et FBN représentent de solides candidats comme agents antioxydants et anticancéreux.

Mots clés:

Benzonitrilferrocène, paramètres de liaison, ADN, BSA, l'amarrage moléculaire.

TABLE OF CONTENTS

Chapter 3: Biological interaction studies

Second part

Chapter 4: Characterization

Chapter 5: Anticancer activity evaluation

Chapter 6: Antioxidant activity evaluation

LIST OF FIGURES

LIST OF TABLES

LIST OF ABBREVIATIONS

Fc	Ferrocene
NPF	Nitrophenylferrocene
FBN	Ferrocenylbenzonitril
HOMO	Highest occupied molecule orbital
LUMO	Lowest un-occupied molecular orbital
CV	Cyclic voltammetry
E_{pa}	Anodic peak potential
E_{pc}	Cathodic peak potential
DNA	Deoxyribonucleic acid
BSA	Bovine serum albumin
UV	Ultraviolet
DPPH	2,2-diphenyl-1-picrylhydrazyl
NMR	Nuclear magnetic resonance
DMSO	Dimethyl sulfoxide
DMF	Dimethylformamide
$\mathbf{I_{pa}}$	Anodic peak current
$\mathbf{I_{pc}}$	Cathodic peak current
EDTA	Ethylenediaminetetraacetic acid
ΔE_0	Potiential standart change
$O_2^{-\cdot}$	Superoxide anion radical
ΔG	Free Gibbs energy change
K_b	Binding constant
K_{ox}/K_{red}	Ratio of Binding constant
IC_{50}	Half-maximal inhibitory concentration

General introduction

In recent decades, the research curiosity pushed many scientists to investigate the interactions of protein-drug and free radical-antioxidant with a view to study the eventual activity and fate of drugs after entering the bloodstream as well as recognize the results of the binding types between them using simple and modern techniques[1-2].

DNA is a long polymer structured of only four kinds of subunits, which resemble one another chemically. Also, it is the most significant molecule in the organism and plays a fundamental role in the regulation of transcription[3]. The DNA mutation has been targeted by many studies in order to figure out the real causes that led to its occurrence, as well as to find the appropriate way to overcome this cellular problem as the preparation effective compounds able to block the diffusion of mutation in the organism[4-5]. Double-stranded DNA includes a highly negatively -charged sugar-phosphate backbone; this previous property of DNA widely exploited by biologists to prepare new drugs that bear positive charges on its external structures (as the generated oxidized form of ferrocene derivatives in this study) which much help in increasing the binding affinity of the drugs towards the active sites of DNA. In addition, these drugs are linked with DNA structure via non-covalent contacts in various forms such as intercalation, electrostatic, major and groove interactions[6-7].

Bovine serum albumin (BSA) structure consists from three domains and each one has two subdomains. It is the most abundant proteins in blood circulation and also acts as a transporter protein for large number of drugs, as well as possesses many pivotal functions in organism system as the distribution, metabolism and excretion[8]. BSA role is famous for its ability to attach with small molecules during the circulatory system of all vertebrate organisms. It is also considered from the proteins which have a high interaction potential with numerous bioactive compounds. Its three-domain design supplies many targetable-active sites, which have a high flexibility of adaptation with ligands[9-10].

The non-toxic properties of nitriles promoted researchers to investigate their pharmaco-chemistry as potential drugs. The prevalence of nitrile-containing drugs displays the biocompatibility of the nitrile functionality[11-12]. Recently many pharmaceuticals drugs containing nitriles are either prescribed for many different types of diseases or are in clinical trial[12]. In addition, the high chemical features of ferrocene and its easy incorporation into a large number of bio-substances have made it one of the key compounds in pharmaceutical industries, which can be used to prepare new potential drugs having an excellent activity against different types of human diseases[13]. The antioxidant and anticancer investigations were carried out to understand how ferrocene derivatives interact with DNA, BSA, $O_2^{-\cdot}$ and DPPH$^{\cdot}$ and providing a full overview for studied compounds behaviours inside the organism using voltammetric, spectroscopic and molecular docking techniques.

The plan of thesis consists of two main parts; each part divided into three chapters.

The first part :

The first chapter highlights the spotlights on the discovery of ferrocene structure and describes their physicochemical and thermodynamic properties. Furthermore, represents some synthesis methods that we can use to prepare ferrocene molecules and explains our interest mechanism in this work, which is the diazonium reaction; finally, it describes some applied aspects of ferrocene in medicine.

The second chapter represents the properties and characterizations of cyclic voltammetry and electronic spectroscopy methods are used for evaluating the interaction between the studied ligands and (DNA / BSA) with a full explanation for molecular docking approach has been used in such research.

The third chapter describes the structural features of BSA and DNA and also explains the principles of antioxidant activity study.

The second part :

The fifth chapter was exploited for evaluation of the electrochemical and kinetic behaviours of ferrocene derivatives toward DNA and BSA; and also, interpreting the docking results of the optimized structures of NPF and FBN with the crystal structures of BSA and DNA.

The last chapter was used to investigate the antioxidant capacity and determine the binding parameters of all the studied compounds with the radicals of superoxide anion and $DPPH^{\cdot}$.

References

1-Lu, H., Zhou, Q., He, J. et al. Recent advances in the development of protein–protein interactions modulators: mechanisms and clinical trials. Sig Transduct Target Ther 5, 213 (2020).

2-Asghar, Faiza, et al. "Ferrocene-functionalized anilines as potent anticancer and antidiabetic agents: Synthesis, spectroscopic elucidation, and DFT calculations." Journal of Molecular Structure 1249 (2022): 131632.

3-Alberts B, Johnson A, Lewis J, et al. Molecular Biology of the Cell. 4th edition. New York: Garland Science; 2002. The Structure and Function of DNA. Available from: https://www.ncbi.nlm.nih.gov/books/NBK26821/

4- Douki T, Reynaud-Angelin A, Cadet J, Sage E (August 2003). "Bipyrimidine photoproducts rather than oxidative lesions are the main type of DNA damage involved in the genotoxic effect of solar UVA radiation". Biochemistry. 42 (30): 9221–26.

5-Cadet J, Delatour T, Douki T, Gasparutto D, Pouget JP, Ravanat JL, Sauvaigo S (March 1999). "Hydroxyl radicals and DNA base damage". Mutation Research. 424 (1–2):9–21.

6-Paul, Ananya, and Santanu Bhattacharya. “Chemistry and Biology of DNA-Binding Small Molecules.” Current Science, vol. 102, no. 2, Temporary Publisher, 2012, pp. 212–31.

7-Almaqwashi, Ali A., et al. "Mechanisms of small molecule–DNA interactions probed by single-molecule force spectroscopy." Nucleic acids research 44.9 (2016): 3971-3988.

8-Ravindran, Aswathy, et al. "Studies on interaction of colloidal Ag nanoparticles with bovine serum albumin (BSA)." Colloids and Surfaces B: Biointerfaces 76.1 (2010): 32-37.

9- Rahmani, Turaj, Ali Hajian, Abbas Afkhami, and Hasan Bagheri. "A novel and high performance enzyme-less sensing layer for electrochemical detection of methyl parathion based on BSA templated Au–Ag bimetallic nanoclusters." New Journal of Chemistry 42, no. 9 (2018): 7213-7222.

10- Amlan, Chakraborty, and Dasgupta Abhijeet. "Effect of Low Power mm wave Irradiation on sedimentation, coagulation and light absorbance of purified Bovine Serum Albumin." Helix 3 (2012): 165-168.

11- S. T. Murphy, H. L. Case, E. Ellsworth, S. Hagen, M. Huband, T. Joannides, C. Limberakis, K. R. Marotti, A. M. Ottolini, M. Rauckhorst, J. Starr, M. Stier, C. Taylor, T. Zhu, A. Blaser, W. A. Denny, G. L. Lu, J. B. Smaill, F. Rivault, Bioorganic and Medicinal Chemistry Letters 17(8) (2007) 2150-2155.

12- F. F. Fleming, L. Yao, P. C. Ravikumar, L. Funk, B. C. Shook, Journal of Medicinal Chemistry 53(22) (2010) 7902-7917.

13-Astruc, Didier. "Why is ferrocene so exceptional?." European Journal of Inorganic Chemistry 2017.1 (2017): 6-29.

First part

Chapter 1

Chemistry of ferrocene

1. Background

1.1. Ferrocene structure

Ferrocene, an organometallic complex containing iron, stirred up a great deal of attention directly after its discovery in the early fifties of the last century by Kealy and Pauson[1-2]. Geometric structure of such discovered compound contains an iron atom sandwiched between two flat cyclopentadiene (Cp) rings; additionally, it represents valuable alternative compounds which combine among the unique features with remarkable properties and all types of typical metallocene identified after the comprehensive revealing of ferrocene molecule[3]. Furthermore, the hypothesis of aromatic character for ferrocene and ferrous position amongst two parallel rings was confirmed by Orgel and Dunitz[4], Eiland and Repinsky[5], and Moffitt[6] using X-Ray crystallography. Some earlier works related to drug preparation showed that increasing in activity when being include iron atom based molecule as ferrocene instead of many known organic compounds[7-8]. In this context, higher aromaticity of sandwich compound plays an important role during electrophilic substitution reactions, such as Friedel-Crafts acylation, which have excellently been conducted[9-10]. In recent years, the discussion on the most stable conformer of ferrocene, whether it is the eclipsed or the staggered, with both experimental and other information, still without conclusive evidence; despite the major number of studies that describe the properties of both conformers[11].

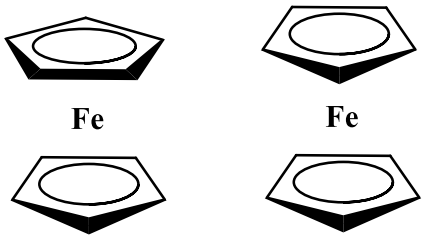

Figure 1: Representation of the two different molecular conformations of staggered form (left) and eclipsed form (right) of ferrocene

Antiprismatic and staggered form of solid-state of Cp rings, have elevated stability in contrast with other metallocenes (osmocene and ruthocene) of the same category. The previous feature may be attributed to small-distance between the Cp rings. As an additional advantage, staggered conformation has the ability to minimize non-bonded interactions between heteroannular carbons of cyclopentadienyl rings[5]. Differentiation of ferrocene arrangements is a result of a meager energy barrier value between the highest occupied molecular orbitals HOMOs and the lowest unoccupied molecular orbitals LUMOs of the eclipsed and staggered conformer[12]**.** Moreover, several theoretical and experimental detailed-investigations on the structure of ferrocene proved that staggered conformation in the solid phase that can be obtained

by a way of the minimum-value of crystal repulsion backing forces of carbon-carbon and hydrogen-hydrogen that existing between the two rings. The carbon-carbon bond distances are 1.40 Å and the Fe-C bond distances are 2.04 Å. The energy difference between staggered and eclipsed approximately is 4kj/mol. Meanwhile, The CpFeCp has tow a point groups d_5d (staggered form) and D_{5h} symmetry (eclipsed form). The study related to the d-electrons of Fe in ferrocene that has done by Shawkat Islam and Feng Wang suggests to nature of contacts between Fe–Cp bonds is a covalent bonding [13]. Two C_5H_5 rings grouped in coplane regular manner which binds together via the equally bonds to the central atom "Fe" by π electrons and as another supportive property for the stability, hydrogen atoms are slightly bind towards their counterpart in the opposite Cp ring[15]. Besides, C_{2p} orbitals of the transition metal structure of ferrocene are very appropriate to form molecular orbitals extending around the ring, and this mainly depends on the extent of electron delocalization[16]. On molecular orbital theory, five P orbitals (one on each carbon atom) are available for orbital formation. Linear combinations of orbitals lead to three bonding and two antibonding molecular orbitals.

The general molecular orbital diagram for generic metallocenes, Cp_2M is elucidated in schematic representation below; it has been taken ferrocene as example.

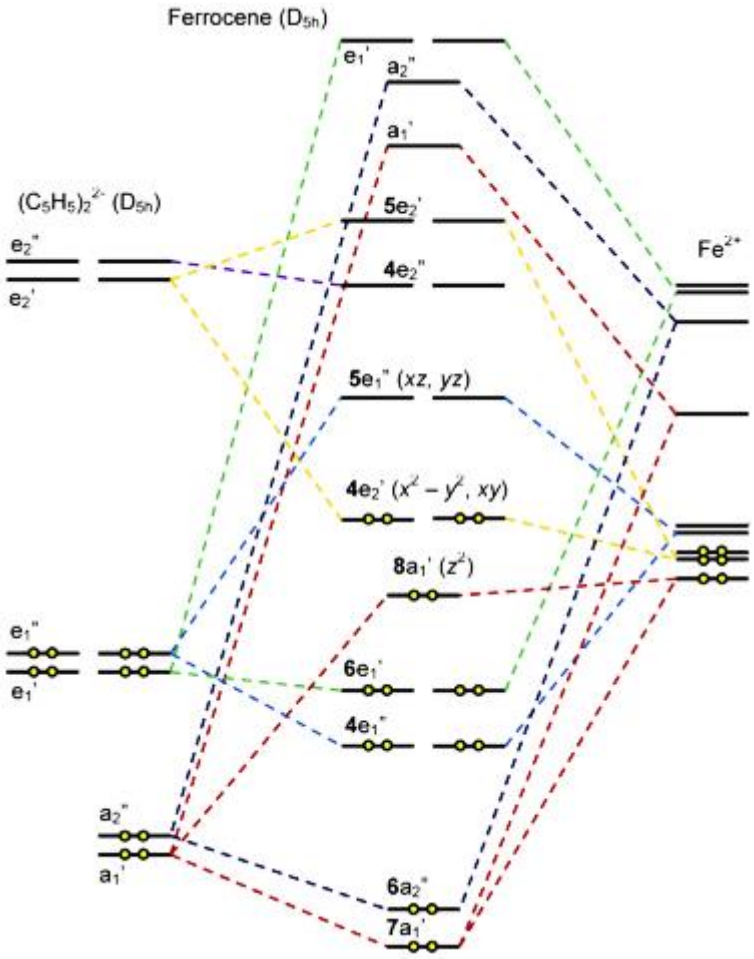

Figure 2: Molecular orbital diagram of ferrocene molecule. Orbitals on the left show the p system of two Cp^- and Orbitals on the right represent valence orbitals of the iron atom.[17]

Ferrocene is notably stable compared to other majority organometallic substances, as well as its ability to form bonds with acids and alkalis, this considered as a new achievement in inorganic, organic, and applied chemistry[4]. The high thermal stability of ferrocene mainly attributed to the aromaticity of the Cp rings. The oxidation state of the iron atom in ferrocene is +2 and also each Cp ring bear only one conjugated negative charge. Both 5electrons of rings with 8 electrons of Fe, the total electron count brought to 18 (eighteen electron rule of configuration**)**, which is what to support stability and elucidated the general diamagnetic behaviour of external/internal shape of ferrocene[19]. A three-dimensional structure of ferrocene so contributed in derivatives preparation based on electrophile and nucleophile substation reactions. Upon its characteristics are previously mentioned, it paved the way to synthesize a vast class from $[Fe(C_5H_5)_2]$, which has never been described before in chemistry. Moreover, Its electrochemical behaviour is monitorable and much help scientists to make ferrocene a valuable building block for elaboration electroactive compounds using various methods[20]. Additionally, the importance of protonation behaviour in electrophile substitution reaction with ferrocene, have been elucidated using more than one theoretical and experimental investigation; which gave new molecules having a ferrocene as central nucleus.

1.2 Physicochemical and thermodynamic properties

In various research fields, the robustness of the extraordinary structure of ferrocene attributed to containing significant functions and remarkable advantages especially inside its organometallic molecule. Chemically, the melting point and molar mass of ferrocene are 448 K, 186.04 g/mol respectively and its boiling point has been accurately determined at 522 K[21], as well as, possesses a reversible behaviour, crystallized in orange / yellow form with a camphor-like odor[22]. The changing of ferrocene color to deep-blue is an outcome for losing one electron by oxidation at +0.4 v using a saturated calomel electrode in cyclic voltammetric technique[23]. Among the key factors for the use of ferrocene is super-stability at room temperature[24], low toxic compound[25], insoluble in water[26], unaffected by air[27], soluble in majority of hydrocarbon solvents[28]. On the other hand, the density of ferrocene is equal to 1.490 kg/m³; (at 293.15K) at standard atmospheric pressure[29] and ferrocene also underwent a single-step thermal decomposition with almost 100% mass loss at ˜ 453 K. One of the leading causes for involving ferrocene with certain substances is that it has the ability to donate an electron from the higher non-bonding level of energy molecular orbital, converting the neutral, diamagnetic compound to a positively charged, paramagnetic ferricenium ion radical (Fc^+)[30]. As for the thermodynamic

properties, the average sublimation value of enthalpy of ferrocene at 298.15 K can be measured using three experimental techniques, differential scanning calorimetry (d.s.c.), Calvet calorimetry and Langmuir's equation and its values respectively are: 73.1 ± 1.2, 74.2 ±1.2, 71.7 ± 1.3 ($kJ.mol^{-1}$)[31], in parallel, d.s.c technique has been devoted to calculate the values of enthalpy fusion at 448.5, 447.6 K and its results were as follows: 17.8, 17.49 ($kJ.mol^{-1}$)[32-33]. Crystal ferrocene was used to obtain the entropy of transition by dividing the transition enthalpy (as an average of four measurements) on the transition temperature "242 K" to be (17.13 ± 0.02) $J.K^{-1}.mo1^{-1}$[27].

1.3. Synthesis

Since the discovery of ferrocene and identified its unknown structure, a large number of synthetic route for its preparation have rapidly appeared and can be synthesized by more than one efficient preparative procedure, which begins by reacting cyclopentadienide containing-reagent such as sodium cyclopentadienide[34], Grignard reagent[35] and cyclopentadienylthallium[34] with $FeCl_2$ (it was and still one of the most easily accessible sources of iron-oxide) in ethereal solvents. Given the essential role played, frequently, only the strong bases able to provide a good yield.

Indeed, the reaction of the sodium salt of cyclopentadiene with ferrous chloride in tetrahydrofuran is a widely used way for preparing ferrocene and the direct contribution of the weak acidic behaviour of cyclopentadiene and strength fundamental behaviour of sodium gave rise to produce a salt $C_5H_5^-Na^+$. Resulting-mixture reacts with ferrous chloride to generate ferrocene[36].

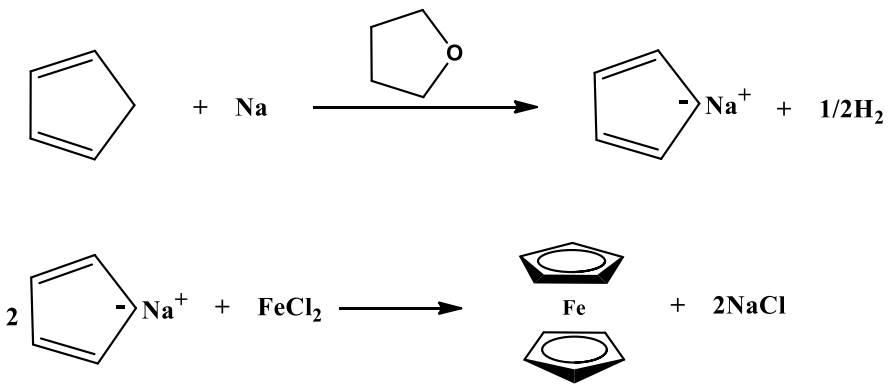

As another way to prepare ferrocene, is to use the Grignard or cyclopentadienyl magnesium bromide reagent, as an intermediate during the reaction. The oxidation state of iron reduces from ferric chloride "$FeCl_3$" to ferrous chloride "$FeCl_2$" after it added to a solution involving an excess of Grignard reagent and the suggested mechanism may be described as follows[35]:

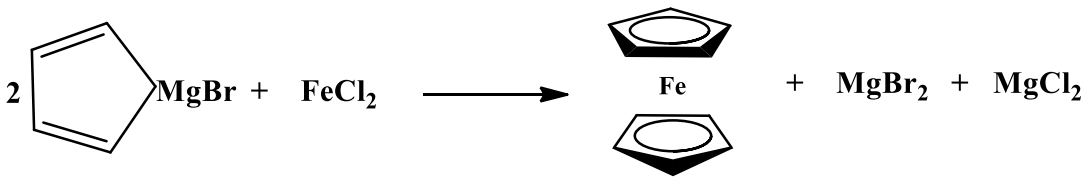

Entirely solubility of ferric chloride with most organic solvents deems great proof to the synthetic path success, and this allows cyclopentadienyl group to become "aromatic" by the acquisition of a negative charge. Generally, the quick and timely reaction requires to be ferrous-halide having high-soluble; still, ferrocene may give a good yield through solubilizing a ferrous ion with a chelating agent for enhancing the affinity of chelating ligands for the metal ion "Fe^{2+}" and to generate more activity of Grignard reagent towards the chelating agent, this is only possible by the addition of excess from C_5H_5MgBr[4].

Among helpful ways to make a cyclopentadienylthallium, as the first stage, is the reaction of thallium sulfate with sodium hydroxide to obtain thallium hydroxide, which played the role of strong-base and thallium source, in an aqueous medium[39-37]. It is easily stored, as a second step it was mixed a resulting solution "TlOH" with C_5H_5 for getting TlC_5H_5 then such a latter product reacts with $FeCl_2$ for finally getting a ferrocene molecule. These reactions are shown below[40-41].

$$Tl_2SO_4 + 2NaOH \longrightarrow 2TlOH + Na_2SO_4$$

$$2TlOH + 2C_2H_6 \longrightarrow 2TlC_2H_5 + 2H_2O$$

$$FeCl_2 + 2TlC_2H_5 \longrightarrow Fc + 2TlCl$$

In 1952, a research team published a new synthetic way for preparation a ferrocene molecule utilizing the reduction reaction among iron pentacarbonyl with cyclopentadiene vapor at an elevated temperature in nitrogen and atmospheric pressure. Such a reaction is written, bellow [42]:

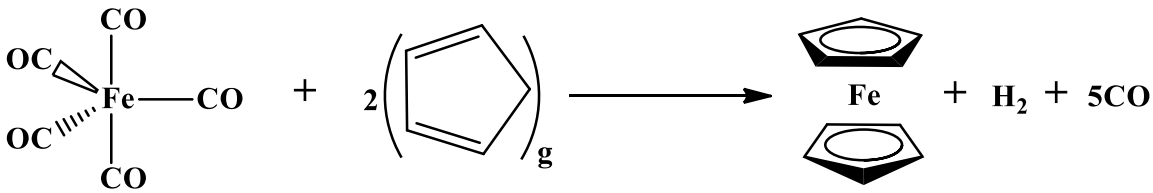

2. Diazotization reaction:

2.1 Background

Diazotization in organic chemistry is one of the older and most commonly used reactions with permits the formation of diazonium salts. Nearly all primary aromatic amines can be converted into its diazonium salts [43]. Nevertheless, the highly reactive nature of the diazonium functionality gave rise to the evolution of numerous reactions for elaborating several antibiotics. Besides, can be combined between the most recent processing methods and new active agents, for enhancing the reactions path based on diazonium mechanism[44].

2.2. Diazonium salts

The German chemist Johann Peter Griess reported a first paper related to diazonium salt in 1858. His discovery has been widely exploited in the chemistry of dyes[45]. The general structure in form $R\text{-}N_2^+ X^-$; R represents an aryl or alkyl and X^- also represents an organic or inorganic weak nucleophilic anion. In theory, however, a wide range of combinations for R/X^- pair can be generated according to the two groups' nature that has a direct and robust effect on the whole stability of the salt, which makes it unstable in room temperature, even explosive in some cases. The use of such compounds in synthesis is therefore tricky. Also, alkyl diazonium is non-isolable caused by the conjugation between the aromatic cycle and the diazene group[46].

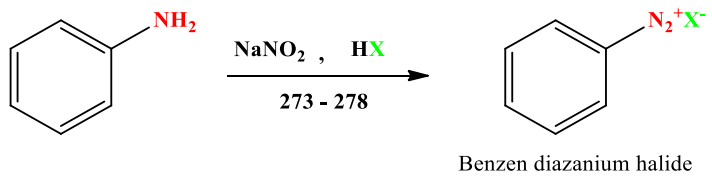

Figure 3: Diazonium salt formation

2.3. Arylation of ferrocene

Of particular ferrocene moieties have extraordinary importance caused by its high electrochemical features and its inhalable role when attached with an active functional group and can quickly transform into active biological compounds[47]. Among these compounds is phenylferrocene, because of the phenyl group's well-known high reactivity toward many reagents.[48]. Ferrocene undergoes aromatic substitution reactions like benzene. However, after four decades of the discovery of this metallocene, the increased interest by the unusual reactivity of ferrocene has not stopped. In addition, not surprisingly, all mechanisms of these transformations attracted significant attention. As a general rule, the electrophilic attack able occur at two different sites: it may target any carbon atom from cyclopentadienyl rings on the opposite face for metal-carbon bonds (Exo attack) or on the same face as the metal-carbon bonds (endo attack)[49].

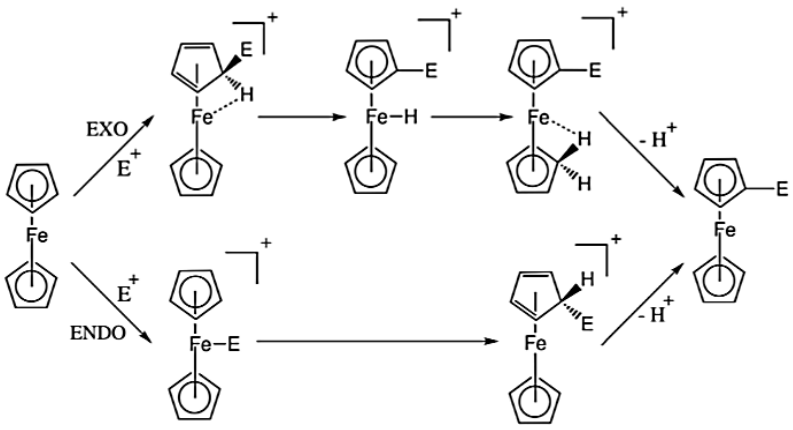

Figure 4: Exo and endo routes for electrophilic substitution mechanism of ferrocene [50]

3. Applied aspects in medicine

Nowadays, the most promising research projects are rushing toward the preparation of drugs bearing an inorganic part that featured by effective therapeutic abilities against large categories of intractable diseases especially in the medicinal chemistry range and their chemotherapeutic properties have been extensively exploited in many requirements of trials.[51-52]. As there is no doubt in their efficacy, notably the compounds derived from ferrocene. By focusing on the papers are published in the few last years, ferrocene's reactivity attracted particular interest due to its distinctive properties such as neutrality, lipophilicity and the catalytic role during the organic reactions[53-54], which have shown a high antimicrobial[55] and anticancer [56] and antioxidant activity[57]. The use of ferrocene in the vital research areas demonstrated that some ferrocenyl compounds possess high activity and tested in vitro and in vivo against the different types of viruses. This research path is among the promising strategies to combine between ferrocenyl groups with known drugs or drug candidates to get new drugs. However, there are still obstacles in finding ways to obtain the clinical approval that allows ferrocene-having molecules to change over from being synthetic curiosities to effective medicaments that can be used in medical treatments[58].

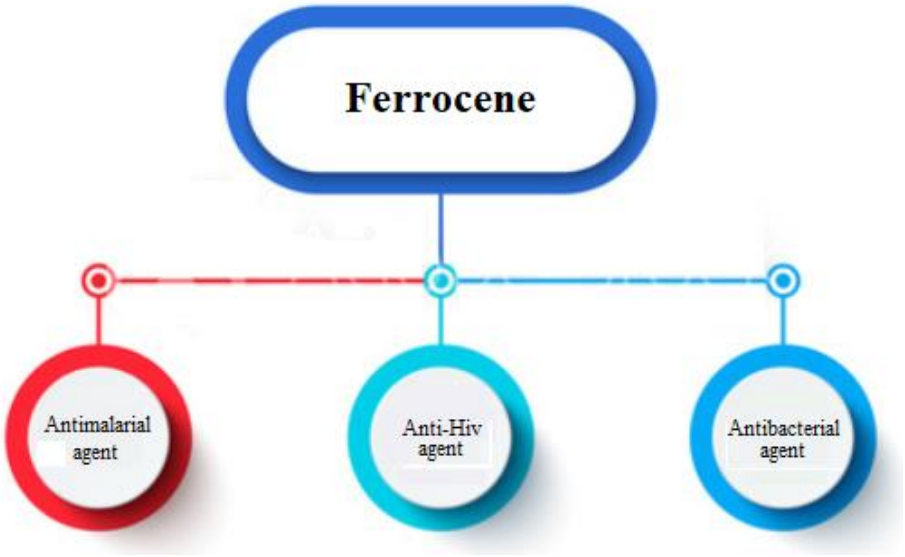

Figure 5: Some medicinal aspect of ferrocene

As stated earlier, ferrocene may be the starting point for modern therapeutic drugs [59] that biologically assessed to identify their efficiency. The following highlights summarize the role of incorporation ferrocene molecules in the medicinal drugs field, particularly the antimalarial, anti-HIV and antibacterial agents.

3.1. Antimalarial agent

More recently, multiple pathways have been devoted to elaborating the following class of antimalarials, one of the principal aims is to synthesize new drugs being less prone to body resistance. One of this application is an exploitation of the metal-based compounds in the drug industries field [60]. Nevertheless, the suggestion of use such a strategy requires facing significant challenges[61-62], Drugs containing metal were utilized since-longstanding but, its use is quickly decreased when proved their toxicity. However, numerous investigations were carried out to demonstrate their intrinsic activity and high efficacy based on the experimental results of these investigations, pharmaceutical researchers are able to improve the old structures or find out alternative methods for preparing chemotherapeutic having safer metals. Hence, such metallocenic strategy has been used for obtaining new antimalarials that could surmount the challenges are mentioned above. In fact, depending on derivatization reactions, it is possible providing large classes containing ferrocene that may increase the activity of such derivatives. All these specifications with each other; have made ferrocene one of the better-suggested molecule that can be introduced into medicinal drugs. The following content describes several molecules that was categorized as an antimalarial agent and which include a ferrocene moiety.

In the early 1990s, it has been reported the first successful attempt for interbreeding ferrocene moieties with an effective antimalarial agent like chloroquine. By the substitution reaction, it has facilely been prepared ferroquine from chloroquine in 1994 by Biot and co-collaborators at Lille University. Also, it has more potent activity than chloroquine toward plasmodium falciparum and is featured by non-toxic in vivo[63-64]. By replacement methylene group of chloroquine by a ferrocene moiety, gave a ferroquine. Figure 6 elucidates such chemical reaction.

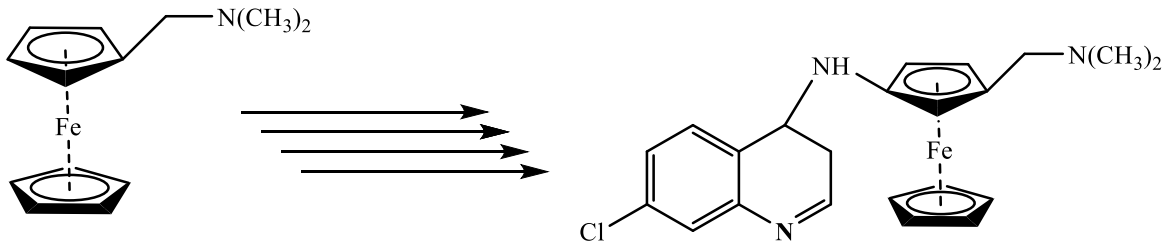

Figure 6: Synthesis path of ferroquine

Bellot and collaborators reported a new series of ferroquine derivatives, including trioxaferroquines. They have a high efficacy toward chloroquine-resistant strains (FcB1-Colombia and FcM29-Cameroon) with the half-maximal inhibitory concentration in the range of 16–43 nM. In vitro evaluation studies on antimalarial agents, compound (C) from the represented series in figure 7 showed a good response toward FcB1 and FcM29 with IC50 values equal to 17 and 29 nM, respectively[64-65].

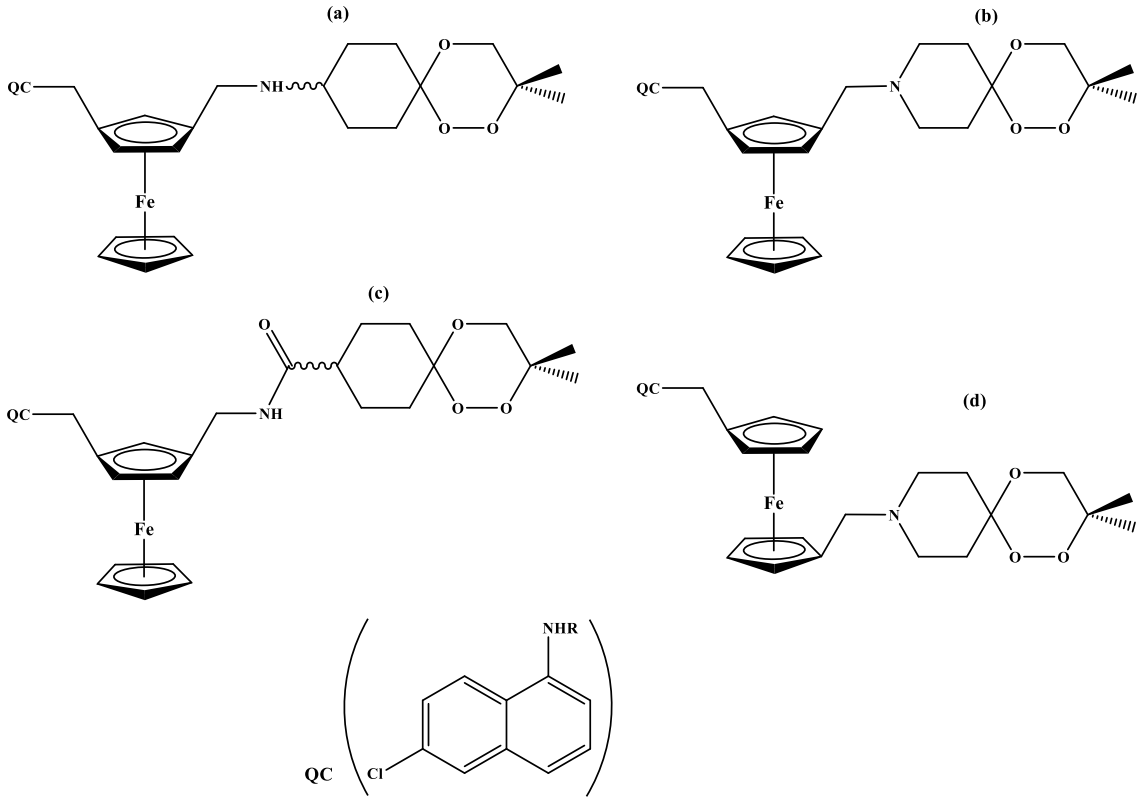

Figure 7: Chemical structures of trioxaferroquine derivatives

3.2. Anti-HIV Agent

The increasingly applications on ferrocene for producing new drugs against HIV; attracted the attention of Champdore and collaborators. Such group acted to preparing new compounds by incorporating the ferrocenemethyl moiety into a heterocyclic base then evaluated it toward HIV. Only two compounds from the prepared series of ferrocenyl derivatives showed remarkable activity against HIV[66].

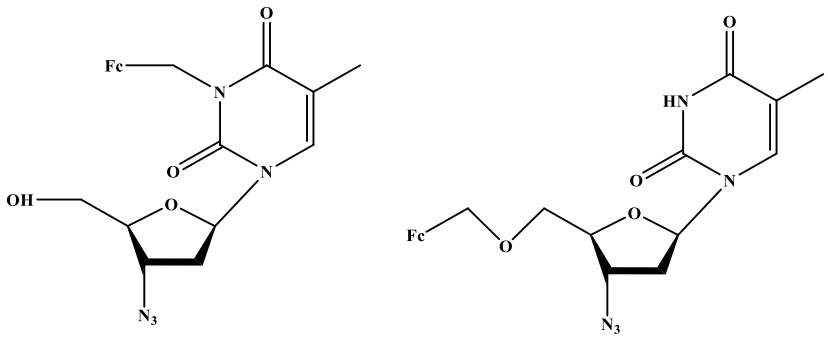

Figure 8: Chemical structures of anti-HIV compounds

On the other hand, in over two decades of elaborating IN inhibition-containing anti-HIV agent, a significant number of synthetic products are appeared as IN inhibitors, among these compounds, ferrocenyl-2-hydroxy-4-oxo-2-butenoic acid (a), hydroxyferrocene chalcone (b)

and ferrocenyl chalcones, which are displayed a considerable potency during the strand transfer inhibition[67].

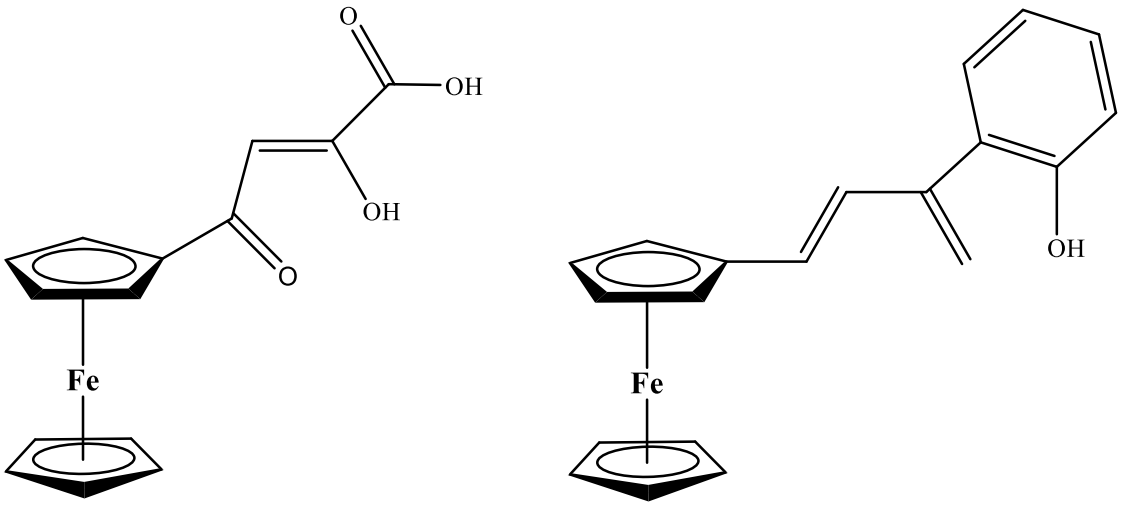

Figure 9 :β-diketo acids examinated as potential HIV-1 integrase inhibitors compounds

To surmount viral resistance of HIV, the current and future efforts will improve a chemical performance of authentic IN inhibitors, which may play an essential role in finding a drug having a capacity to inhibit the activity of HIV.

3.3. Antibacterial agent

Most antibiotics have a high efficacy for inhibition the chronic influence of unhealthy bacteria. Nevertheless, the resistance of bacterial diseases toward the current antibiotics has kept, for instance, gonorrhea and tuberculosis diseases that are become so difficult to curb their activity with present antibiotics and this is attributed to developing the target bacteria cells, its resistance against the successively use of the same antibiotic (without any elaboration). According to limiting the production of laboratories, researchers suggested using many different solutions to overcoming these cases. Among these ideas incorporating the ferrocenic group inside a drug that previously used as an antibiotic for enhancing both its inhibiting influence and its selectivity behaviour[68].

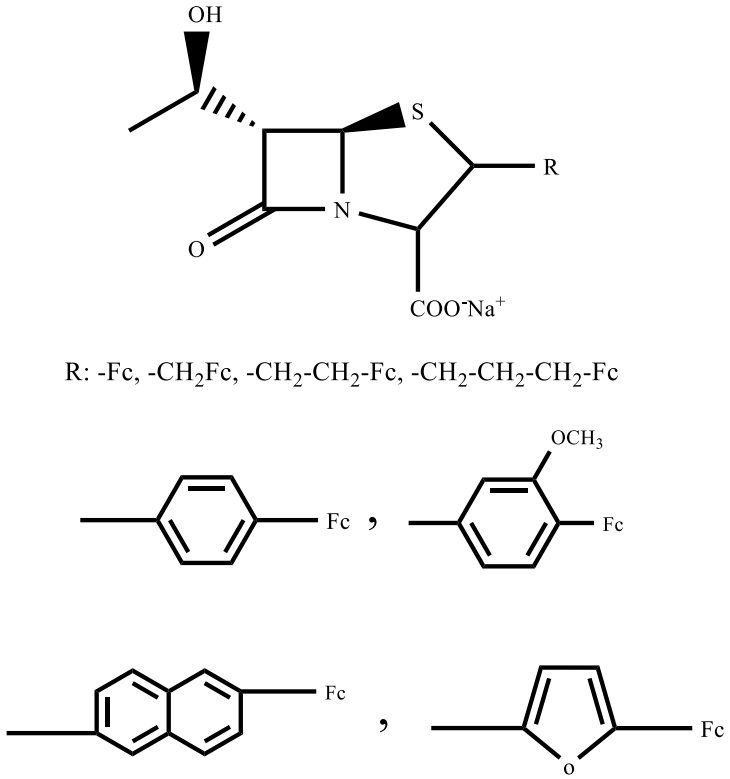

Figure 10: Chemical structures of some antibacterial agents

Bohua Long and collaborators prepared a new penems family containing ferrocene molecule linked to C-2 site of the penem unit as shown in Figure 10 and the antibacterial activities against Gram-positive/negative bacteria were in vitro studied. Besides, strains-of Methicillin-resistant Staphylococcus aureus (MRSA) was evaluated in the same experimental conditions. Furthermore, the majority of the penems having an excellent activity against antibacterial-action as well as super stability to human DHPI compared to faropenem (the reference active compound in this study), in particular, penem derivative (b) showed significant antibacterial activity against two-types of bacteria that mentioned above[69].

Chapter 2

Experimental techniques

1 .Cyclic voltammetry technique

Cyclic voltammetry (CV) became a common way since the middle of the last century to study the electrochemical reactions; it also represents a hallmark in electro-analytical methods[70]. A CV is known by two basic operations the accuracy of its functions and the high electrochemical information content obtained from potentiodynamic measurement of studied bioactive compounds[71]. Besides, CV analysis is used to identify the electrochemical-properties of oxidized and reduced analyte forms near the electrode surface in the chemical medium. The CV can also be used to obtain the diffusion coefficient, free Gibbs energy, and binding-site size parameters[72].

At the use of cyclic voltammetry, the electrode potential changes linearly with time between two predetermined limits[73]. For more details, the change in potential is called "triangular" and characterized by the scanning speed "R", such that R=dE/dt (Figure11- left)[74]. The obtained data exploits to plot the graph of intensity (i) versus potential (E). The resulting current from the studied system is often symbolized as ($A.cm^2$) to simplify comparisons between electrodes with different geometric surfaces[75]. The supporting electrolyte concentration is ranging from 50 to 100 times greater than that of electro-active components for overcoming noise challenge generating from migration currents as well as it worked to increase the conductivity of the solution[76-77]. The purpose of supporting electrolyte is to ensure that the ionic strength of the solution will act in high electric-performance at the surface-electrode[78-79]. The magnitude of anodic and cathodic peak current (I_{pa}, I_{pc}) and the anodic and cathodic potential peaks (E_{pa} and E_{pc}), are the essential parameters in cyclic voltammetry[80]. The mostly used electrode in this category of research is glassy carbon and this attributed to its significant abilities either chemical-resistant or high conductivity[81]. The next section will discuss the redox species' result from cyclic voltammetry method that used for several electrochemical analysis purposes (Figure12-Right). The studied ligand has two behaviours "reduction" and "oxidation", it can exchange one electron with the electrode, when to be reached by a specific value of potential[82]. The active molecule is reduced by accepting an electron from the electrode surface (ES), and this electrochemical procedure is being possible when the potential energy of the empty molecular orbital of the analyte is less than the potential energy of the electrons that exist in (ES). In such an energetically favorite state, the electron able to jump from the electrode toward the studied ligand, and vice versa, the analyte is oxidized by losing an electron to (ES); it must be there a remarkable difference in energy level among a studied compound and (ES) for occurring the electron transformation. The electrochemical

benefit of electrons conversion in these reactions is keeping the potential energy of such total system[83].

1.1. Reversible system

In electrochemistry, the reversible reaction (it is a very fast equilibrium reaction where one electron exchanges between two basic electro-states of the substance). The potential forces (E) applied on the particular concentrations of Ox and Red species at the working electrode surface (are,c_{Ox}^{0} and c_{Red}^{0}) in a ratio agrees with the Nernst equation:

$$E = E^{0} - \frac{RT}{nF} ln \frac{C_{Red}^{0}}{C_{Ox}^{0}} \qquad (1.1)$$

Where R is the molar gas constant (8.3 J.mol^{-1}.K^{-1}), T is the absolute temperature (K), n is the number of electrons transferred, F = Faraday constant (96.485 C/equiv), and E_0 is the standard reduction potential for the redox couple. If the potential force applied to the electrode is altered, the ratio $(c_{Red}^{0})/(c_{Ox}^{0})$ will also change. If the potential is made more negative the ratio being larger (Oxidized molecule is reduced) and, meanwhile, if the potential is made more positive the ratio being small (reduced molecule is oxidized)[73].

1.2. Half -Wave Potential ($E_{1/2}$)

CV data able to give several characteristics of forward / reverse behaviour for the studied compound, half-wave potentials symbolized by "E_0" (standard electrochemical potentials),

i.e., $E_{1/2} \approx E_0$ for the reversible system and can be obtained directly from a cyclic voltammogram as the average between the anodic "E_a" and the cathodic "E_c" potentials. The measured-half-wave potential is influenced by the diffusion behaviour of oxidized and reduced form of the studied ligand, furthermore, the direct relationship with a formal potential, it is shown below:

$$E_{1/2} = \frac{E_{pc}+E_{pa}}{2} = E^{0} + \frac{RT}{2nF} ln\left(\frac{D_{Red}}{D_{Ox}}\right) \qquad (1.2)$$

Where D_{Ox} is the diffusion coefficient of Ox; D_{Red} is the diffusion coefficient of Red. When the diffusion coefficients of the oxidized and reduced species are too similar, the half-wave potential provides an excellent approximation to the formal potential[84].

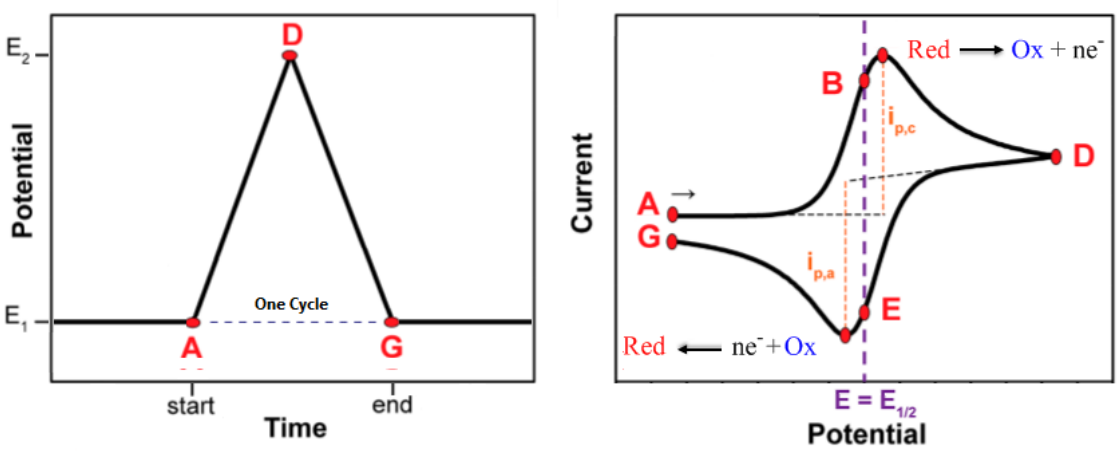

Figure 11: (Right) Electrochemical reversible system of cyclic voltammetry; (left) Diagram shows the variation of potential as function with time of oxidation and reduction reactions

Upon the criteria of reversibility, it became possible to use cyclic voltammetry as a method to examine the response of reversible system. The CV can also be used to estimate the diffusing behaviour of electroactive substances and estimate the concentration of a substance that has diffusion-limited. By determination of the currents i_{pc} and i_{pa}, the diffusion coefficients can be accessed through the Randles-Sevcik equation:

$$i_p = 2.69.10^5 n^{3/2} A.D^{1/2} V^{1/2} C_0 \qquad (1.3)$$

Where i_p is the peak current (cathodic or anodic), n represents the electron number exchanged (n = 1 for ferrocene), A is the area of the electrode (cm^2), D is the diffusion coefficient ($cm^2.s^{-1}$), v is the scan rate (Vs^{-1}), and C_o is the concentration of electroactive species in the solution ($mol.cm^{-3}$)[85].

1.3. Instruments

1.3.1. Potentiostat

A potentiostat is an electronic device that works to monitor the voltage conversion of working electrode according to reference electrode. The potentiostat conducts this task by subjecting the studied electroactive-species into a range of potential corresponding with the target procedure (oxidation or reduction). As another function, the potentiostat devotes to measure the flow of current among the working and counter electrodes. Two main variables can be obtained from the electrochemical measurements, which generated by a mathematical relationship between the potential (mV) and the current density ($\mu A/cm^2$)[86].

1.3.2. Electrochemical cell

An ideal electrochemical cell contains a studied sample dissolved in an organic or aqueous medium, electrolyte support, and three electrodes types. Cells have assortment sizes and shape; additionally, it is manufactured with different materials. The utilized type depends mainly on the amount, sample kind, voltammetry technique, and analytical information. The substances were used in the manufacturing of a cell are (polyethylene, glass, Teflon), for order avoiding the side reactions with a studied sample[87].

1.3.3. The Electrodes

The electrochemical electrodes are: (1) working electrode (WE) is an electrode having a specific function, by imposing the corresponding potential value for studied species which are contacted with the electrode surface for implementing the oxidation or reduction reactions;(2) reference electrode (RE), possess a constant potential, also, has an essential role in usually electrochemical evaluation studies[88]. All the potential values record according to a constant potential of (RE). (3) auxiliary electrode (AE), is an electrode that is employed to close the current circuit in the three-electrode electrochemical system [89].

2. UV/VIS technique

Besides chemical analysis, the optical spectroscopy characterizations of substance mixtures are carried out with many physical methods. Among analysis tools used in different research areas are UV/VIS techniques. This method is often applied to monitoring the kinetic behaviour of studied samples in near-ultraviolet and visible regions during the biological binding-investigations to find out the corresponding values of free binding energy (ΔG), binding constant (K_b), resulted from the specific types of interactions between the studied proteins and ferrocene derivatives, additionally it also used for evaluating the efficiency and affinity of newly prepared compounds[90]. Meanwhile, the use of the previous method is exploited to understand how the drug molecules interacting with DNA, these chemical and biological topics have become an active research area in chemistry, molecular biology and medicine[91].

In vitro aspect, thus a simple way employed to estimate the interaction types among studied compound and double-strands-DNA by recording the change in absorbance as a function with wavelength. Also, based on the shift of maximum absorption value obtained from the increasing additions of the studied compound, all binding parameters can be calculated depending on the obtained data[92].

The primary three binding modes that can be obtained from the valuable information of UV/vis technique are involved: intercalative binding, groove binding and electrostatic interaction caused by structural sandwiching of some molecules between the aromatic, heterocycles DNA base pairs. The intercalation-binding mode is the most vital kind of attachment[93]. The general UV-vis behaviour of all compounds affected by the additions of DNA concentrations indicates an attachment between them. Meanwhile, if the increasingly additions of DNA samples being accompanied by increases in maximum absorption, DNA structure is damaged [94].

2.1. Denaturation of DNA

DNA denaturation (or melting) occurred at high temperature or elevated pH. Such phenomena lead to disengaged the double strand of DNA, as a result of breaking hydrogen bonds between DNA bases[95].

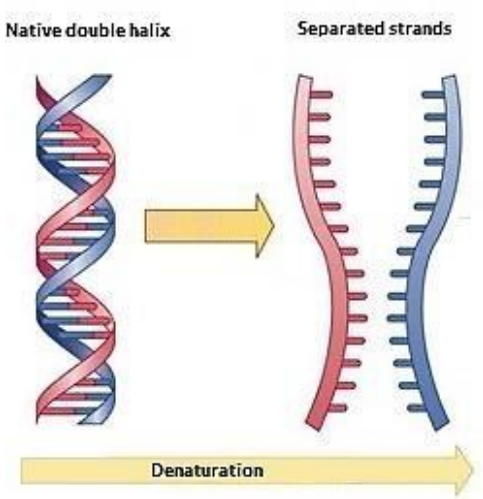

Figure 12: Denaturation phenomenon of DNA[96]

The unexpected increase of UV absorption resulted from the denaturation of DNA, named a hyperchromic effect. DNA bases of purine and pyrimidine strongly absorb ultraviolet light. As another characteristic, when double-strands of DNA are bound, its absorption ability being less than when to be in denatured form and this is a consequence for the nature stacking interactions among bases. The single structure of deoxynucleotides is strongly absorbed compared to double strand of DNA in basic state[94].

Natural absorption spectrum curve (ASC) of DNA in the denatured state is always being above the spectrum of DNA in a natural state, and the other ASCs of DNA in the interacting state are always under the spectrum of DNA in a natural state. As an example, figure 15 illustrates the

absorption spectrum curve of DNA in the interacting state as a function with a studied concentrations range (inverse relationship) for the ferrocene derivative.

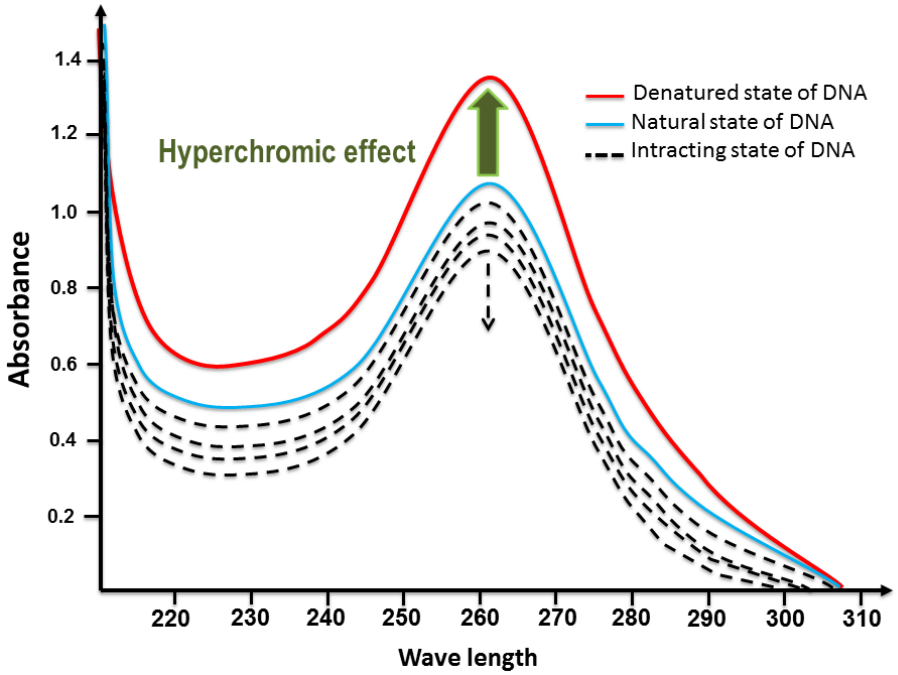

Figure 13: Spectroscopic absorption curves of DNA in denatured, natural and interacting states

2.2. Theory of molecular docking

Molecular docking (MD) is an efficacious technique and utilizes upon the obtained experimental-data to predict theoretically the preferred orientation of a small molecule (ligand) in a macromolecule (target) to form a stable complex; On the other hand, it can also predict the suitable ligand site inside the protein structure[97].

2.2.1. Molecular docking

In the last three decades, the investigations number of informatics applied chemical increased. Also, it is one of the highest fast-growing fields in applied sciences. MD is a speedy means for predicting a manifold of the complex intermolecular structures between at least two objects. It is also a tool for a structural-optimization where the goal is to determine the best position for the receptor (ligand itself) inside acceptor (macromolecule). The simulation-based on algorithmic calculations which are designed to find the correct orientation and conformation of the ligand into the binding site of a target macromolecule (when the ligand is docked into the active site of rigid macromolecule such as "DNA")[98]. Thus, theoretical calculations, 3D visualization and manipulation of molecular systems can be used to develop algorithms having a high accuracy performance and increasing the computational power that still somewhat limited, until able to solve complex problems of the docking approach. A standard docking

protocol involves two principal stages; first, a search algorithm predicts the ligand's different configurations within the targeted binding pocket. In the second stage, each docked pose evaluated and classified according to the intermolecular attachment's tightness after calculating the free energy of each complex. Optimally, the correlation among the most suitable free-energy values (ΔG) and the best-predicted poses, must be in an excellent agreement between them[99].

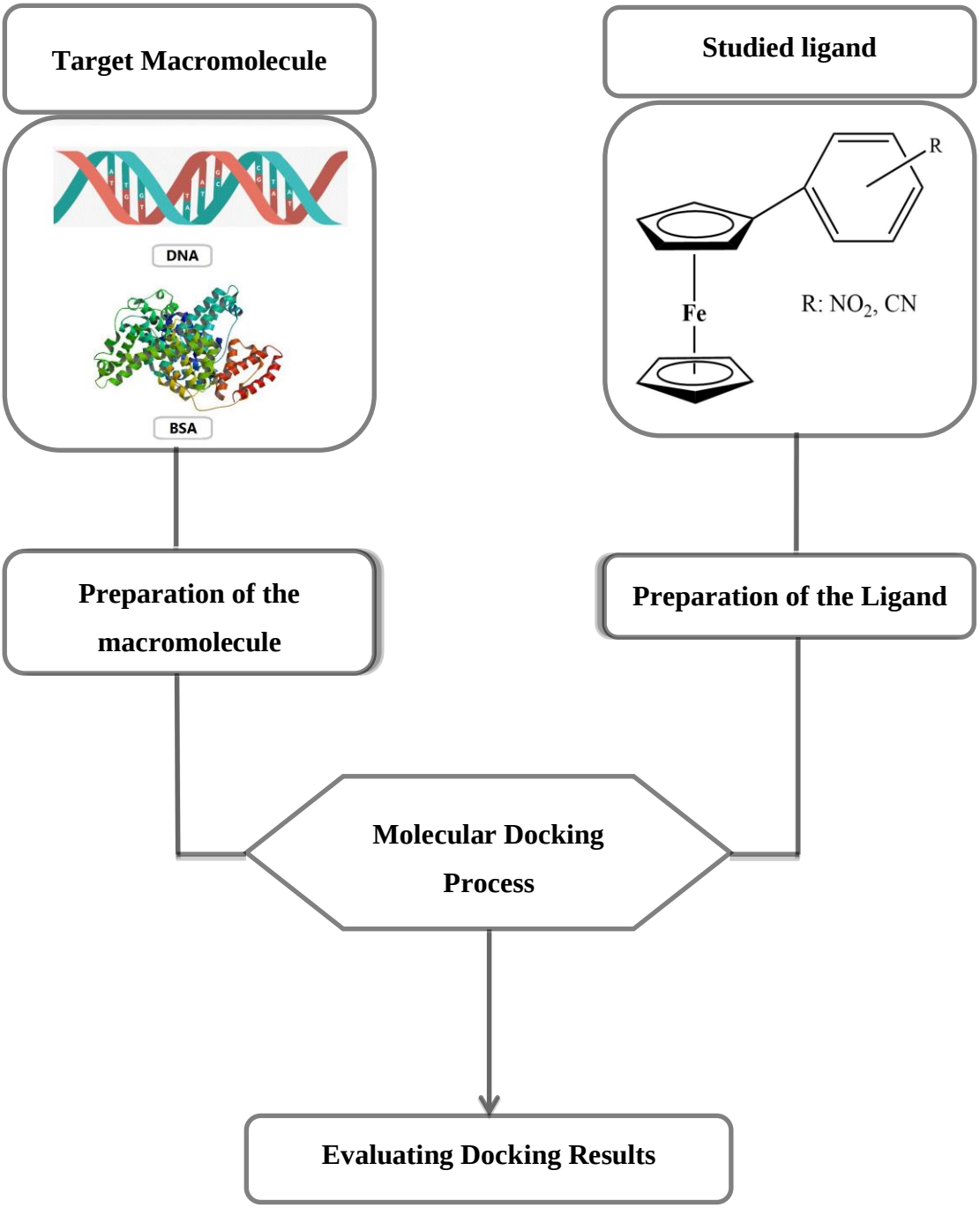

Figure 14: Flowchart of main steps for all docking protocols

2.2.2. Molecular modeling

Molecular modelling is a comprehensive name for all the computational techniques and theoretical processes to mimic or simulate molecules' response in some binding poses. These techniques are often applied in computational biochemistry and materials science to understand the intramolecular binding between the small bio-compounds and large biological molecules in the human body. Notably, the combination of simulation and experimental studies have vastly supported these fields, where gave important information in various a life sciences domains[100].

2.2.3. Molecular dynamic

Simulation modern techniques are one of the common subjects in structural and molecular biology. Computational molecular dynamics (MD) are usually used to perform two basic tasks; for exploring the conformational aspects of biological systems and highlighting the types of protein-ligand interaction; also, protein-ligand binding studies are so important to understand the mechanisms of strong reactions and provide a useful theoretical data to prepare new drugs[101]. MD technique could help the modelling systems' free energy calculations to determine the binding affinity among the examined molecules. (The output file of the software contains all the predicted poses, the topmost stable pose in the output file is used for completing the other steps) physicochemical properties, site size and binding constant are directly related to the potency of protein−ligand interaction[102].

2.3. Applications of molecular docking

Molecular docking is an essential tool in computational chemical research. It could show the feasibility of any function or property of the studied compounds before used in the experimental part of any investigation. Accuracy prediction of molecular docking it gives excellent findings excellent finding, in particular when studying the interaction amongst a small molecule and macromolecule which give much information about its vital role (activation or inhibition). The obtaining of such information type before carrying out any experimental study may help the researchers design new drugs with distinctive characterizations[103].

2.4. Types of docking process

It exists three types of molecular docking as demonstrated by the following figure,

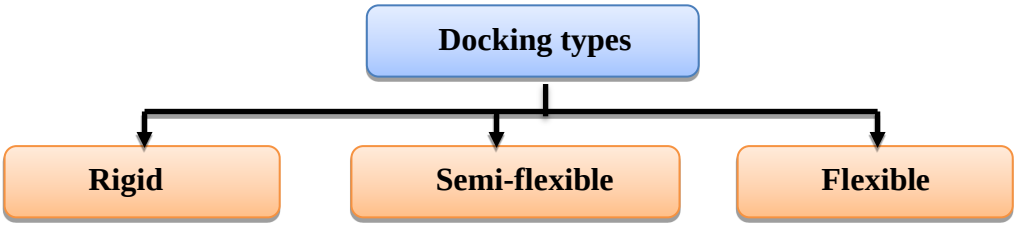

Figure 15: three types of molecular docking

2.4.1. Rigid Docking

Rigid docking is the simplest-way employed for studying the binding relationship between two rigid molecules like (ligand/protein or protein/protein). It only estimates six transitional degrees and rotational freedom. DOCK is an excellent example of rigid docking method and utilizes to superimpose the ligand at the fit binding groove.

2.4.2. Semi-flexible Docking

Just one of two molecules is subjected to the theoretical process (generally the ligand), while the protein is rigid. Docking methods employ to fix the protein conformation that may correspond with the ligands to be docked.

2.4.3. Flexible Docking

The computational methods of flexible docking are generally employed to analyze the intramolecular interaction of superposition between the flexible macro/small molecules. FLIPDock docking software is mostly used in the automated docking process among a flexible ligand and an ensemble of flexible receptor conformations obtained from either experimental or specific computational tools.

The most common docking algorithms use the rigid-receptor/flexible-ligand model for visualization the interaction between ligands and proteins, this type of docking is used in our work using Autodock software[104].

2.5. Calculation of free binding energy

The essential aim of (MD) simulation is access to optimized stability-state of the studied entries to obtain the system's lowest energy. Estimating the free Gibbs energy is one of the computational means to evaluate a ligand's affinity toward a target macromolecule. ΔG can be determined starting from the ligand's change in energy when to be in the free and bound case with the macromolecule. Autodock software used to calculate binding free energy based on the following equation[105]:

$$\Delta G_{bind} = \Delta G_{vdW} + \Delta G_{elec} + \Delta G_{hbond} + \Delta G_{desolv} + \Delta G_{tors} \qquad (.14)$$

Final predicted binding free energy ($\Delta G_{\mathbf{bind}}$) is modeled in terms of dispersion & repulsion ($\Delta G_{\mathbf{vdw}}$), hydrogen bond ($\Delta G_{\mathbf{hbond}}$), desolvation ($\Delta G_{\mathbf{desolv}}$), electrostatic ($\Delta G_{\mathbf{elec}}$), torsional free energy ($\Delta G_{\mathbf{tor}}$), final total internal energy ($\Delta G_{\mathbf{total}}$) and unbound system's energy ($\Delta G_{\mathbf{unb}}$). Thus, a detailed understanding of the fundamental principles related to the binding free energy ($\Delta G_{\mathbf{bind}}$) it provides auxiliary data about the nature types of interactions that performed by simulation method[106].

Chapter 3:

Biological interaction studies

1. DNA interaction study

1.1. Structural features of DNA

Deoxyribonucleic acid or DNA is the most significant molecule in all organisms, it can attach with various types of compounds that possess bioactive characteristics (organic/inorganic compounds and complexes). It has two main strands and is exploited to establish a double helix by coiling around its vertical axis. Structurally, DNA-strands are antiparallel in all kinds of DNA (A, B and Z conformations) additionally its 5', 3'-phosphodiester bonds moved in opposite directions along with the DNA structure[107]. The hydrophilic regions with phosphate groups have negative charges, both located outside of DNA double-helix. In parallel, the hydrophobic regions of the bases being inside the DNA double helix. In molecular biology, two strands' conformational structure generates two forms of binding-pockets called the major and minor groove. The major and minor grooves are in different magnitudes depending on the distance between the bases pairs of DNA. Confirmation of the DNA molecule (A, B and C) can play an essential structural role in the interactions between DNA and bioactive compounds. The electrostatic interactions with the sugar-phosphate-backbone, hydrophobic intercalative binding with the bases, and mixed interactions with the major and minor grooves, all of them represent the significant classes of non-covalent binding in the field of ligand-protein interaction studies[108].

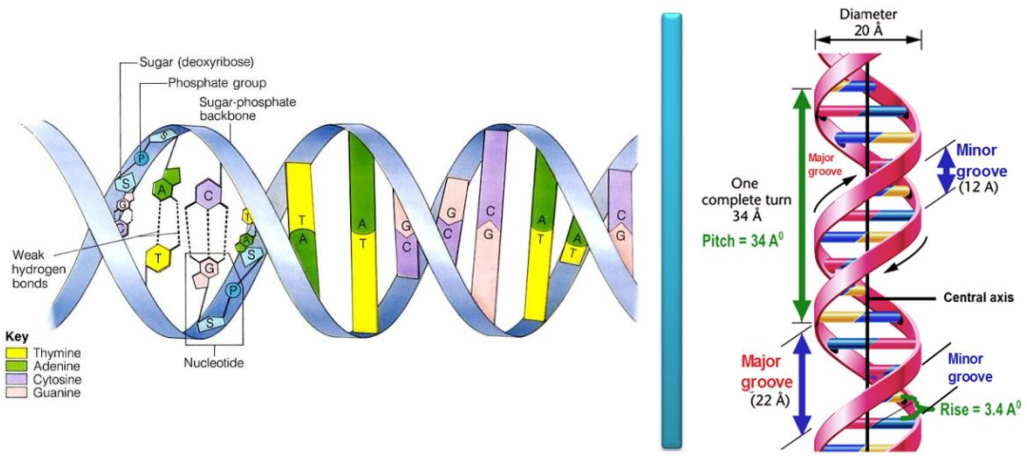

Figure 16: Double helical structure of DNA[109]

1.2. Alternative forms of the double helix (DNA)

The leading three configurations of DNA linked via interactions amongst complementary base pairs. Furthermore, the most common conformations: A-form, B-form, and Z-form. In body cellular DNA, there are some apparent deviations in the structural model that proposed by Watson and Crick, but they do not impact on particular physical and chemical fundamental properties of DNA[110].

Firstly, the A-DNA double helix is a bit wider than B and Z forms of DNA, in addition, the A-conformation is scarce, it only has one status, which is a dehydrated state and it differs from B-conformation in deviation of 20° concerning the double-helical axis of DNA molecule. Second, the Z-DNA is a left-handed Duplex structure with a 4.4 nm turn length and twelve base pairs per helical turn in which the double helix winds to the left in a diagonal zigzag pattern. Third, Watson and Crick proposed the known structure of B-DNA and its structure is more stable compared to other forms of DNA. As a consequence of the conformation of the backbone and sugars, (B) double-stranded of DNA has two grooves form of approximately equal depth, the principal (very wide) and minor (slightly narrow)[111]. Most importantly, B-DNA is the expected standard reference point for any thorough bio-study about DNA properties. It is the most used-form in modulation studies under the PDB code (ID: 1bna) which can be downloaded (www.rcsb.org).

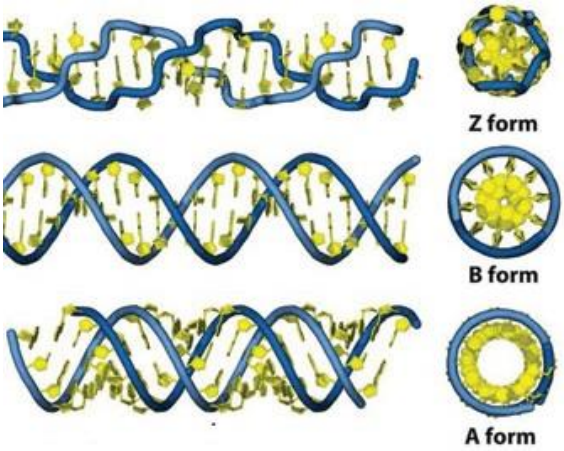

Figure 17: Different conformations of DNA (A, B and Z)[112]

1.3. Ligand-DNA Interaction

Cellular DNA is the essential target of a large number of anticancer drugs and many therapeutic antibodies. In addition, in the major number of papers, the interaction mode of initial-drugs toward DNA was widely evaluated using an assortment of physical biochemistry methods. Most of the outcomes gained from in vitro and in silico studies are devoted to understanding the basic principles of structural relationship of drugs with DNA. These investigations are so important to elucidate and determine the interaction mechanism, in order to short the research-rout for designing effective anticancer drugs[113-114].

Mostly, drugs are non-covalently bound with DNA structure, the interaction modes were categorized into four groups:

- **Intercalating agents**

It is a biomolecule capable to incorporate itself among the planar bases of natural DNA via special mechanism as well as properly prevent his action may lead to mutations.

- **Minor groove binders**

Minor groove binder is a large family of crescent-shaped molecules that interacted selectively with the minor groove of DNA. Also, it is a shallow furrow inside a specific sequence from DNA helix.

- **Major groove binders**

Most of the drugs choose a minor groove as a target binding pocket and the other remain-regions from DNA have represented the major grooves, where the strands are far apart, and the classical analysis of DNA structure indicated that positive charges cover the outer space of the major groove.

- **External binders**

This type of binding is established by electrostatic force. Several bio-compounds have the potential to form outward edge stacking interactions with the sugar-phosphate backbone of DNA. This kind of interaction occurs when the outer negative cover of DNA attached with a species bearing a positive charge.

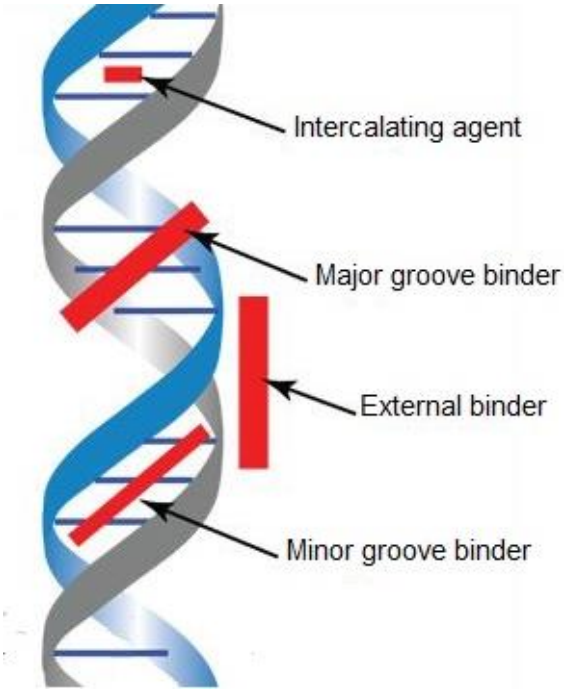

Figure 18: The non-covalent binding pose of drugs to DNA [115].

In our investigations related to interaction study between ferrocene derivatives and DNA, it has been used three standard methods (Cyclic voltammetry, UV-Vis spectroscopy, Molecular Docking) to evaluate and determine the binding types.

2. BSA interaction study

2.1. Structural features of BSA

Bovine serum albumin (BSA) is among the most abundant proteins in the vertebral organism system and it does the most exist in plasma. Furthermore, BSA is considered a bio-tool for studying bio-compound-protein interactions due to its low cost and the easy protocol used to isolate it, and 76% of its homology sequence corresponds with human serum albumin. As for its molecule flexibility, BSA molecule is not in a static, "platonic" state described by Weber (1975) as flexible and rapidly changing in shape [116]. Bovine Serum Albumin's molecule includes 583 amino acids, bound with a single chain cross-linked with 17 cysteine residues (residues (one thiol set with eight disulfides bonds), and the total molecular mass of BSA protein: 66400 Da. The long amino acids chain, structurally, they are ordered in three reiterated domains that possess homologue featured compositions (sites I, II, and III), each one involved two differentiated fundamental sub-domains (A and B) and its stability realized by 17 disulfide bridges. The subdomains can accommodate several ligands as well[117].

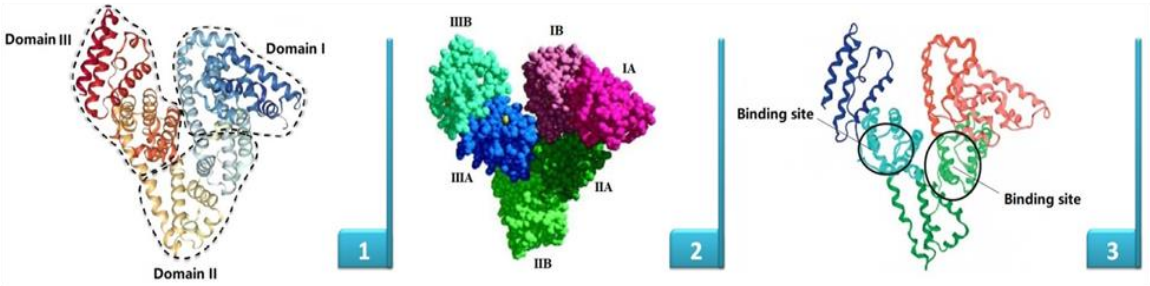

Figure 19: represents an overall three-dimensional structure of BSA with domains (I, II and III); (2) elucidate the subdomains (A and B) of pre basic-domain ;(3) potential binding sites of BSA[118]

2.2. Function of BSA

BSA is the most abundant protein in the blood circulation and is well-known as a carrier protein. Besides, this protein has the most important function: the transportation of various organic and inorganic compounds, including drugs and playing a pivotal role in distribution, metabolism and excretion of drugs molecules. Also has an influential role in the regulation of plasma buffer, antioxidant function and an anticoagulant effect. It acts to transport several types of the endogenous and exogenous substances (such as medication, hormones, xenobiotics and fatty acids), once inside it the bloodstream. This class of proteins also provides colloid blood

osmotic pressure. However, one of the significant property of BSA, it is the reversibly bind with diverse types of complex compounds. One of its primary functions is a direct contribution to inhibit the effectiveness of some chronic diseases[119-120].

2.3. Ligand-BSA interaction

BSA behaviour is famous for its ability to bind with small molecules during the circulatory system of all vertebrate organisms. It is also considered from the proteins which have a high potential for interacting with numerous bioactive compounds. The flexibility of the model protein structure easily adapts with ligands, as well as its three-domain design supplies various sites. The bovine serum albumin tertiary structure has distinct binding sites with various particular characteristics; the main ones include by the site(I) and site (II), which located in subdomains A and B (hydrophobic cavities), respectively[121-122]. Experimentally, the complex structure of BSA must be used in constant temperature for conducting the evaluation studies. The thermodynamic processes predominantly used to define the movement of BSA and the active compounds. The resulting forces from the processes of attachment include: hydrogen bonding, hydrophobic interaction and electrostatic force. The weak binding behaviour between all the charged functions of ligand and protein binding sites has noted in some metal complexes. A large number of studies indicate that drugs usually target the residue of Trp134 which is located on the outer space of BSA[123-124].

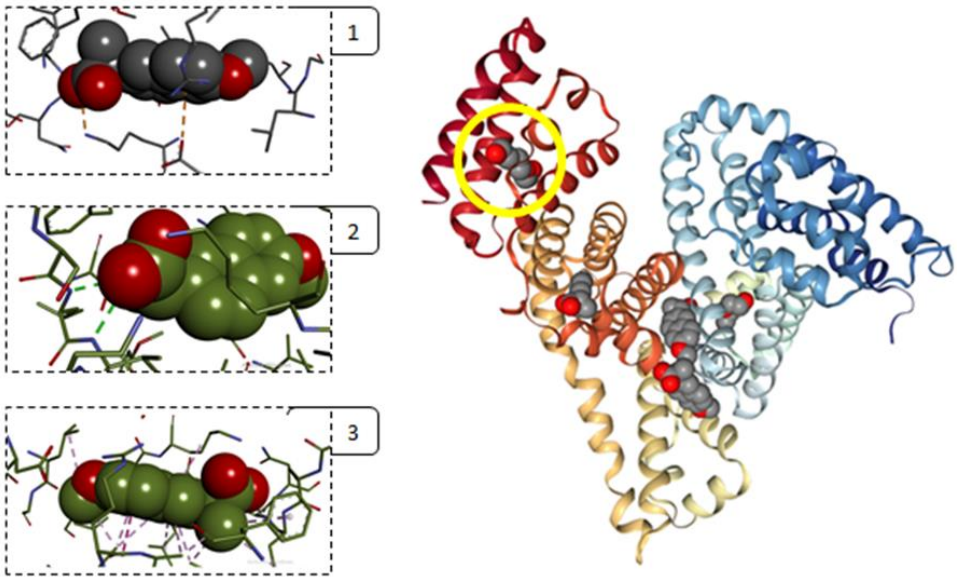

Figure 20: Crystal structure of human serum albumin represented by the ribbon structure[125]

The illustration displays a BSA molecule in a complex form with naproxen (PDB: 4OR0) and figures (1), (2), (3) appear binding types of complex inside the yellow circle, which are

electrostatic forces (brown dashed line), hydrogen bonds (green dashed line) and hydrophobic interaction (purple dashed line) respectively.

Study and evaluation of BSA and its capacity to conserve the vital body functions in blood circulation is an essential step in developing new effective medicament. In this regard, the types and strengths of drug-BSA interactions have also been determined using a simple analytical and electrochemical instruments such as UV-Vis and cyclic voltammetry then were confirmed the obtained experimental results by simulation tools[124].

3. Antioxidant activity study

The increase interests of the biologic antioxidant functions have attracted significant attention. Although there is a great multiplicity of the used methods for determining the efficacity of antioxidant activity; in our antioxidant capacity evaluations of ferrocene derivatives were used two known methods in this exploratory range: CV and UV-VIS method[126].

3.1. Free radical ($O_2^{-\cdot}$) scavenging activities study

3.1.1. Oxidative stress

Oxidative stress means existing a disturbance in the production of free radicals (ex: Reactive oxygen species) and antioxidant defences. All cells are regularly subjected to different stresses that can damage the vital functional capabilities of organisms, whether it is a result of exogenous oxidative stress such as the unwanted influence of chemical or physical agents; certain of these agents could induce oxidative stress. Biomolecules of living organisms could also be forcefully subjected to endogenous oxidative stress; this leads to damage for nuclear acids, proteins, carbohydrates, and polyunsaturated lipids, leading to death cells[127]. According to the effective enzyme and non-enzyme antioxidant mechanism, in biological processes, if a misfire occurs in the oxidative stress, the ratio of balance (pro-oxidant / antioxidant) in our organism system also will be affected. Also, it gives rise to excessive in free radical production or decreases the elimination rate. On the other hand, to understand how oxidative stress increases the susceptibility of a particular disease, the associations among oxidative stress and disease should be carefully examined[128].

3.1.2. Molecular structure of free radical

Every chemical substance possesses unpaired number electrons can be classified as free radicals. Unpaired electrons act to elevate the chemical reactivity of atom and molecule. Experimentally, the hydroxyl radical (OH●), superoxide anion ($O_2^{-\cdot}$), transition metals such as

iron and copper, nitric oxide (NO●), and peroxynitrite (ONOO-) are among the interesting free radicals and extensively used in physicochemical experiments[128].

3.1.3. Role of antioxidant

The body is packed with a wide range of endogenous and exogenous antioxidants. Both components prevent cellular composites from the damage. In the current study, all antioxidant activity evaluation steps are mainly based on the exogenous compounds (synthetic antioxidants). Antioxidants are molecules that can give an electron to a free radical without becoming unstable[129].

3.1.4. The use of cyclic voltammetry in antioxidant activity study

The antioxidant function of the system plays an essential role in defence of biological systems from the danger of free radicals. Cyclic voltammetry method uses to generate $O_2^{-\cdot}$ by reducing the oxygen in an aprotic solvent such as DMF, DMSO.... etc at ambient temperature (298 ± 1°C). The scavenging of radical is monitored by the remarkable decreasing in anodic current in the face with the studied sample's increasing concentration. In this exploring study, the strength of the interaction is quantified through calculation the binding constant (K_b), IC_{50} and diffusion coefficient values. With regard to the action of superoxide-ion radical resulting from the cyclic voltammetric process, one-electron is generated due to the reduction of O_2, as shown in Figure 21. Also, a radical of superoxide ion is characterized by its reversible behaviour (Reduction then Oxidation)[130-131].

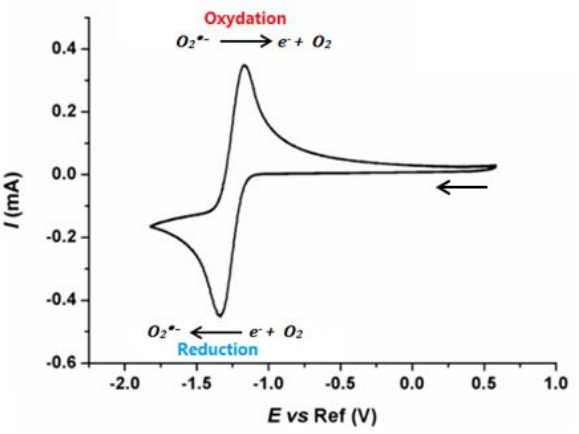

Figure 21: Typical cyclic voltammogram of dioxygen/superoxide redox couple

3.1.5. Ferrocene based antioxidants

Ferrocene widely used in antioxidant drugs preparation. By adding this compound to a specific organic molecule, we can provide new selective properties and enhance the antioxidant properties of the resulting compounds. In general, the goal of the evaluation studies was to

tackle the problem of drug efficiency through the provision of a method to improve the pharmacokinetics preparation of antioxidants. This aim has been accomplished by combining organometallic compounds containing antioxidant drug models with water-soluble macromolecular carriers is designed according to special biomedical specifications[132]. However, although synthetic medicines have developed mainly by systemically applying the new techniques, there is a big obstacle to improve their therapeutic role. The preparation of numerous derivatives of ferrocene and their antioxidant evaluations are reported in many noteworthy articles like the research of T. Lanez and collaborators for the preparation of antioxidant compounds having a ferrocene as a basic nucleus [133]. The obtained results of free radical assays are indicated that to the potency of their antioxidant behaviour and figure 22 represents two structures from the synthesized series.

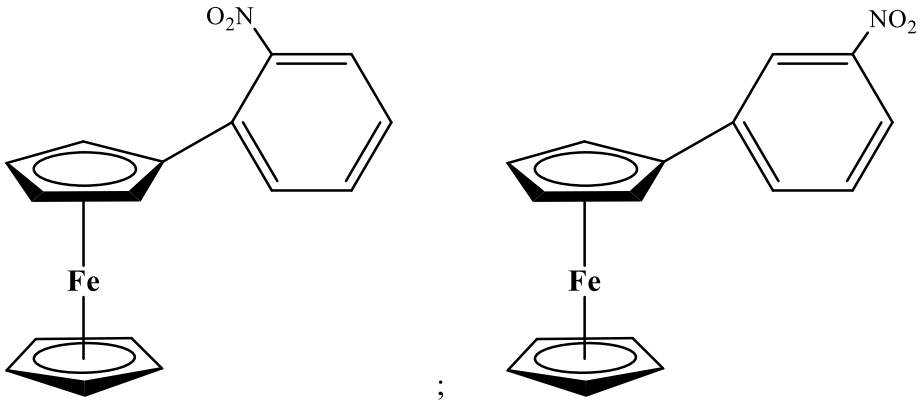

Figure 22: Chemical structures of 2-and 3-nitrophenyl ferrocene

3.2. DPPH scavenging activities study

3.2.1. Technical features

The most straight forward strategy to estimate the antioxidant capacity of bio-compounds or any other biological source is DPPH free radical scavenging assay. It is an unpretentious and easy way, the studied compound mixed with the DPPH solution, and after a fixed time, we can identify the sample that has maximum absorbance. With speedy development in a domain of technical instruments, many changes were conducted on its working way to meet the chemical and physical structure needs of studied samples and for obtaining results more accuracy[134-135].

3.2.2. Physicochemical testing conditions

These tests were conducted under various chemical conditions. The excess of DPPH reagent should be utilized for exhausting the ability of the potentially antioxidant compound to donate more H^+. Nevertheless, the initial concentration of DPPH in a cuvette should be chosen to obtain an absorption value that must be less than 4; in line with Beer's rule and standard

spectrophotometry principals. When used, the UV quartz cuvette the range of DPPH solution concentration ranging from 25 to 70 µM. Certain laboratory staff employs DPPH concentration above 200 µM (in our DPPH assays we used the first range). Predominantly substances that contain antioxidant characteristics their reactions with DPPH to be biphasic in the first few minutes with a quick decay in the absorbance, pursued by a slow stage named degradation kinetic until access to the balance. Kinetic rates of reaction differ from compound to others. DPPH test is mostly streamlined by calculating the DPPH concentration before and after the incubation period; the original test suggested the reaction time: 30 minutes. Nevertheless, the short-period not to be less than 4-16 minutes was utilized, whereas some papers have also utilized 24-hour as the incubation period. This gives rise to obtaining different outcomes for identical samples.[135-136]

3.2.3. Characteristics and applications

DPPH• is a stable free radical, and it can become a stable diamagnetic molecule by accepting an electron-hydrogen radical and it also is a snare "scavenger" for the most kinds of radicals. Consequently, the rate of reduction of a kinetic reaction of DPPH use as an indicator for monitoring the reaction-path through adds it to the studied solution. Approximately, at the wavelength 520 nm, DPPH has a high absorption band. Also, the solution of DPPH can take a dark violet colour, and thus last colour change to pale yellow when the reaction is completed. This characteristic permits this characteristic permit surveillance the reaction visually. On the other hand, Radical of DPPH• in polar solvents is poorly soluble while soluble in different polar organic solvents. In water, at ambient temperature, its solubility is virtually nil[137-138].

Several chemicals react with DPPH• by H-atom donation or electron transfer or the combination of both mechanisms. Based on chemical reactions to be studied; types of antioxidant activity investigations can be classified into two subgroups: firstly, the tests that dependent on hydrogen atom Transfer (HAT) reaction; secondly, tests that depend on Single electron transfer (SET) reaction. In SET mechanism, only a single redox reaction with unwanted-oxidant is carried out additionally it also is represented the endpoint indicator for the reaction. In HAT mechanism, the free radical removes one hydrogen atom from antioxidant, and the antioxidant itself becomes a radical[138-141]. Figure 23 summarized HAT mechanisms in three reactions:

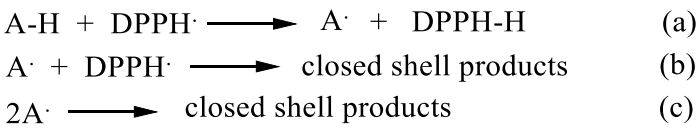

Figure 23: Three reactions of hydrogen atom transfer mechanism

A closed shell product can be formed by recombination radicals (b) or by means of producing a new radical pair (c).

3.2.4. Ferrocene based antioxidants under in vitro conditions

The biochemical uses of organometallic compounds have experienced remarkable development over past years due to their crucial role in the therapeutic intervention (probably the most famous in the coordination chemistry is ferrocene). For that reason, transition metals are particularly appropriate compared to other kinds of molecules, which can adapt it with many compounds. Among common ferrocene-containing substances are antioxidants. Besides, enhancement of the activity of antioxidants by ferrocene has been the subject of numerous studies. The incorporation of ferrocene in a significant number of antioxidants series is the main reason behind the increased inhibitory effects against many oxidants, such as peroxides and peroxynitrites. Consequently, the development of ferrocene-related antioxidants will open worthwhile search fields for preparing novel drugs, having iconic characterizations. On the other hand, a significant number of papers focused on estimating the antioxidant capacity of some ferrocene derivatives using a spectrophotometric method by DPPH assay. E. R. Milaeva et al carried out like this biologic investigation on two compounds, and their structures are shown below.

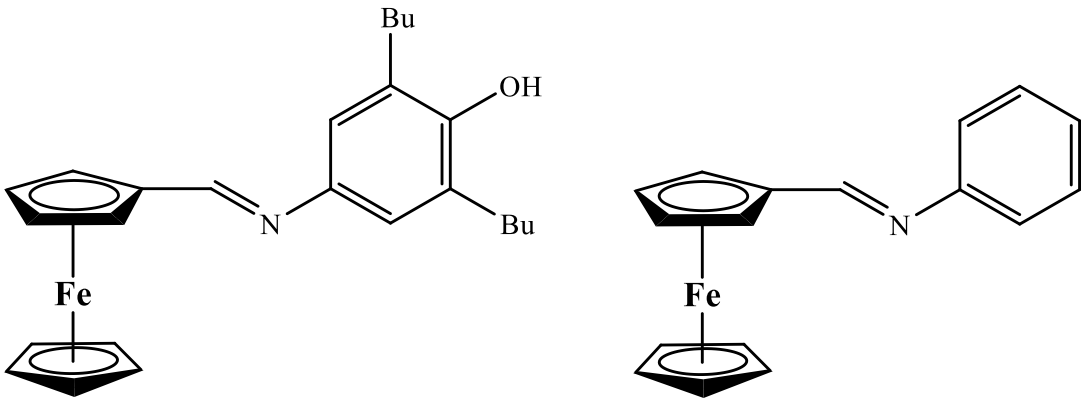

Figure 24: Two structures of compounds bearing di-tert-butyl-4-hydroxyphenyl or phenyl substituents linked with ferrocene by similar spacer[140]

1.Werner, H., At least 60 years of ferrocene: the discovery and rediscovery of the sandwich complexes. *Angewandte Chemie International Edition* **2012,***51* (25), 6052-6058.
2.Chirik, P. J., Group 4 transition metal sandwich complexes: Still fresh after almost 60 Years. *Organometallics* **2010,***29* (7), 1500-1517.
3.Astruc, D., Why is ferrocene so exceptional? *European Journal of Inorganic Chemistry* **2017,***2017* (1), 6-29.
4.Kauffman, G. B., The discovery of ferrocene, the first sandwich compound. *Journal of Chemical Education* **1983,***60* (3), 185.
5.Lydon, C. E. Towards the synthesis of ferrocene nucleic acids. University of Birmingham, 2009.
6.Seibold, E.; Sutton, L., Structure of ferrocene. *The Journal of Chemical Physics* **1955,***23* (10), 1967-1967.
7.Sánchez-Delgado, R. A.; Anzellotti, A., Metal complexes as chemotherapeutic agents against tropical diseases: trypanosomiasis, malaria and leishmaniasis. *Mini reviews in medicinal chemistry* **2004,***4* (1), 23-30.
8.Beagley, P.; Blackie, M. A.; Chibale, K.; Clarkson, C.; Meijboom, R.; Moss, J. R.; Smith, P. J.; Su, H., Synthesis and antiplasmodial activity in vitro of new ferrocene–chloroquine analogues. *Dalton Transactions* **2003,** (15), 3046-3051.
9.Newirth, T. L.; Srouji, N., Acetylation of ferrocene: a study of the friedel-crafts acylation mechanism as measured by hplc using an internal standard. *Journal of chemical education* **1995,***72* (5), 454.
10. Rosenblum, M.; Santer, J.; Howells, W. G., The Chemistry and Structure of Ferrocene. VIII. Interannular Resonance and the Mechanism of Electrophilic Substitution. *Journal of the American Chemical Society* **1963,***85* (10), 1450-1458.
11. Seiler, P.; Dunitz, J. D., A new interpretation of the disordered crystal structure of ferrocene. *Acta Crystallographica Section B: Structural Crystallography and Crystal Chemistry* **1979,***35* (5), 1068-1074.
12. Mohammadi, N.; Ganesan, A.; Chantler, C. T.; Wang, F., Differentiation of ferrocene D5d and D5h conformers using IR spectroscopy. *Journal of Organometallic Chemistry* **2012,***713*, 51-59.
13. Islam, S.; Wang, F., The d-electrons of Fe in ferrocene: the excess orbital energy spectrum (EOES). *RSC Advances* **2015,***5* (16), 11933-11941.
14. Turner, J. F.; Soper, A. K., On the determination of the structure of ferrocene in solution. *Polyhedron* **2004,***23* (17), 2975-2983.
15. Bermúdez-García, J.; Yáñez-Vilar, S.; Castro-García, S.; Señarís-Rodríguez, M.; Sánchez-Andújar, M., New properties in old systems: cooperative electric order in ferrocene and ammonia-borane. *RSC advances* **2015,***5* (102), 83818-83824.
16. Lu, Y.; Jiang, Y.; Wu, H.; Chen, W., Ferrocene-functionalized graphene oxide nanosheets: efficient electronic communication between ferrocene centers across graphene nanosheets. *Electrochimica Acta* **2015,***156*, 267-273.
17. Bean, D. E., Fowler, P. W., & Morris, M. J. (2011). Aromaticity and ring currents in ferrocene and two isomeric sandwich complexes. Journal of Organometallic Chemistry, 696(10), 2093-2100.
18. Wendlandt, W., Handbook of organometallic compounds (Hagihara, Nobue; Kumada, Makoto; Okawara, Rokura). ACS Publications: 1971.
19. Metlesics, W.; Zeiss, H., The Action of Alkali Metals on Phenylgermanium Halides1. *Journal of the American Chemical Society* **1960,***82* (13), 3321-3323.
20. Mohammadi, N.; Wang, F.; Best, S.; Appadoo, D.; Chantler, C. T., Dominance of eclipsed ferrocene conformer in solutions revealed by the IR fingerprint spectral splitting. *arXiv preprint arXiv:1306.0633* **2013**.
21. Bhattacharjee, A.; Rooj, A.; Roy, D.; Roy, M., Thermal decomposition study of ferrocene [(C5H5) 2Fe]. *Journal of Experimental Physics* **2014,***2014*.

22. Barr, T.; Watts, W., Bridged ferrocenes—IV: Intramolecular cyclization of ferrocene derivatives containing αβ-unsaturated carbonyl functions. *Tetrahedron* **1969,***25* (4), 861-869.
23. Connelly, N. G.; Geiger, W. E., Chemical redox agents for organometallic chemistry. *Chemical Reviews* **1996,***96* (2), 877-910.
24. Xi, Y.; Yang, D.; Hou, Z.; Zhang, C., Effect of reaction conditions on the morphology of elemental metals by composite-hydroxide-mediated approach. *Physica E: Low-dimensional Systems and Nanostructures* **2012,***44* (10), 2078-2081.
25. Fouda, M. F.; Abd-Elzaher, M. M.; Abdelsamaia, R. A.; Labib, A. A., On the medicinal chemistry of ferrocene. *Applied Organometallic Chemistry* **2007,***21* (8), 613-625.
26. Okabe, T.; Nakazaki, K.; Igaue, T.; Nakamura, N.; Donnio, B.; Guillon, D.; Gallani, J.-L., Synthesis and physical properties of ferrocene derivatives. XXI. Crystal structure of a liquid crystalline ferrocene derivative, 1,1'-bis[3-[4-(4-methoxyphenoxycarbonyl)phenoxy]propyloxycarbonyl]ferrocene. *Journal of Applied Crystallography* **2009,***42* (1), 63-68.
27. Werner, H., At Least 60 Years of Ferrocene: The Discovery and Rediscovery of the Sandwich Complexes. *Angewandte Chemie International Edition* **2012,***51* (25), 6052-6058.
28. Yousefinejad, S.; Honarasa, F.; Solhjoo, A., On the Solubility of Ferrocene in Nonaqueous Solvents. *Journal of Chemical & Engineering Data* **2016,***61* (1), 614-621.
29. Patnaik, P.; Knovel, *Handbook of Inorganic Chemicals*. McGraw-Hill: 2003.
30. Rooj, A.; Roy, M.; Bhattacharjee, A., Thermal decomposition reaction of ferrocene in the presence of oxalic acid. *International Journal of Chemical Kinetics* **2017,***49* (5), 319-332.
31. Organometallic Compounds in Biomedical Applications. In *Macromolecules Containing Metal and Metal-Like Elements*, 2004; pp 1-18.
32. Rojas, A.; Vieyra-Eusebio, M. T., Enthalpies of sublimation of ferrocene and nickelocene measured by calorimetry and the method of Langmuir. *The Journal of Chemical Thermodynamics* **2011,***43* (11), 1738-1747.
33. Lousada, C. M.; Pinto, S. S.; Canongia Lopes, J. N.; Minas da Piedade, M. F.; Diogo, H. P.; Minas da Piedade, M. E., Experimental and Molecular Dynamics Simulation Study of the Sublimation and Vaporization Energetics of Iron Metalocenes. Crystal Structures of Fe(η5-C5H4CH3)2 and Fe[(η5-(C5H5)(η5-C5H4CHO)]. *The Journal of Physical Chemistry A* **2008,***112* (13), 2977-2987.
34. Slocum, D. W.; Jones, W. E.; Ernst, C. R., Fundamental studies of substituted ferrocene systems. VII. Electronic effects in the alkylferrocenes. *The Journal of Organic Chemistry* **1972,***37* (26), 4278-4281.
35. Kealy, T. J.; Pauson, P. L., A New Type of Organo-Iron Compound. *Nature* **1951,***168* (4285), 1039-1040.
36. Jones, K.; Lappert, M. F., Amino derivatives of metals and metalloids: III. Metal amines as reagents for synthesis of organometallics; especially the reactions of aminostannanes with protic species. *Journal of Organometallic Chemistry* **1965,***3* (4), 295-307.
37. Bitterwolf, T. E.; Hubler, T. L.; Rheingold, A. L., Synthesis and chemistry of 1-acetyl, 2-methylsubstituted cyclopentadienyl thallium and its chiral manganese and rhodium carbonyl derivatives. The molecular structure of [1-CH3CO, 2-CH3C5H3] Rh (CO)[P (C6H5) 3]. *Journal of organometallic chemistry* **1992,***431* (2), 199-214.
38. Blais, M. S.; Rausch, M. D., A new synthetic route to functionally substituted (η5-cyclopentadienyl) dicarbonyliridium compounds. *Journal of organometallic chemistry* **1995,***502* (1-2), 1-8.
39. Blais, M. S.; Rausch, M. D., A new synthetic route to functionally substituted (η5-cyclopentadienyl) dicarbonyliridium compounds. *Journal of Organometallic Chemistry* **1995,***502* (1), 1-8.

40. Birmingham, J. M., Synthesis of cyclopentadienyl metal compounds. In *Advances in Organometallic Chemistry*, Elsevier: 1965; Vol. 2, pp 365-413.
41. Leigh, T., 624. Ferrocene derivatives containing tertiary alkyl groups. Synthesis by the Friedel–Crafts and other methods. *Journal of the Chemical Society (Resumed)* **1964,** (0), 3294-3302.
42. Miller, S. A.; Tebboth, J. A.; Tremaine, J. F., 114. Dicyclopentadienyliron. *Journal of the Chemical Society (Resumed)* **1952,** (0), 632-635.
43. Butler, R. N., Diazotization of heterocyclic primary amines. *Chemical Reviews* **1975,***75* (2), 241-257.
44. Shah, J.; Jan, M. R.; Khan, M. A., Determination of furosemide by simple diazotization method in pharmaceutical preparations. *Journal of the Chinese Chemical Society* **2005,***52* (2), 347-352.
45. Bensghaïer, A.; Mousli, F.; Lamouri, A.; Postnikov, P. S.; Chehimi, M. M., The Molecular and Macromolecular Level of Carbon Nanotube Modification Via Diazonium Chemistry: Emphasis on the 2010s Years. *Chemistry Africa* **2020**, 1-35.
46. Schantl, J. G., Cyclic azomethine imines from diazenes (azo compounds). In *Advances in Heterocyclic Chemistry*, Elsevier: 2010; Vol. 99, pp 185-207.
47. Larik, F. A.; Saeed, A.; Fattah, T. A.; Muqadar, U.; Channar, P. A., Recent advances in the synthesis, biological activities and various applications of ferrocene derivatives. *Applied Organometallic Chemistry* **2017,***31* (8), e3664.
48. Ornelas, C., Application of ferrocene and its derivatives in cancer research. *New Journal of Chemistry* **2011,***35* (10), 1973-1985.
49. Sharma, N.; Ajay, J. K.; Venkatasubbaiah, K.; Lourderaj, U., Mechanisms and dynamics of protonation and lithiation of ferrocene. *Physical Chemistry Chemical Physics* **2015,***17* (34), 22204-22209.
50. Sharma, Nishant, et al. "Mechanisms and dynamics of protonation and lithiation of ferrocene." Physical Chemistry Chemical Physics 17.34 (2015): 22204-22209.
51. Geckeler, K.; Zhou, R., Polymer-induced interaction and quasi-micellar molecular organization in dynamic equilibrium. *Naturwissenschaften* **1992,***79* (7), 325-327.
52. Guo, Z.; Sadler, P. J., Medicinal inorganic chemistry. In *Advances in inorganic chemistry*, Elsevier: 1999; Vol. 49, pp 183-306.
53. N'Da David, D.; Jaco, C. B.; Peter, J. S.; Lategan, C., Synthesis, cytotoxicity and antimalarial activity of ferrocenyl amides of 4-aminoquinolines. *Arzneimittelforschung* **2010,***60* (10), 627-635.
54. Yeary, R. A., Chronic toxicity of dicyclopentadienyliron (ferrocene) in dogs. *Toxicology and applied pharmacology* **1969,***15* (3), 666-676.
55. Li, S.; Wang, Z.; Wei, Y.; Wu, C.; Gao, S.; Jiang, H.; Zhao, X.; Yan, H.; Wang, X., Antimicrobial activity of a ferrocene-substituted carborane derivative targeting multidrug-resistant infection. *Biomaterials* **2013,***34* (4), 902-911.
56. Realista, S.; Quintal, S.; Martinho, P. N.; Melato, A. I.; Gil, A.; Esteves, T.; Carvalho, M. d. D.; Ferreira, L. P.; Vaz, P. D.; Calhorda, M. J., Electrochemical studies and potential anticancer activity in ferrocene derivatives. *Journal of Coordination Chemistry* **2017,***70* (2), 314-327.
57. Zaltariov, M.-F.; Rudic, V.; Rudi, L.; Chiriac, T.; Shova, S.; Vlada, A.; Cazacu, M., Synthesis, characterization and evaluation of antioxidant activity of a new ferrocenyl-imine containing siloxane sequence. *Rev Roum Chim* **2015,***60* (7), 797-802.
58. Janka, V.; Žatko, D.; Ladislav, V.; Pál, P.; Janka, P.; Gabriela, M., Some ferrocenyl chalcones as useful candidates for cancer treatment. *In Vitro Cellular & Developmental Biology-Animal* **2015,***51* (9), 964-974.

59. Gielen, M.; Tiekink, E. R., *Metallotherapeutic drugs and metal-based diagnostic agents: the use of metals in medicine*. John Wiley & Sons: 2005.
60. Gasser, G.; Metzler-Nolte, N., Metal compounds as enzyme inhibitors. *Bioinorganic Medicinal Chemistry* **2011**, 351-382.
61. Dyson, P. J.; Sava, G., Metal-based antitumour drugs in the post genomic era. *Dalton Transactions* **2006,** (16), 1929-1933.
62. Blanck, S.; Maksimoska, J.; Baumeister, J.; Harms, K.; Marmorstein, R.; Meggers, E., The art of filling protein pockets efficiently with octahedral metal complexes. *Angewandte Chemie International Edition* **2012,***51* (21), 5244-5246.
63. Herrmann, C.; Salas, P. F.; Patrick, B. O.; de Kock, C.; Smith, P. J.; Adam, M. J.; Orvig, C., 1, 2-Disubstituted ferrocenyl carbohydrate chloroquine conjugates as potential antimalarial agents. *Dalton Transactions* **2012,***41* (21), 6431-6442.
64. Wani, W. A.; Jameel, E.; Baig, U.; Mumtazuddin, S.; Hun, L. T., Ferroquine and its derivatives: new generation of antimalarial agents. *European journal of medicinal chemistry* **2015,***101*, 534-551.
65. Patra, M.; Gasser, G., The medicinal chemistry of ferrocene and its derivatives. *Nature Reviews Chemistry* **2017,***1* (9), 1-12.
66. Mukumoto, K.; Ohtsuka, K.; Nojima, T.; TAKENAKA, S., Preparation of carbodiimide-terminated dithiolane self-assembly monolayers as a new DNA-immobilization method. *Analytical sciences* **2006,***22* (3), 349-355.
67. Monserrat, J.-P.; Al-Safi, R. I.; Tiwari, K. N.; Quentin, L.; Chabot, G. G.; Vessières, A.; Jaouen, G.; Neamati, N.; Hillard, E. A., Ferrocenyl chalcone difluoridoborates inhibit HIV-1 integrase and display low activity towards cancer and endothelial cells. *Bioorganic & medicinal chemistry letters* **2011,***21* (20), 6195-6197.
68. Organization, W. H., Critically important antibacterial agents for human medicine for risk management strategies of non-human use: report of a WHO working group consultation, 15-18 February 2005, Canberra, Australia. **2005**.
69. Long, B.; He, C.; Yang, Y.; Xiang, J., Synthesis, characterization and antibacterial activities of some new ferrocene-containing penems. *European journal of medicinal chemistry* **2010,***45* (3), 1181-1188.
70. Kissinger, P. T.; Heineman, W. R., Cyclic voltammetry. *Journal of Chemical Education* **1983,***60* (9), 702.
71. Gosser, D. K., *Cyclic voltammetry: simulation and analysis of reaction mechanisms*. VCH New York: 1993; Vol. 43.
72. Shah, A.; Zaheer, M.; Qureshi, R.; Akhter, Z.; Nazar, M. F., Voltammetric and spectroscopic investigations of 4-nitrophenylferrocene interacting with DNA. *Spectrochimica Acta Part A: Molecular and Biomolecular Spectroscopy* **2010,***75* (3), 1082-1087.
73. Mabbott, G. A., An introduction to cyclic voltammetry. *Journal of Chemical education* **1983,***60* (9), 697.
74. Verbrugge, M. W.; Liu, P., Electrochemical characterization of high-power lithium ion batteries using triangular voltage and current excitation sources. *Journal of Power Sources* **2007,***174* (1), 2-8.
75. Ward, K. R.; Lawrence, N. S.; Hartshorne, R. S.; Compton, R. G., The theory of cyclic voltammetry of electrochemically heterogeneous surfaces: comparison of different models for surface geometry and applications to highly ordered pyrolytic graphite. *Physical Chemistry Chemical Physics* **2012,***14* (20), 7264-7275.
76. LeSuer, R. J.; Buttolph, C.; Geiger, W. E., Comparison of the Conductivity Properties of the Tetrabutylammonium Salt of Tetrakis(pentafluorophenyl)borate Anion with Those of Traditional Supporting Electrolyte Anions in Nonaqueous Solvents. *Analytical Chemistry* **2004,***76* (21), 6395-6401.

78. Inzelt, G.; Szabo, L.; Chambers, J. Q.; Day, R. W., Cyclic voltammetric and potentiometric behavior of tetracyanoquinodimethane polymer film electrodes: Effect of the nature and the concentration of the supporting electrolyte. *Journal of Electroanalytical Chemistry and Interfacial Electrochemistry* **1988,***242* (1), 265-275.
79. Belding, S. R.; Compton, R. G., Cyclic voltammetry in the absence of excess supporting electrolyte: The effect of analyte charge. *Journal of Electroanalytical Chemistry* **2012,***683*, 1-13.
80. Dickinson, E. J. F.; Limon-Petersen, J. G.; Rees, N. V.; Compton, R. G., How Much Supporting Electrolyte Is Required to Make a Cyclic Voltammetry Experiment Quantitatively "Diffusional"? A Theoretical and Experimental Investigation. *The Journal of Physical Chemistry C* **2009,***113* (25), 11157-11171.
81. Nicholson, R. S., Theory and Application of Cyclic Voltammetry for Measurement of Electrode Reaction Kinetics. *Analytical Chemistry* **1965,***37* (11), 1351-1355.
82. Masui, M.; Sayo, H.; Tsuda, Y., Anodic oxidation of amines. Part I. Cyclic voltammetry of aliphatic amines at a stationary glassy-carbon electrode. *Journal of the Chemical Society B: Physical Organic* **1968,** (0), 973-976.
83. Paim, L. L.; Stradiotto, N. R., Electrochemical behavior of a glassy-carbon electrode chemically modified with cadmium pentacyanonitrosylferrate in the presence of tetrahydrothiophene. *Journal of Electroanalytical Chemistry* **2011,***663* (1), 43-47.
84. Bowers, M. L.; Yenser, B. A., Electrochemical behavior of glassy carbon electrodes modified by electrochemical oxidation. *Analytica Chimica Acta* **1991,***243*, 43-53.
85. Gueshi, T.; Tokuda, K.; Matsuda, H., Voltammetry at partially covered electrodes: Part II. Linear potential sweep and cyclic voltammetry. *Journal of Electroanalytical Chemistry and Interfacial Electrochemistry* **1979,***101* (1), 29-38.
86. Wang, Y.; Rogers, E. I.; Compton, R. G., The measurement of the diffusion coefficients of ferrocene and ferrocenium and their temperature dependence in acetonitrile using double potential step microdisk electrode chronoamperometry. *Journal of Electroanalytical Chemistry* **2010,***648* (1), 15-19.
87. Dryden, M. D.; Wheeler, A. R., DStat: A versatile, open-source potentiostat for electroanalysis and integration. *PloS one* **2015,***10* (10), e0140349.
88. Elgrishi, N.; Rountree, K. J.; McCarthy, B. D.; Rountree, E. S.; Eisenhart, T. T.; Dempsey, J. L., A practical beginner's guide to cyclic voltammetry. *Journal of Chemical Education* **2018,***95* (2), 197-206.
89. Nazri, A.; Sudibyo, N.; Murat, M., Application of electro analytical chemistry for the corrosion process on the stainless steel electrodes in the acidic thiourea. *MS&E* **2019,***478* (1), 012010.
90. EC08, Autolab Application Note. "Basic overview of the working principle of a potentiostat/galvanostat (PGSTAT)–Electrochemical cell setup." Metrohm Autolab. BV (2011): 1-3.
91. Muñoz Caro, G. M., Photochemistry in Ice Layers. In *Encyclopedia of Interfacial Chemistry*, Wandelt, K., Ed. Elsevier: Oxford, 2018; pp 545-552.
92. Perveen, F.; Qureshi, R.; Ansari, F. L.; Kalsoom, S.; Ahmed, S., Investigations of drug–DNA interactions using molecular docking, cyclic voltammetry and UV–Vis spectroscopy. *Journal of Molecular Structure* **2011,***1004* (1-3), 67-73.
93. Shah, A.; Qureshi, R.; Janjua, N. K.; Haque, S.; Ahmad, S., Electrochemical and spectroscopic investigations of protonated ferrocene-DNA intercalation. *Analytical Sciences* **2008,***24* (11), 1437-1441.
94. Shah, A.; Qureshi, R.; Khan, A. M.; Khera, R. A.; Ansari, F. L., Electrochemical behavior of 1-ferrocenyl-3-phenyl-2-propen-1-one on glassy carbon electrode and evaluation of its interaction parameters with DNA. *Journal of the Brazilian Chemical Society* **2010,***21*, 447-451.

95. Sirajuddin, M.; Ali, S.; Badshah, A., Drug–DNA interactions and their study by UV–Visible, fluorescence spectroscopies and cyclic voltametry. *Journal of Photochemistry and Photobiology B: Biology* **2013,***124*, 1-19.
96. Ackerman, M. M.; Ricciardi, C.; Weiss, D.; Chant, A.; Kraemer-Chant, C. M., Analyzing Exonuclease-Induced Hyperchromicity by UV Spectroscopy: An Undergraduate Biochemistry Laboratory Experiment. *Journal of Chemical Education* **2016,***93* (12), 2089-2095.
97. Yazdi, SM Hossein Tabatabaei, et al. "DNA-based storage: Trends and methods." IEEE Transactions on Molecular, Biological and Multi-Scale Communications 1.3 (2015): 230-248.
98. Yuriev, E.; Holien, J.; Ramsland, P. A., Improvements, trends, and new ideas in molecular docking: 2012–2013 in review. *Journal of Molecular Recognition* **2015,***28* (10), 581-604.
99. Gupta, R. K.; Sharma, G.; Pandey, R.; Kumar, A.; Koch, B.; Li, P.-Z.; Xu, Q.; Pandey, D. S., DNA/protein binding, molecular docking, and in vitro anticancer activity of some thioether-dipyrrinato complexes. *Inorganic chemistry* **2013,***52* (24), 13984-13996.
100. Shi, J.-H.; Chen, J.; Wang, J.; Zhu, Y.-Y., Binding interaction between sorafenib and calf thymus DNA: spectroscopic methodology, viscosity measurement and molecular docking. *Spectrochimica Acta Part A: Molecular and Biomolecular Spectroscopy* **2015,***136*, 443-450.
101. Holtje, H.-D.; Folkers, G.; Mannhold, R.; Kubinyi, H.; Timmerman, H., *Molecular modeling: basic principles and applications*. John Wiley & Sons, Inc.: 1997.
102. Alonso, H.; Bliznyuk, A. A.; Gready, J. E., Combining docking and molecular dynamic simulations in drug design. *Medicinal research reviews* **2006,***26* (5), 531-568.
103. Naqvi, A. A.; Mohammad, T.; Hasan, G. M.; Hassan, M., Advancements in docking and molecular dynamics simulations towards ligand-receptor interactions and structure-function relationships. *Current topics in medicinal chemistry* **2018,***18* (20), 1755-1768.
104. Grinter, S. Z.; Zou, X., Challenges, applications, and recent advances of protein-ligand docking in structure-based drug design. *Molecules* **2014,***19* (7), 10150-10176.
105. Totrov, M.; Abagyan, R., Flexible ligand docking to multiple receptor conformations: a practical alternative. *Curr Opin Struct Biol* **2008,***18* (2), 178-184.
106. Lee, H. S.; Jo, S.; Lim, H.-S.; Im, W., Application of binding free energy calculations to prediction of binding modes and affinities of MDM2 and MDMX inhibitors. *J Chem Inf Model* **2012,***52* (7), 1821-1832.
107. Agarwal, S.; Mehrotra, R. In *An overview of Molecular Docking*, 2016.
108. Sinden, R. R., CHAPTER 1 - Introduction to the Structure, Properties, and Reactions of DNA. In *DNA Structure and Function*, Sinden, R. R., Ed. Academic Press: San Diego, 1994; pp 1-57.
109. Watson, J. D.; Crick, F. H. C., Molecular Structure of Nucleic Acids: A Structure for Deoxyribose Nucleic Acid. *Nature* **1953,***171* (4356), 737-738.
110. Güllü, Ömer, and Abdülmecit Türüt. "Electronic properties of Cu/n-InP metal-semiconductor structures with cytosine biopolymer." (2015).
111. Boon, E. M.; Barton, J. K., DNA electrochemistry as a probe of base pair stacking in A-, B-, and Z-form DNA. *Bioconjugate chemistry* **2003,***14* (6), 1140-1147.
112. Ricciardi, A., The Molecules of Life: Physical and Chemical Properties. *Yale J Biol Med* **2015,***88* (1), 101-102.
113. Boon, Elizabeth M., and Jacqueline K. Barton. "DNA electrochemistry as a probe of base pair stacking in A-, B-, and Z-form DNA." Bioconjugate chemistry 14.6 (2003): 1140-1147.

114. Ricci, C. G.; Netz, P. A., Docking studies on DNA-ligand interactions: building and application of a protocol to identify the binding mode. *J Chem Inf Model* **2009,***49* (8), 1925-1935.
115. Nelson, S. M.; Ferguson, L. R.; Denny, W. A., Non-covalent ligand/DNA interactions: minor groove binding agents. *Mutation Research/Fundamental and Molecular Mechanisms of Mutagenesis* **2007,***623* (1-2), 24-40.
116. Almaqwashi, Ali A., et al. "Mechanisms of small molecule–DNA interactions probed by single-molecule force spectroscopy." Nucleic acids research 44.9 (2016): 3971-3988.
117. Bloomfield, V., The structure of bovine serum albumin at low pH. *Biochemistry* **1966,***5* (2), 684-689.
118. Majorek, K. A.; Porebski, P. J.; Dayal, A.; Zimmerman, M. D.; Jablonska, K.; Stewart, A. J.; Chruszcz, M.; Minor, W., Structural and immunologic characterization of bovine, horse, and rabbit serum albumins. *Mol Immunol* **2012,***52* (3-4), 174-182.
119. Naik, Keerti M., Deepa B. Kolli, and Sharanappa T. Nandibewoor. "Elucidation of binding mechanism of hydroxyurea on serum albumins by different spectroscopic studies." SpringerPlus 3.1 (2014): 1-13.
120. Rahmani, T.; Hajian, A.; Afkhami, A.; Bagheri, H., A novel and high performance enzyme-less sensing layer for electrochemical detection of methyl parathion based on BSA templated Au–Ag bimetallic nanoclusters. *New Journal of Chemistry* **2018,***42* (9), 7213-7222.
121. Acton, Q. A., Metalloproteases : advances in research and application : 2011 edition : scholarlyBrief. **2012**.
122. Jeremias, H. F.; Lousa, D.; Hollmann, A.; Coelho, A. C.; Baltazar, C. S.; Seixas, J. D.; Marques, A. R.; Santos, N. C.; Romão, C. C.; Soares, C. M., Study of the interactions of bovine serum albumin with a molybdenum(II) carbonyl complex by spectroscopic and molecular simulation methods. *PLOS ONE* **2018,***13* (9), e0204624.
123. Sułkowska, A.; Równicka, J.; Bojko, B.; Sułkowski, W., Interaction of anticancer drugs with human and bovine serum albumin. *Journal of molecular structure* **2003,***651*, 133-140.
124. Yue, Q.; Shen, T.; Wang, C.; Gao, C.; Liu, J., Study on the Interaction of Bovine Serum Albumin with Ceftriaxone and the Inhibition Effect of Zinc (II). *International Journal of Spectroscopy* **2012,***2012*, 284173.
125. Fekri, R.; Salehi, M.; Asadi, A.; Kubicki, M., DNA/BSA interaction, bio-activity, molecular docking simulation study and electrochemical properties of hydrazone Schiff base derived Cu (II)/Ni (II) metal complexes: influence of the nuclearity and metal ions. *Polyhedron* **2017,***128*, 175-187.
126. Crystal structure of human serum albumin. Available from protein data bank: https://www.rcsb.org/structure/4OR0
127. Gulcin, İ., Antioxidants and antioxidant methods: an updated overview. *Archives of Toxicology* **2020,***94* (3), 651-715.
128. Pizzino, G.; Irrera, N.; Cucinotta, M.; Pallio, G.; Mannino, F.; Arcoraci, V.; Squadrito, F.; Altavilla, D.; Bitto, A., Oxidative Stress: Harms and Benefits for Human Health. *Oxid Med Cell Longev* **2017,***2017*, 8416763-8416763.
129. Shankar, K.; Mehendale, H. M., Oxidative Stress. In *Encyclopedia of Toxicology (Third Edition)*, Wexler, P., Ed. Academic Press: Oxford, 2014; pp 735-737.
130. Sardesai, V. M., Role of antioxidants in health maintenance. *Nutrition in clinical practice : official publication of the American Society for Parenteral and Enteral Nutrition* **1995,***10* (1), 19-25.

131. Chevion, S.; Roberts, M. A.; Chevion, M., The use of cyclic voltammetry for the evaluation of antioxidant capacity. *Free Radical Biology and Medicine* **2000,***28* (6), 860-870.
132. Lanez, T.; Henni, M., Antioxidant activity and superoxide anion radical interaction with 2-(ferrocenylmethylamino) benzonitrile and 3-(ferrocenylmethylamino) benzonitrile. *Journal of the Iranian Chemical Society* **2016,***13* (9), 1741-1748.
133. Liu, Z.-Q., Potential applications of ferrocene as a structural feature in antioxidants. *Mini reviews in medicinal chemistry* **2011,***11* (4), 345-358.
134. Benabdesselam, S.; Izza, H.; Lanez, T.; Guechi, E. K., Synthesis, antioxidant and antibacterial activities of 3-nitrophenyl ferrocene. *IOP Conference Series: Materials Science and Engineering* **2018,***323*, 012007.
135. Kedare, S. B.; Singh, R. P., Genesis and development of DPPH method of antioxidant assay. *J Food Sci Technol* **2011,***48* (4), 412-422.
136. Arteaga, J. F.; Ruiz-Montoya, M.; Palma, A.; Alonso-Garrido, G.; Pintado, S.; Rodríguez-Mellado, J. M. Comparison of the simple cyclic voltammetry (CV) and DPPH assays for the determination of antioxidant capacity of active principles *Molecules* [Online], 2012, p. 5126-5138. PubMed.

137. Pyrzynska, K.; Pękal, A., Application of free radical diphenylpicrylhydrazyl (DPPH) to estimate the antioxidant capacity of food samples. *Analytical Methods* **2013,***5* (17), 4288-4295.
138. Foti, M. C., Use and Abuse of the DPPH• Radical. *Journal of agricultural and food chemistry* **2015,***63* (40), 8765-8776.
139. Xie, J.; Schaich, K. M., Re-evaluation of the 2,2-Diphenyl-1-picrylhydrazyl Free Radical (DPPH) Assay for Antioxidant Activity. *Journal of Agricultural and Food Chemistry* **2014,***62* (19), 4251-4260.
140. Song, J.; Jang, E. Y.; Kim, M.-J.; Kim, Y.-J.; Lee, J., Development of a spectroscopic method to determine the content of free radical scavenging compounds and oxidation products in thermally oxidised oils. *International Journal of Food Science & Technology* **2016,***51* (11), 2424-2432.

140.Meleshonkova, N. N., et al. "Synthesis and redox properties of novel ferrocenes with redox active 2, 6-di-tert-butylphenol fragments: the first example of 2, 6-di-tert-butylphenoxyl radicals in ferrocene system." Journal of Organometallic Chemistry 692.24 (2007): 5339-5344.

Second part

Chapter 4

Characterization

1. Preparation of ferrocene derivatives

1.1. Preparation of nitrophenylferrocene and ferrocenylbenzonitril

This work has been carried out on two types of derivatives, the first type contains three derivatives (2, 3, and 4-nitro-phenylferrocene) which previously prepared by our group[1] based on the coupling reaction between ferrocene and the diazonium salts of aminoaniline. The second type is 2, 3, and 4-ferrocenylbenzonitril was also previously synthesized by our research team[2-3]. The obtained derivatives were fully characterized by a combination of ^{1}H, ^{13}C NMR[1-2], UV-VIS spectroscopy and cyclic voltammetry methods.

The preparation of ferrocene derivatives was conducted in conformity with the method of Lanez[4]. The general synthesis approach of studied derivatives is presented in Figure 25. It is widespread and includes a diazotization reaction according to the primary amine position (NH_2R) followed by an arylation of ferrocene "coupling reaction" with the formed diazonium salt.

In all reactions, the synthesis of substituted-phenylferrocene takes place in two steps, the first step is the diazotization of substitutedaniline by sodium nitrite, and the second step is arylation of ferrocene. It is realized by the attack of substitutedbenzene diazonium chloride (it was formed in the earlier step) on cyclopentadienyl rings.

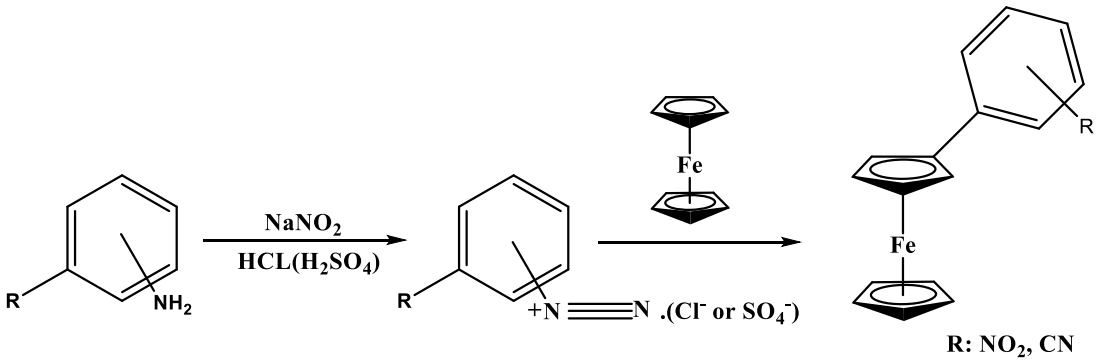

Figure 25: path for the arylation of ferrocene

Below are figures representing the chemical structures of the prepared derivatives {(a) 2-Nitrophenylferrocene, (b) 3-Nitrophenylferrocene, (c) 4-Nitrophenylferrocene}.

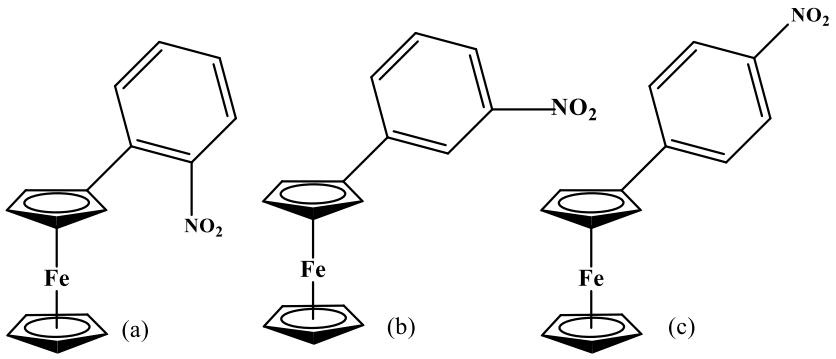

Figure 26: Chemical structures of 2 (a), 3(b) and 4-nitrophenyl ferrocene(c)

A series of 2-ferrocenylbenzonitrile (2FBN), 3-ferrocenylbenzonitrile (3FBN) and 4-ferrocenylbenzonitrile (4FBN) were also prepared by the same diazotization reaction pathway, as presented in Figure 25. It was also characterized using cyclic voltammetry, UV-vis spectroscopic methods.

1.2. Characterizations of ferrocenylbenzonitriles

1.2.1. Ortho-ferrocenylbenzonitrile

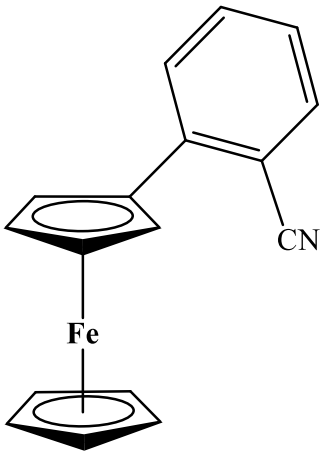

Figure 27: Chemical structure of 2-ferrocenylbenzonitril

1.2.1.1. Cyclic voltammetric characterization

The electrochemical properties of the title compound were studied by cycle voltammetry in dimethylsulfoxide with supporting electrolyte 0.1 M Bu_4NBF_4 at scan rate 100 $mV.s^{-1}$ on glass carbon disk electrode at (298 K).

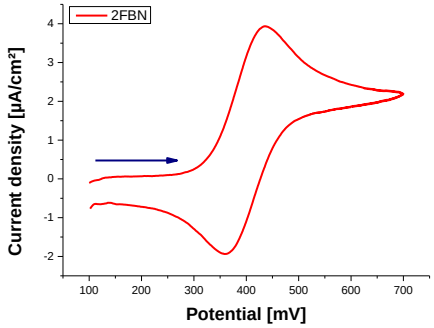

Figure 28: Cyclic voltammogram of 0.5 mM of 2-ferrocenylbenzonitril

The electrochemical data obtained from the cyclic voltammogram of 2-ferrocenylbenzonitril are summarized in the following table.

Table 1: Electrochemical parameters of 2FBN obtained from the cyclic voltammogram in Figure 28

Compound	I_{pa} (µA)	I_{pc} (µA)	$\lvert I_{pa}/I_{pc} \rvert$	$E_{1/2}$	E_{pa} (mV)	E_{pc} (mV)	E_{pa}-E_{pc}
2FBN	3.93	-3.78	1.04	397.66	435.33	359.99	75.34

Upon the obtained ratio of the anodic and cathodic current peak $\lvert I_{pa}/I_{pc} \rvert$ of 2FBN, which equal 1.04, hence 2FBN is a reversible system. E_{pa} and E_{pc} values of 2FBN are higher compared to ferrocene potentials. This change may be explained by the conjugated system in the phenyl cycle, as shown in Figure 28. The estimated value of peak-to-peak separation obtained from the application of E_{pa}-E_{pc} is equal to 75.34 mV, as compared with the suggested value (60 mV) of a fully reversible one-electron process a potential-range of the studied compound shifted to more positive potential values. This observation may be attributed to two main reasons (1) a combination of uncompensated solution resistance and (2) slightly slow electron-transfer kinetics.

1.2.1.2. UV-VIS Spectroscopic characterization

Ultraviolet / visible spectroscopy absorptions experiments were measured in DMSO at ambient temperature.

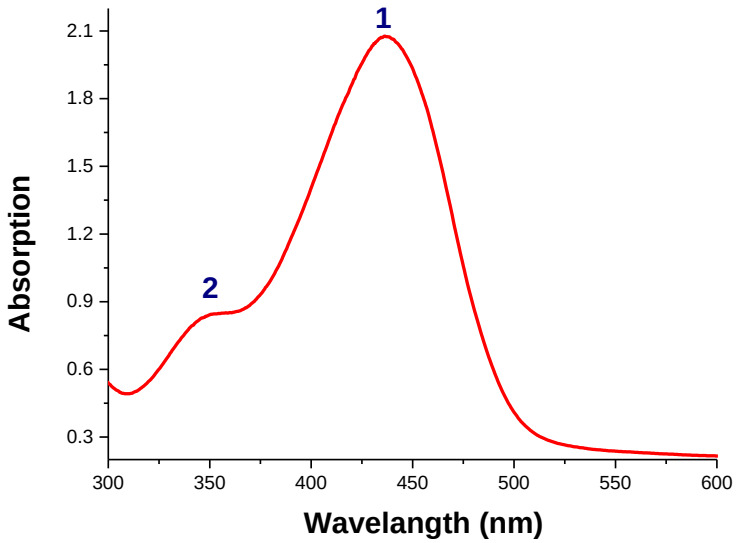

Figure 29: UV-visible absorption spectrum of 1 mM of 2-ferrocenylbenzonitril

The UV-Vis behaviour of 2FBN in Figure 29 shows two absorption bands, the first one located at λ = 437 nm (for the more intense band) is attributed to the π→π* electronic transitions of the conjugated system of the phenyl cycle and the second band centred at λ = 350 nm is corresponding to the n→π* electronic transitions of the CN function.

1.2.2. Metha-ferrocenylbenzonitrile

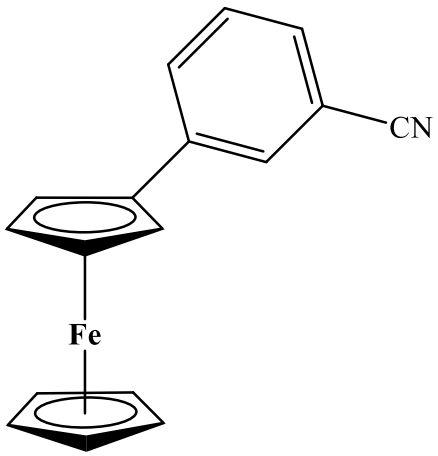

Figure 30: Chemical structure of Metha-ferrocenylbenzonitril

1.2.2.1 Characterizations of Metha-ferrocenylbenzonitril

1.2.2.2. Cyclic Voltammetric characterization

The electrochemical redox-behaviour of Metha-ferrocenylbenzonitril was recorded by the same method and experimental conditions of first one.

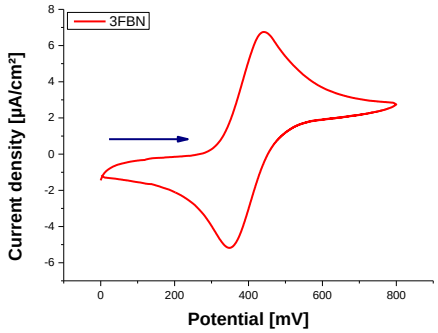

Figure 31: Cyclic voltammogram of 1mM Metha-ferrocenylbenzonitril

Table 2: Electrochemical parameters of 3FBN obtained from the cyclic voltammogram in figure 31

Compound	I_{pa} (µA)	I_{pc} (µA)	$\lvert I_{pa}/I_{pc} \rvert$	$E_{1/2}$	E_{pa} (mV)	E_{pc} (mV)	E_{pa}-E_{pc}
3FBN	6.74	-7.14	0.94	396.76	443.36	350.16	93.2

Upon the obtained data of anodic and cathodic current peaks of 3FBN derivative, this compound has a reversible system according to calculated parameter $\lvert I_{pa}/I_{pc} \rvert$ that equal 0.94. E_{pa} and E_{pc} values of 3FBN are higher compared to formal ferrocene potentials. This change may be explained by the conjugated system in the phenyl cycle, as showing in figure 30. The estimated value of peak-to-peak separation obtained from the application of E_{pa}-E_{pc} is equal to 39.2 mV, as compared with the suggested value (60 mV) of a fully reversible one-electron process, the potential range of the studied compound shifted to more positive potential values. This observation may be attributed to two main reasons (1) a combination of uncompensated solution resistance and (2) slightly slow electron-transfer kinetics.

1.2.2.3. UV-VIS Spectroscopic characterization

UV spectroscopic spectrum of metha-ferrocenylbenzonitril was recorded by Ultraviolet and visible spectrophotometer using a quartz cuvette (3cm) in DMSO at ambient temperature.

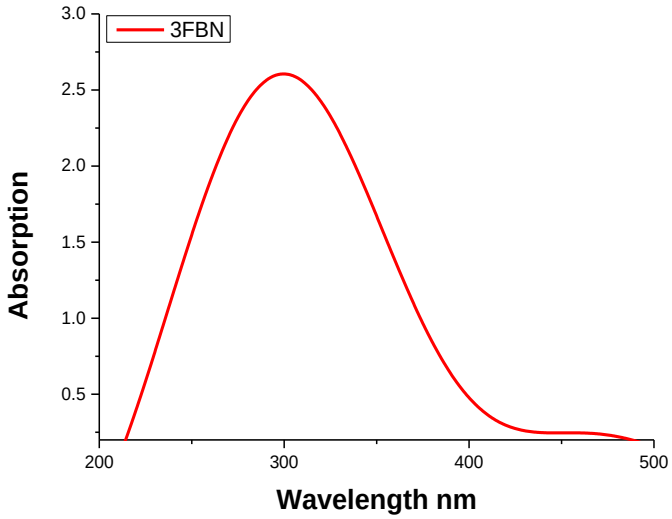

Figure 32: UV-visible absorption spectrum of 1 mM Metha-ferrocenylbenzonitril

Figure 32 represents the spectrum of 3FBN, and it displays one absorption band at λ = 300 nm and corresponds with n→π* electronic transitions CN function.

1.2.3. Para-ferrocenylbenzonitrile

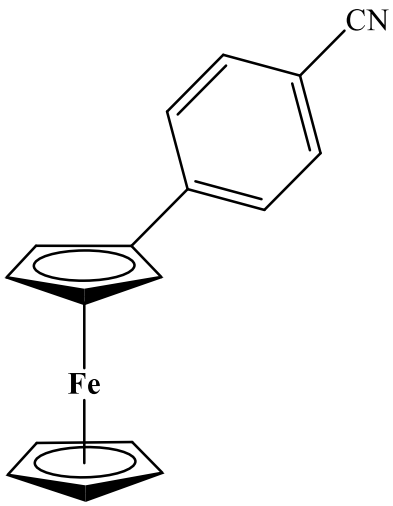

Figure 33: Chemical structure of para-ferrocenylbenzonitril

1.2.3.1. Characterizations of para- ferrocenylbenzonitril

1.2.3.2. Cyclic Voltammetric characterization

Also, it has been used a fully similar manipulation of earlier compounds to record the electrochemical response of 4-ferrocenylbenzonitril.

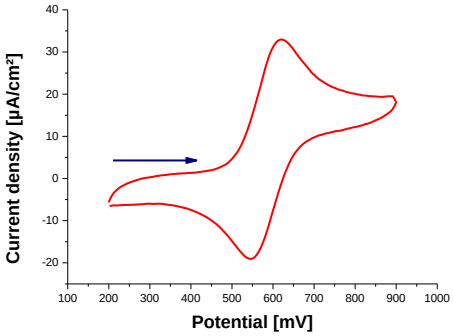

Figure 34: Cyclic voltammogram of 1mM 4-ferrocenylbenzonitril

Table 3: Electrochemical parametres of 4FBN obtained from the cyclic voltammogram in figure 34

Compound	I_{pa} (µA)	I_{pc} (µA)	$\lvert I_{pa}/I_{pc} \rvert$	$E_{1/2}$	E_{pa} (mV)	E_{pc} (mV)	E_{pa}-E_{pc}
4FBN	32.99	-31.6	1.04	582.635	619.69	545.58	74.11

Upon the obtained data of anodic and cathodic current peak of 4FBN derivative, this compound has a reversible system according to calculated parameter $\lvert I_{pa}/I_{pc} \rvert$ that equal 1.04. E_{pa} and E_{pc} values of 4FBN are higher compared to formal ferrocene potentials. This change may be explained by the conjugated system in the phenyl cycle, as showing in **Figure 34**. The estimated value of peak-to-peak separation obtained from the application of E_{pa}-E_{pc} is equal to 75.11 mV, as compared with the suggested value (60 mV) of a fully reversible one-electron process, the potential range of the studied compound shifted to more positive potential values. This observation may be attributed to two main reasons (1) a combination of uncompensated solution resistance and (2) slightly slow electron-transfer kinetics.

1.2.3.3. UV-VIS Spectroscopic characterization

The spectre Uv-Vis was obtained under the same condition as above.

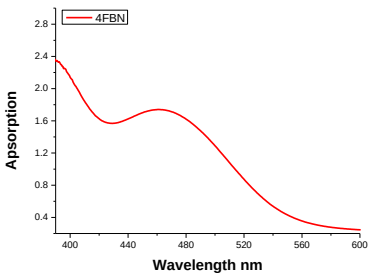

Figure 35: UV-visible absorption spectrum of 1 mM 4-ferrocenylbenzonitril

The spectrum of 3FBN is displayed in Figure 35, and it shows one absorption band at λ = 460 nm, which corresponds with $\pi \rightarrow \pi^*$ electronic transitions of phenyl cycle.

All the resulting mixtures containing 2,3 and 4- binzonitrilferrocene are purified by column chromatography in the gradient of petroleum ether/ether : (8/2).

Chapter 5

Anticancer activity evaluation

1. DNA interaction study

The immune system has strong defenses against infections and represents a critical stage in the monitoring of biological cells' behaviour within the organism. In particular, the enzyme of Topoisomerase II acts to regulate DNA under- and over winding and removes knots and tangles from the genetic material while generating new copies of DNA. The circle replication process of dsDNA is accrued in abnormal and normal cells. In brief, the catalyzed enzymatically role of the active site of Topoisomerase II establishes a bond with the phosphate of the nucleic acid on DNA-backbone via the nucleophilic attack of tyrosine. In structural-biochemistry, this physiological function called the DNA cleavage reaction, and it is the main goal for some highly successful anticancer drugs that presently applied in clinical and medicinal laboratory[4].

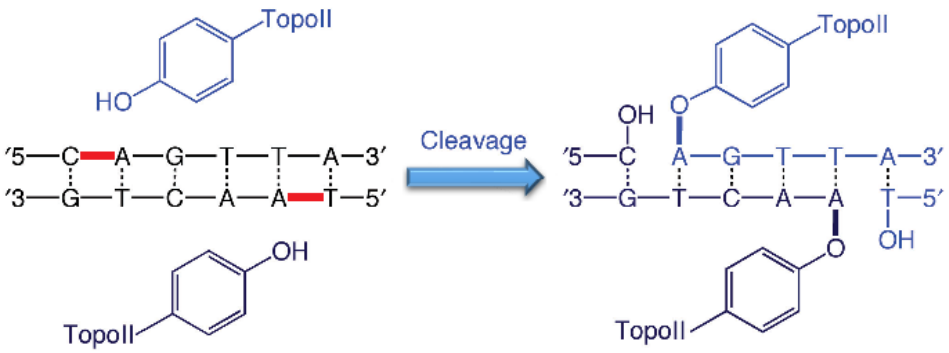

Figure 36: Double-stranded DNA cleavage reaction of Topoisomerase II [5]

Moreover, many biologists prepared several synthetic anticancer by incorporating ferrocene-based agents which acts to inhibit the topoisomerase function by relegating the DNA strands (Figure36) after cleavage-stage and transform the topoisomerase II into a DNA damaging factor, this leads to decrease the concentration of cancer cells[6].

1.1. DNA isolation

Many isolation DNA methods from the blood samples were used to evaluate the anticancer potency of some ferrocene derivatives. DNA isolation is very significant in interaction studies with anticancer drugs. Furthermore, it was a successful way in molecular biology techniques of DNA extraction, which gave a DNA in a high concentration, minimum extraction time, safe, inexpensive, elevated yield.

In this study, we utilized a simple and non-toxic DNA extraction technique called the salting-out[7-8], it developed by Miller et al. This technique has three primary stages: cell lysis, selective release of dsDNA from nuclear matrices, and removed the unwanted materials to recover DNA. In this context, these physical and chemical treatments that used in DNA isolation-protocol can affect the quantity and quality of the obtained DNA [9-10].

1.1.1. Procedure of DNA isolation:

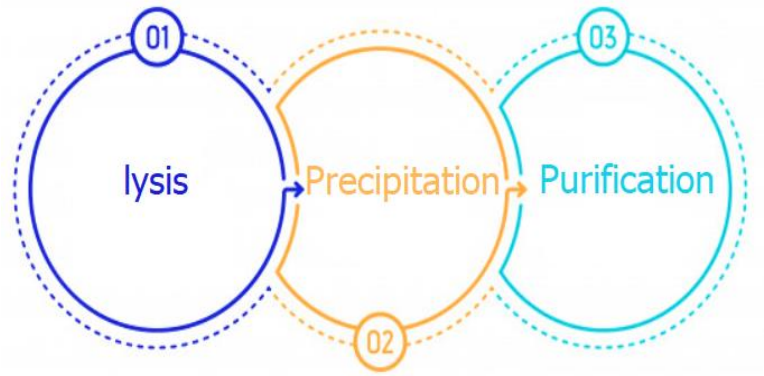

Figure 37: The three main steps of DNA isolation

1. Whole blood samples were collected in microcentrifuge tubes containing EDTA (1/9 from a volume of a chicken blood sample) and stored at 4 °C; also, it can be used directly without storage.

2. The sample of chicken blood is left for 20 min in a similar volume of RBC Lysis Buffer (red blood cell) then put it in equal quantities (a mixture of chicken sample with RBC Lysis Buffer in the microcentrifuge tubes and centrifuged for 15 min at a speed of 2500 rpm (and repeat this step until disposal red blood cells / 3-4 times). In each step, we keep the white precipitate and get rid of the liquid phase.

3. The white blood cells were weed out after the first treated by adding 2 ml of WCLB (White Cell Lysis Buffer) with vortex then adding to each tube 150 SDS (Sodium dodecyl sulfate) with vortexed.

4. Across a cell lysis step, the flacon tubes were placed in shaking incubator for 1.5 h at 55 ° C and fixed speed of 280 rpm, at the end of this step, 4 ml of NaCl was also added to each flacon tube and mixing for 2 minutes by the vortex.

5. The resulting mixtures were centrifuged for 10 min at 1500 rpm and vortexed for 1 min.

6. After centrifugation and vortexing steps, ethanol absolute (must be cold) was added to obtained mixtures in the order 1:3 mixture : ethanol (v/v) then slowly manually mixed for one minute and subjected to centrifugation for 5 at 1500 rpm.

- At the end of previous step, we note the appearance of a thin white filament (which represents DNA) within the microcentrifuge tubes containing a mixture with ethanol absolute.

7. The obtained DNA washed by 70% ethanol (must be cold) then centrifuged for 2 min at 1500 rpm.

- Finally, the obtained DNA was dried in ambient temperature and characterized using spectroscopy technic.

1.1.2. Quantitative and qualitative evaluation of DNA

1.1.3 Quantitative evaluation of isolated DNA

The quantitative evaluation of the extracted DNA was conducted by spectroscopy method; its concentration was determined by measuring the absorbance of nitrogenous bases (purine and pyrimidine), using the molar extinction coefficient value 6600 m-1.cm^{-1} at 260 nm[11].

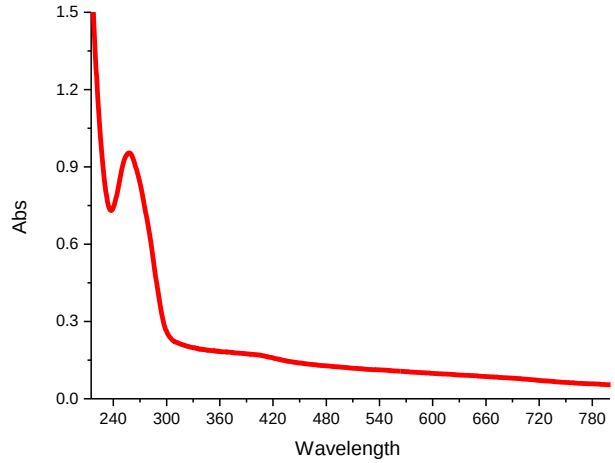

Figure 38: UV absorption curve of isolated DNA sample

1.1.4 Qualitative evaluation of isolated DNA

The double-strand of DNA was quantified by estimating the absorbance from 230 to 320 nm for detection the other possible contaminants using spectrophotometric way. The assay was carried out on a diluted and a well-mixed stock sample of DNA.

The commonest calculation for estimating the purity of DNA is measuring the absorbance ratio at 260 and 280 nm, for high DNA quality, the ratio (A_{260} / A_{280}) must be ranging from 1.7 to 2.0.

Table 4: Absorbance ratio of isolated DNA sample

DNA Sample	Absorption value
A_{260}	0.270
A_{280}	0.150
Ratio (A_{260}/A_{280})	1.85

The samples were collected in a total of 15 ml of chicken blood. They were collected using sterile macrotubes and stored in ethylene diamine tetra-acetic acid solution (EDTA) until the time of isolation.

Finally, the purity and DNA concentration was inside the optimal range; subsequently, it can be used in vitro trails. We conclude; therefore, chicken blood is a good source of DNA and may successfully use in evaluation studies of candidate drugs against undesirable mutations in DNA.

1.2. Cyclic Voltammetric investigation of NPF and FBN interacting with DNA:

1.2.1. Binding constant

All six ferrocene derivatives contain a well-known redox couple (Fc+/Fc). The addition of DNA into the solution containing the studied sample gives rise to a decrease in the redox-peak currents and leads to a shift in the anodic and cathodic peak potential. These two electrochemical phenomena are because the interaction among the studied ferrocene derivatives with DNA through intercalating the phenyl rings attached with ferrocene inside the negatively charged phosphate backbone. Simultaneously, the oxidation current (I_{pa}) of all studied compounds have similar electrochemical behaviour. In this regard, the affinity between target binding sites and ligands in bio-complexes are affected by non-covalent intermolecular forces like hydrogen bonding, electrostatic interactions, hydrophobic and two kinds of Van der Waals forces: weak, London-dispersion forces and dipole-dipole forces. Furthermore, the mentioned binding affinity may be influenced by the presence of another factors[12-13].

Figure 39 represents the voltammograms of ortho-nitrophenylferrocene (2NPF), meta-nitrophenylferrocene (3NPF), para-nitrophenylferrocene (4NPF), ortho-benzonitrileferrocene (2BNF), meta-benzonitrileferrocene (3BNF) and para-benzonitrileferrocene (4BNF). In the absence and presence of DNA the anodic peak potential of 4NPF, 3NPF, 2NPF, 4BNF, 3BNF, 2BNF are as follows: (0.638, 0.555), (0.617,0.552), (505.60,433.01), (394.63,434.44),

(441.66,388.11), (620.75,620.75) in mV respectively .The studied concentration range of all compounds is ranging from 4.76 to 18.92 µM.

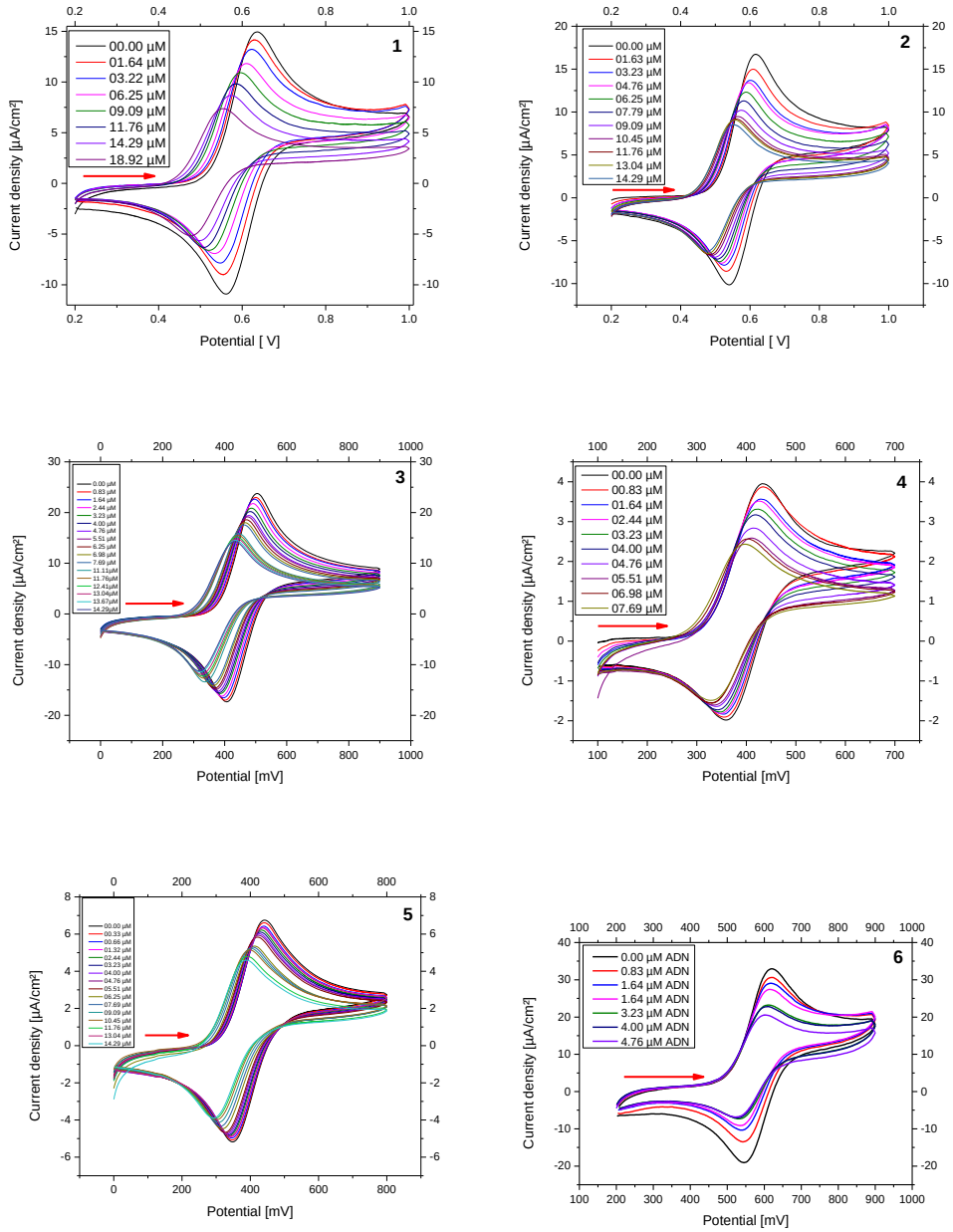

Figure 39: Cyclic voltammograms of 1mM 2NPF (1), 3NPF (2), 4NPF (3), 2BNF (4), 3BNF (5) and 4BNF (6) recorded at 0.1V s^{-1}potential scan rate on GC disk electrode at 298K in the absence and presence of increasing concentration of DNA in DMF for 4FBN, 2NPF, 3NPF and 4NPF; in 9:1(DMSO/H_2O) for 3FBN and 2FBN with supporting electrolyte 0.1 M Bu_4NBF_4.

The binding constant is the strength of the binding interaction among a single bio-macromolecule (DNA) to its experimental partner (The ligand). Besides, in most cases, the binding constant value is determined by the equilibrium among ligand and DNA. Equation (2.1) is utilized to identify the pathway of complexity interaction.

The negative charge in the external surface of DNA backbone along the minor/major groove of its structure, it mainly contributed to the interaction that can be occurred between the four nucleotide bases of DNA with the reduced and oxidized species of NPF or FBN; these latter represent the oxidized and reduced state of NPF and FBN related to reversible electrochemical behaviour. The decrease in shift anodic and cathodic current of cyclic voltammograms is caused by the sandwiched of NPF or FBN derivatives within DNA. The electrostatic interaction is established among the drugs that bear a positive charge (NPF+, PBN+) and all the negative charge position along the outer surface of DNA structure[14-15].

The shift anodic current values of free state for NPF and FBN with the decreasing values of anodic current in bound state NPF-DNA and PBN-DNA have been used to obtain binding constants and free binding energy parameters by applying the following Equation.

$$\log\frac{1}{[DNA]} = logk_b + log\frac{i_p}{i_{p_0}-i_p} \qquad (2.1)$$

Where $[DNA]$ represents the concentration of DNA in molare; k_b is the binding constant (M^{-1}); i_{p_0} and $i_p$are the shift anodic and catodic peaks in free and bound states of studied derivatives with DNA, respectively ($\mu A.cm^2$).

The linear relationship of $log1/[DNA]$ with $log1/1-(i/i_0-i)$ of NPF and FBN gave the plots, which are represented in figure 40 with a straight line and the intercept equal (y) of binding constant k_b.

1.2.2. Binding free Gibbs energy

The free Gibbs energy value was determined using the equation 2.2.

$$\Delta G = -RTlnk_b \qquad (2.2)$$

Where ΔG is the binding free Gibbs energy in KJ/mol, R is the universal gas constant, 8.32 J/(mol.K) and T is the ambient temperature, 298K.

Both electrochemical binding values of all derivatives (NPF, BNF) are listed in table 5.

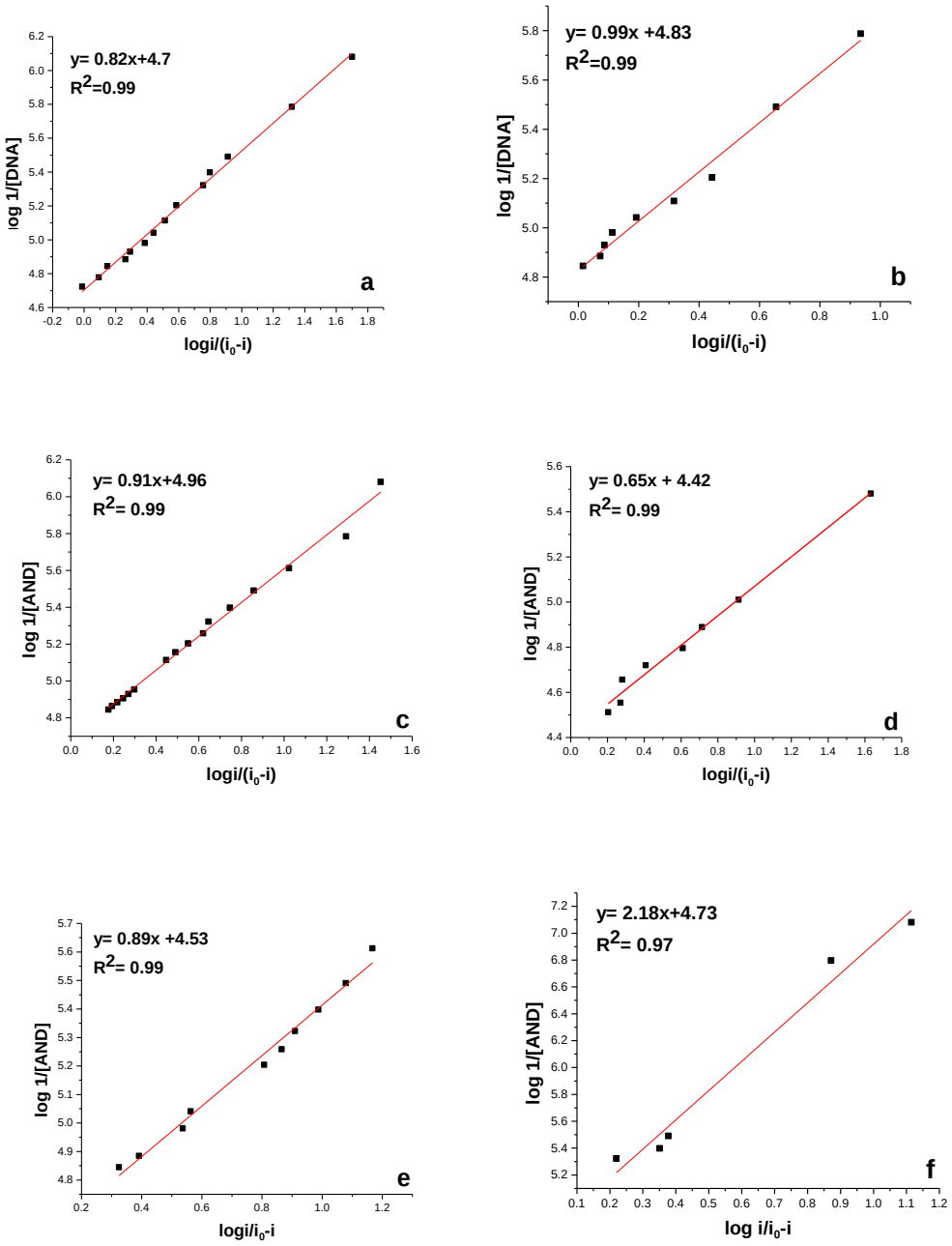

Figure 40: Plots of log 1⁄([DNA]) versus log1⁄(1-(i/i0-i)) used for calculation of the binding constants of ligands NFP and BNF with DNA ((a) 2NPF, (b) 3NPF, (c) 4NPF, (d) 2BNF, (e) 3BNF and (f) 4BNF.

ΔG and k values of two derivatives series for ligands NPF and BNF were determined depending on the obtained equations from the linear regression graphs and are listed below.

Table 5: Values of binding constants and binding free Gibbs energies obtained from in vitro assays for ligands NPF and BNF with DNA at T= 298K by means of the analysis of cyclic voltammetry data

Complex	Equation	R^2	$K(M^{-1})$	$-\Delta G(kj.mol^{-1})$
2NFP-DNA	y = 0.82 x + 4.7	0.99	$5.01x10^4$	26.83
3NFP-DNA	y = 0.99 x + 4.83	0.99	$6.76x10^4$	27.54
4NFP-DNA	y = 0.91 x + 4.96	0.99	$9.12x10^4$	28.28
2BNF-DNA	y = 0.65 x + 4.42	0.99	$2.63x10^4$	25.23
3BNF-DNA	y = 0.89 x + 4.53	0.99	$3.39x10^4$	25.86
4BNF-DNA	y = 2.18 x + 4.73	0.97	$5.37x10^4$	27.00

1.2.3. Binding site size

After carrying out the electrochemical measurements on ferrocene derivatives, the values of binding site size can be determined from the equation (2.3)[16].

$$\frac{c_b}{c_f} = k_b \left\{\frac{freebasepairs}{s}\right\} \qquad (2.3)$$

Where C_f and C_b are the compound-concentrations in free and bound cases with DNA respectively and K_b is the binding constant, s represents the binding site size in terms of base pair, and therefore, the nucleotide phosphate concentration in term [NP] compensated by the considering DNA-concentration term [DNA]/2, thus, so equation (2.3) can be re-expressed as:

$$\frac{C_b}{C_f} = k_b \left\{\frac{[DNA]}{2S}\right\} \qquad (2.4)$$

The bound-to-free ratios of studied derivatives were estimated using the experimental data obtained from the cyclic voltammograms of both studied cases for NPF and FBN.

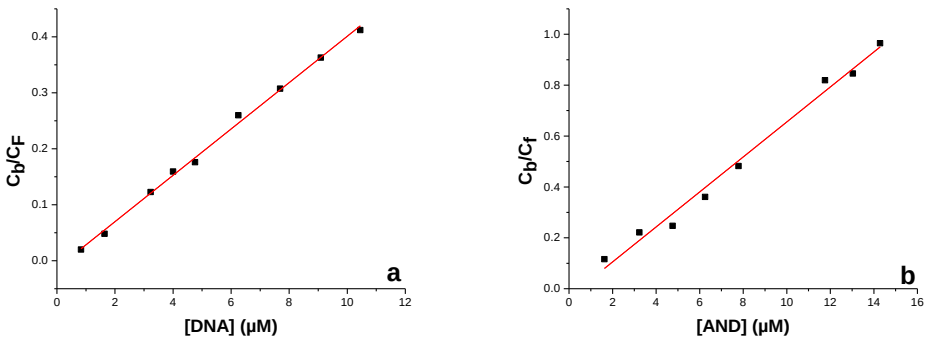

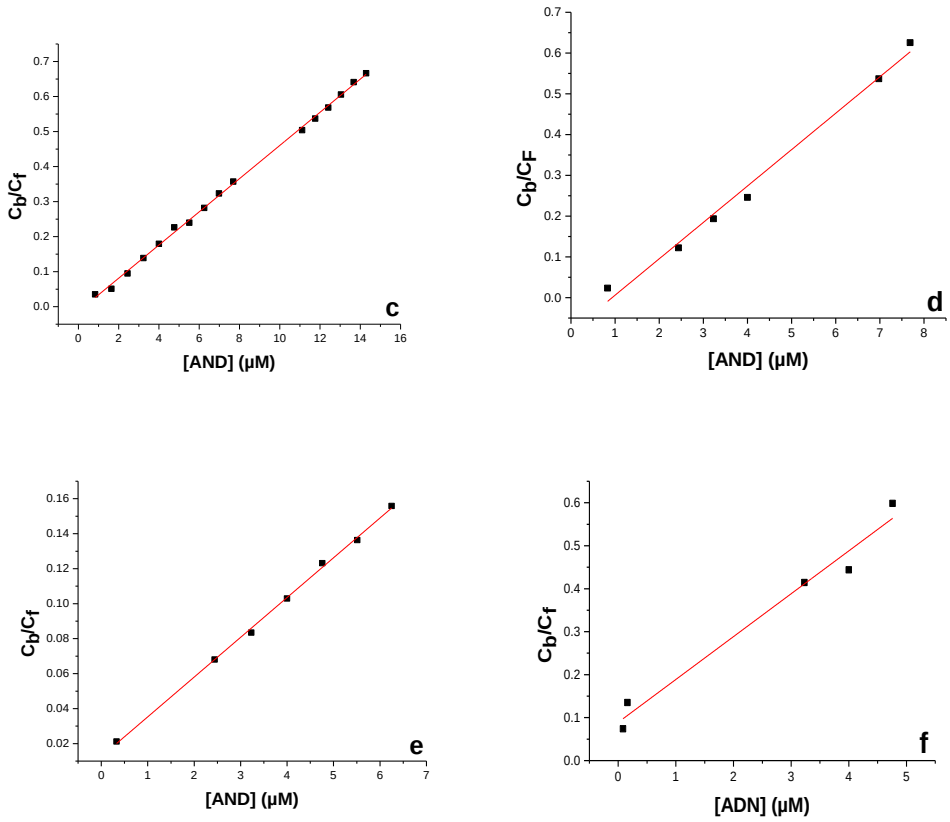

Figure 41: Plots of C_b/C_f ratio vs [DNA] used to determine binding site sizes of (a)2NFP, (b)3NFP, (c)4NFP, (d) 2BNF, (e)3BNF, (f)4BNF

Binding site size values of all studied derivatives NPF and BNF were calculated depending on the obtained equations from the linear regression graphs and are listed in Table 6.

Table 6: Binding site size values of ligands NPF and BNF obtained by Plots of Cb/Cf vs [DNA]

Complex	Equation	R^2	S
2NFP-DNA	y = 0.041x + 0.01	0.996	0.61
3NFP-DNA	y = 0.069x + 0.032	0.986	0.49
4NFP-DNA	y = 0.05x + 0.01	0.988	0.49
2BNF-DNA	y = 0.089x + 0.08	0.999	0.14
3BNF-DNA	y = 0.022x + 0.013	0.998	0.77
4BNF-DNA	y = 0.1x + 0.089	0.996	0.27

1.2.4. Diffusion coefficient

Diffusion coefficients can be calculated using Randles-Sevcik Equation[17-18] at T= 298K as displayed below

$$i_p = 2.69.10^5.n^{\frac{3}{2}}.S.B.D^{\frac{1}{2}}.v^{\frac{1}{2}} \qquad (2.5)$$

Where i_p is the peak current in µA.cm-^{2}, n is the number of electrons transferred through the oxidation reaction, S is the surface area of the electrode in cm^2, C is the bulk concentration of the electro-active species within the electrolyte solution in mol.cm^{-3}, D is the diffusion coefficient in cm^2.s^{-1} and *v* is the scan rate in Vs^{-1}.

Electrochemical behaviour of ligands NPF and BNP have been recorded in different scan rates and their *CV* are showed in Figure 42.

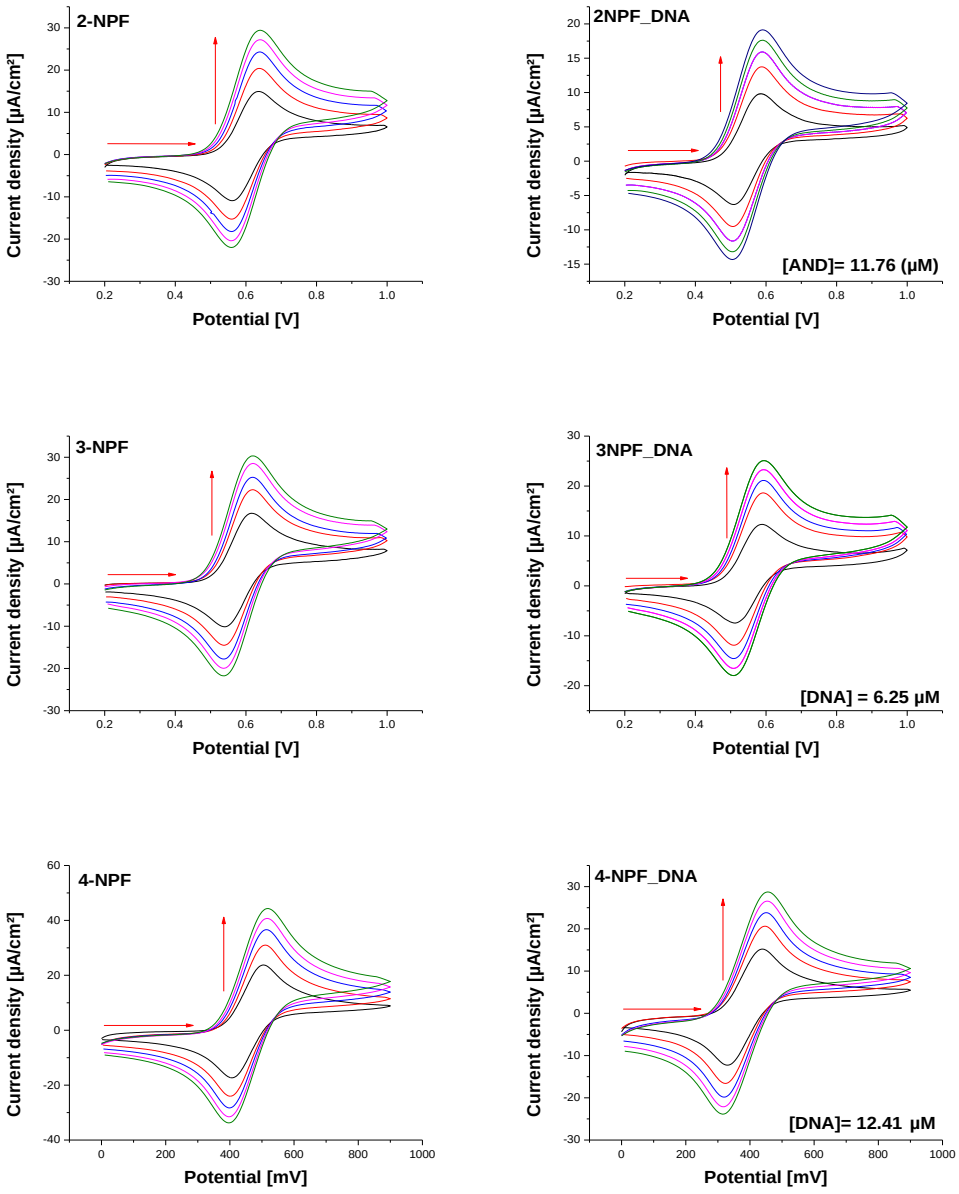

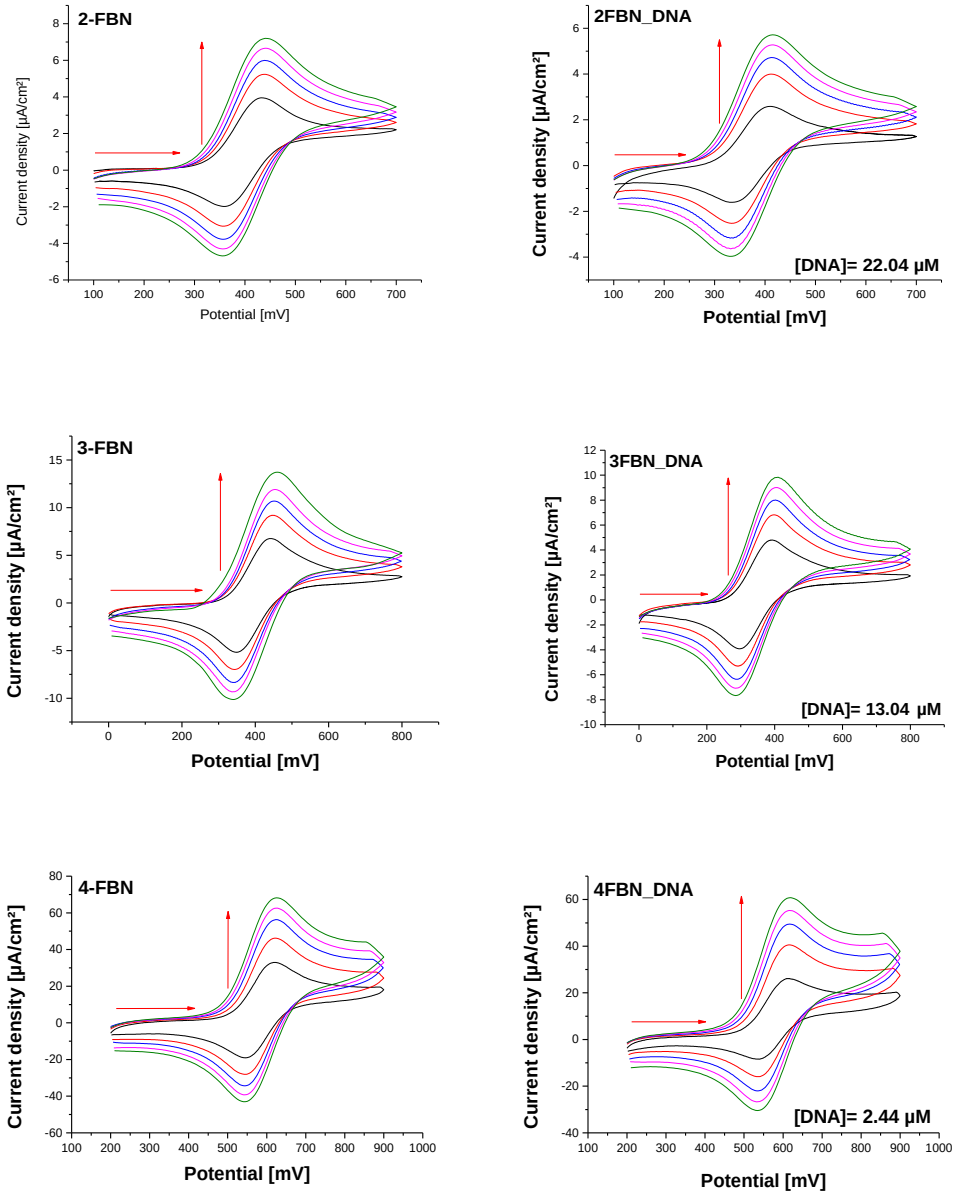

Figure 42: cyclic voltammograms of NPF and FBN (10^{-3}µM) in the absence and presence of DNA in DMF for 2NPF,3NPF,4NPF and 4FBN and in 9:1(DMSO/H2O) solution for 2FBN and 3FBN at scan rates 0.1, 0.2, 0.3, 0.4 and 0.5 v.s^{-1}with supporting electrolyte 0.1 M Bu_4NBF on glass carbon electrode.

Cyclic voltammograms of free and DNA bound NPF and FBN showed that the shift anodic peaks and scan rates are increased together in stable and organized behaviour. The linear regression of i_{pa}values as function with $\sqrt{v}$ used to obtain diffusion coefficients of all studied derivatives are presented in (Figure 43).

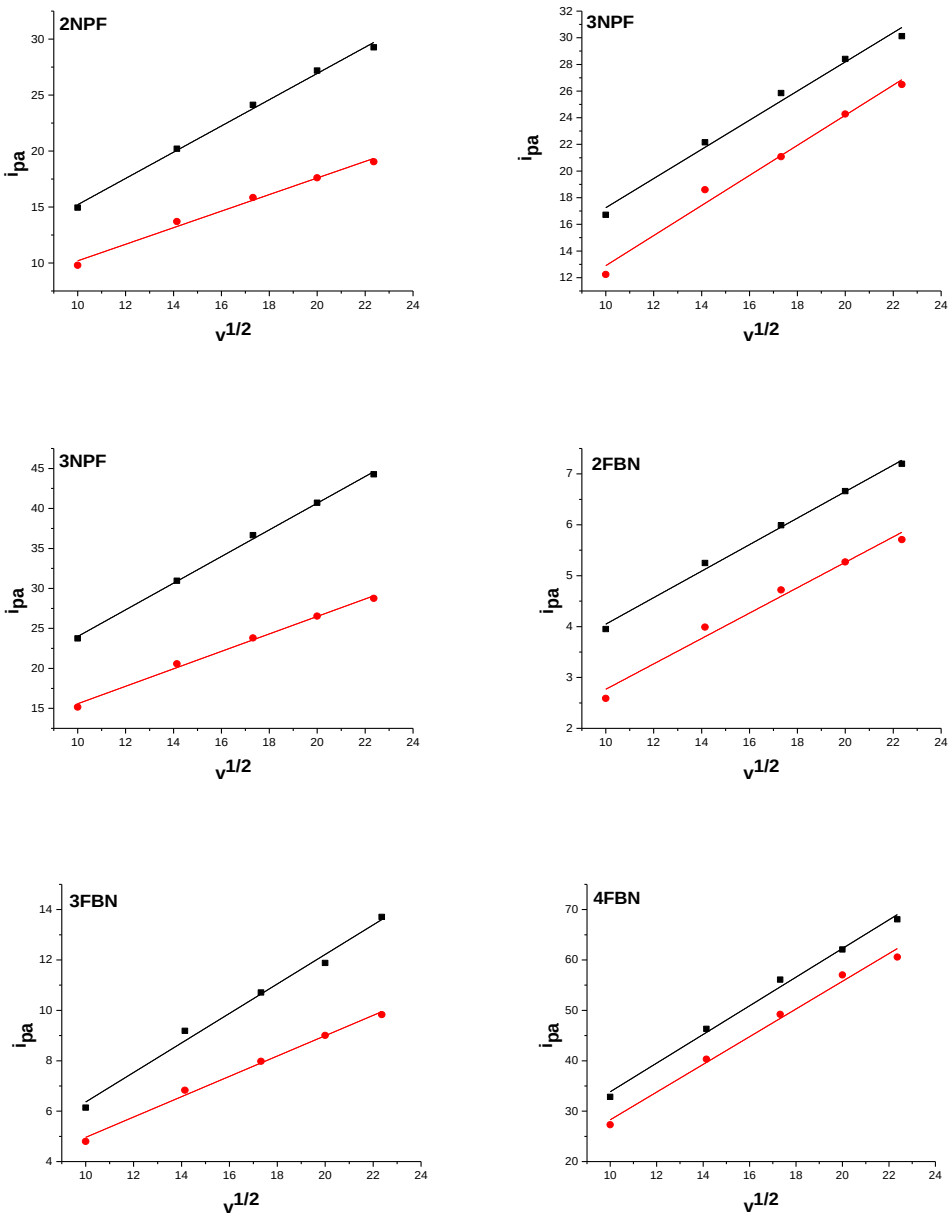

Figure 43: i_{pa} as function with $v^{1/2}$ plots of NPF and FBN in the absence (black lines) and presence of DNA (red lines) at scan rates ranging from 0.1 to 0.5 Vs−1 under the used experimental conditions of Figure 42

The obtained data from the plots of i_{pa} vs $v^{1/2}$ (Figure 43) indicated that the redox species diffused in a controlled manner as well as were used to determine diffusion coefficients of ligands NPF and FBN in free and bound cases with DNA using the equation (2.5) and their values are listed in Table 7.

Table 7: Diffusion coefficients values of the free and DNA-bound NPF and FBN

Ligand/Complex	Equation	R^2	D ($cm^2.s^{-1}$)
2NPF	y = 1.17x + 3.49	0,995	1.12×10^{-7}
2NPF-DNA	y = 0,74x + 2.79	0,987	4.47×10^{-8}
3NPF	y = 1.09x + 6.30	0,986	9.71×10^{-8}
3NPF-DNA	y = 1.12x + 1.61	0,982	4.32×10^{-9}
4NPF	y = 1.67x + 7.32	0,998	4.78×10^{-4}
4NPF-DNA	y = 1.09x + 4.66	0,993	3.12×10^{-4}
2BNF	y = 0.26x +1.44	0.993	7.43×10^{-5}
2BNF-DNA	y = 0.25x +0.27	0.977	7.14×10^{-5}
3BNF	y = 0.59x + 0.51	0.986	2.25×10^{-8}
3BNF-DNA	y = 0.40x + 0.93	0.993	1.44×10^{-8}
4BNF	y = 2.84x + 5.52	0.992	6.60×10^{-7}
4BNF-DNA	y = 2.75x + 0.8	0.988	6.18×10^{-7}

In all studied compounds, the general behaviour of diffusion coefficients can be summarized in the order $D_{ligand} > D_{complex}$; thus, this comparison provides interaction evidence between ligands and DNA.

1.2.5. Ratio of binding constant

In DNA titration study using cyclic voltammetry, the decreased change in anodic current peak (i_{pa}) of NPF and FBN in the absence and presence of DNA are accompanied with the change in anodic potential peak (E_{pa}) to more negatively potential. The constant binding ratio values have been calculated based on the electrochemical behaviour of all DNA bound and free ligands. The formation of DNA-NPF and DNA-FBN complexes led to the decrease of NPF and FBN concentrations, which explains the significant decrease of their i_{pa} with the change of E_{pa} as shown in Figure 44.

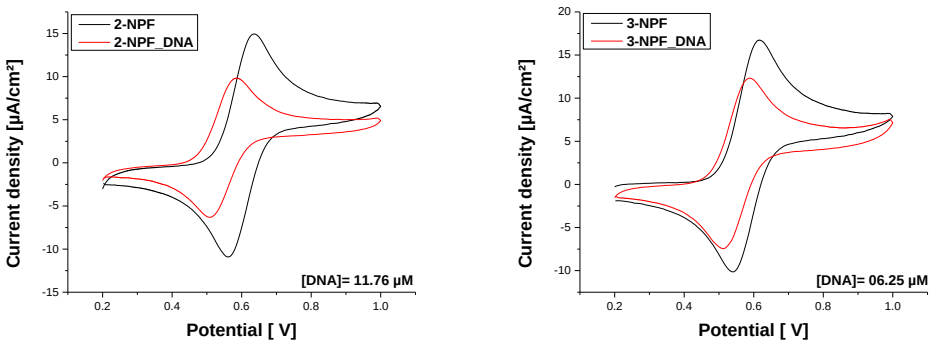

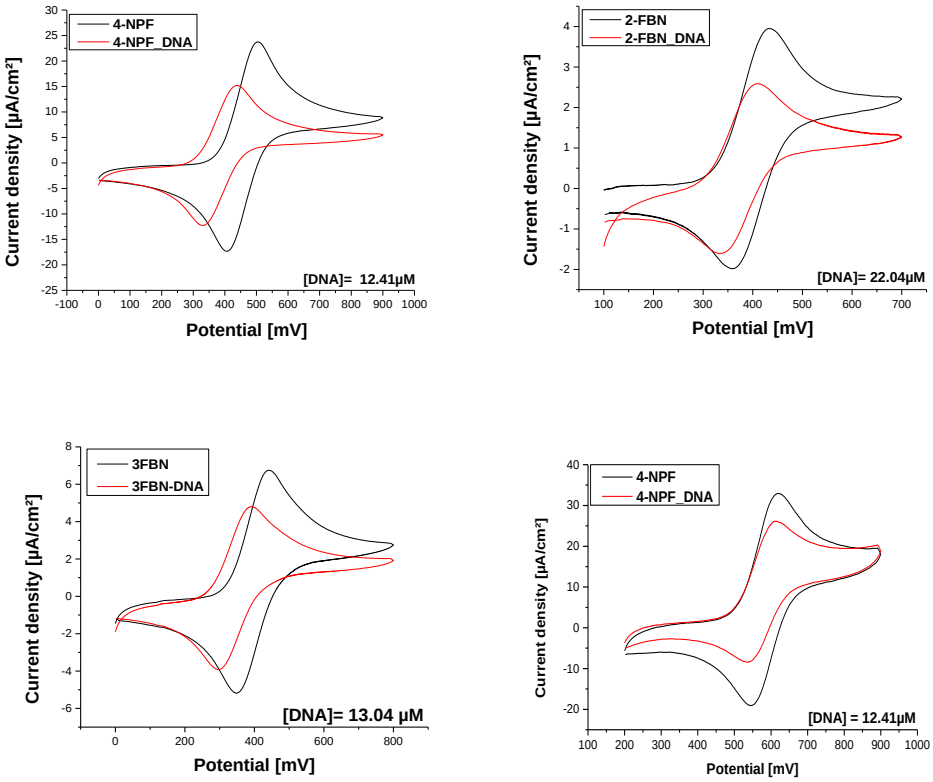

Figure 44: Cyclic voltammograms of NPF and FBN (10^{-3} µM) in the absence (black line) and presence (red line) of DNA in DMF for 2NPF,3NPF,4NPF and 4FBN and in 9:1(DMSO/H2O) solution for 2FBN and 3FBN at scan rate100 mV.s-^{1} with supporting electrolyte 0.1 M Bu_4NBF on glass carbon electrode

In such case when both the anodic and cathodic peak potential values are shifted upon the addition of DNA, the following equilibriums can be applied[19],

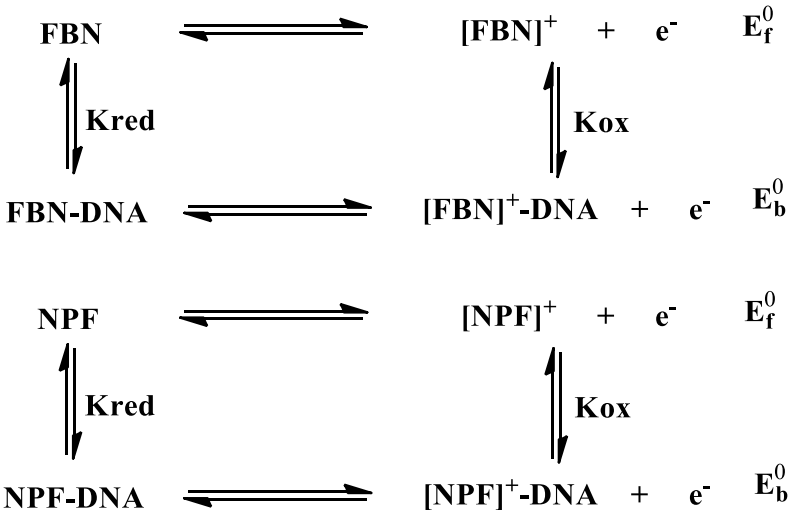

Figure 45: Redox process of the studied compounds with DNA

The application of the Nernst relation to the equilibriums of Figure 45 produces the following equations[20] (1,2),

$$\Delta E^0 = E_f^0 - E_b^0 = E^0(NPF) - E^0(NPF - DNA) = 0.061log\frac{k_{ox}}{k_{red}} \quad (2.6)$$

$$\Delta E^0 = E_f^0 - E_b^0 = E^0(FBN) - E^0(FBN - DNA) = 0.061log\frac{k_{ox}}{k_{red}} \quad (2.7)$$

E_f^0 *and* E_b^0 are the formal potentials of the Fc^+/Fc couple in free and DNA-bound respectively. The formal potential shift was calculated based on electrochemical data from the voltammograms in Figure 44 and were summarized in Table 8. In addition, the ratios of the binding constants were calculated by the equation (2.6) and (2.7) by replacing the value ΔE^0 from Table 8.

Table 8: Electrochemical data of the free and DNA bound NPF and FBN used for calculation the ratio of the binding constants

Ligand/complex	E_{pa}	E_{pc}	E°(mV)	ΔE°(mV)	K_{ox}/K_{red}
2NPF	636	650	643	96	42.37
2NPF-DNA	587	507	547		
3NPF	616.32	539.68	578	26.77	2.84
3NPF-DNA	589.89	512.57	551.23		
4NPF	504.13	406.38	455.25	70.39	15.60
4NPF-DNA	439.36	330.37	384.86		
2FBN	432.27	358.09	395.18	23.02	2.46
3FBN-DNA	411.12	333.2	372.16		
3FBN	442.1	348.34	395.22	51.75	7.54
3FBN-DNA	390.11	296.8	343.45		
4FBN	621.2	544.8	583	6.8	1.3
4FBN-DNA	616	536.4	576.2		

The obtained ratios of the binding constants indicate that the oxidized form of ligands NPF and FBN bind slightly more potent to DNA than their reduced forms.

1.3. UV visible spectroscopic investigation of NPF and FBN interacting with DNA

Beside cyclic voltammetry, UV visible spectroscopy is a useful tool for evaluating the interaction that can be established between a small molecule (ligand) and a macromolecule (DNA); furthermore, the interaction of the studied derivatives with DNA lead to shifting in UV-visible specter of the ligands; subsequently, the maximum of absorption peak and wavelength are changed with increasing DNA concentration[12-21].

The interactions of FBN and NPF with a stock solution of DNA were also tested by absorption spectroscopic titration. The main goal of this study was the validation of the obtained results from the measurements of cyclic voltammetry. The assays were carried out in DMF for 2NPF, 3NPF, 4NPF and 4FBN and in 9:1(DMSO/H_2O) solution for 2FBN and 3FBN. Gradually increasing concentrations of DNA were added to a fixed concentration of a solution of ligands, the used experimental conditions are shown in Figure 46. In the visible region, the derivatives 2NPF, 3NPF, 2FBN, and 4FBN possess only one absorption band, for compounds 4NPF and 3FBN the maximum absorption peaks of were found in the near UV region. All the tested compounds behave a similar pattern and a comparable response in the ultraviolet-visible spectrum. The absorption bands of the studied compounds appeared in ultraviolet and visible regions. The π→π* transition appeared in the visible region and n→π* transition appeared in the ultra-violet region.

After subjected all the compounds to the increase additions of DNA solution, a considerable hypochromic was remarked without any noteworthy change in the maximum wavelength position that distinctly indicated the formation of a complex DNA and NPF or FBN. Hypochromic effect denotes that there are interactions between NPF and FBN with DNA in the major or minor groove[22].

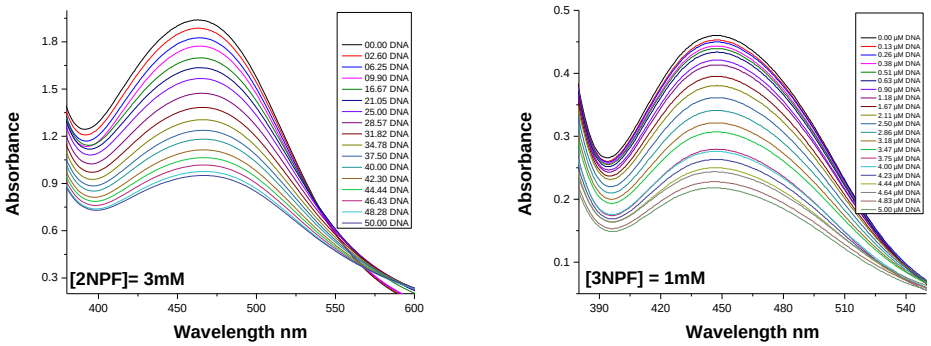

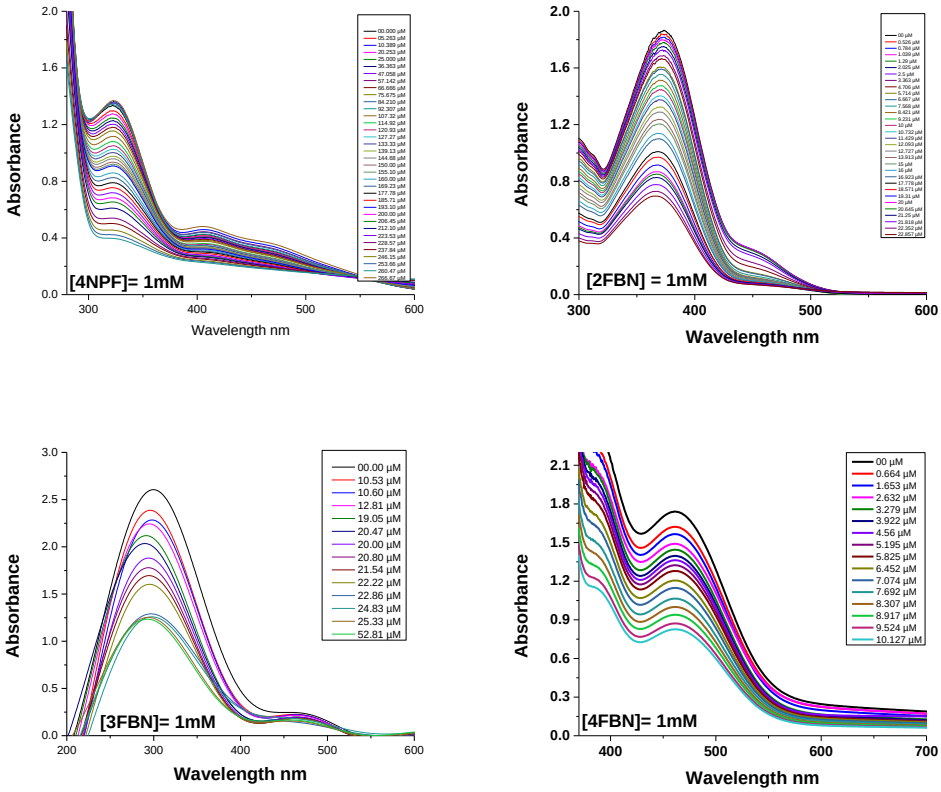

Figure 46: UV-visible absorption spectrums of NPF and FBN in the presence of increasing concentrations of DNA in DMF for 2NPF, 3NPF, 4NPF and 4FBN and in 9:1(DMSO/H_2O) solution for 2FBN and 3FBN at 298K

1.3.1. Binding constant

The obtained data from electronic spectroscopy measurements have been used to calculate the binding constants. The equation (2.8) was used to determine the intrinsic binding constant[23].

$$\frac{A_0}{A-A_0} = \frac{\varepsilon_G}{\varepsilon_{H-G}-\varepsilon_G} + \frac{\varepsilon_G}{\varepsilon_{H-G}-\varepsilon_G}\frac{1}{K_b[DNA]} \qquad (2.8)$$

Where "A_0" and "A" are the absorbances of NPF or FBN in the absence and presence of DNA respectively, and ε_G and ε_{H-G} are their extinction coefficients, [DNA] is the DNA concentration, K_b is the binding constant.

The double-reciprocal plots of $A_0/(A-A_0)$ as a function with 1/[DNA] are represented in Figure 47. The values of k_b were determined from the ratio of the intercept to the slope equations.

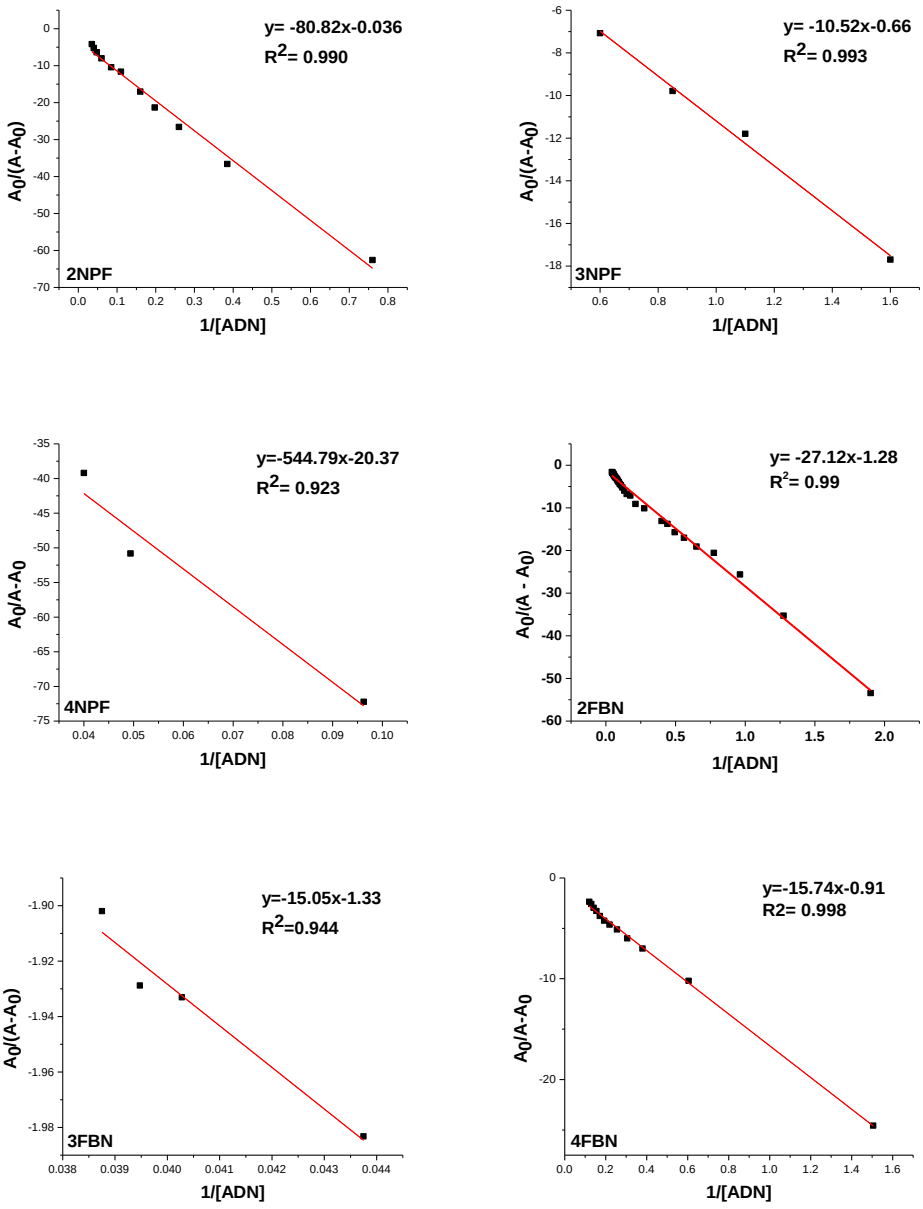

Figure 47: Typical plots of $A_0/(A-A_0)$ as a function of 1/ [DNA] used for calculation of the binding constants of ligands NPF and FBN with DNA

1.3.2. Binding free Gibbs energy

Using further thermodynamic analysis also helps determine the binding free energy change for the free and bound cases of NPF and FBN with DNA using the following equation[24].

$$\Delta G = -RTlnK_b \qquad (2.9)$$

Where ΔG is the binding free energy in KJ.mol^{-1}, R is the gas constant, 8.32 J.mol^{-1}K^{-1} and T is the ambient temperature, 298K. The values of k_b and ΔG of NPF and FBN are listed in Table 9.

Table 9: k_b and ΔG values for the interaction of compounds NPF and FBN with DNA obtained from spectroscopic measurements at T= 298 K

Complex	K (M^{-1})	-ΔG ($KJ.mol^{-1}$)
2NPF-DNA	$4.00x10^4$	26.37
3NPF-DNA	$6.27x10^4$	27.39
4NPF-DNA	$3.74x10^4$	26.11
2FBN-DNA	$4.73x10^4$	26.69
3FBN-DNA	$8.86x10^4$	28.24
4FBN-DNA	$5.66x10^4$	27.13

1.4. Docking study on DNA-Ligand interactions

The docking investigation results on the ligands NPF or FBN gave a comprehensive computational analysis about possible binding modes on DNA structure targeted to the studied compounds. A docking method is an approach that aims to predict the favoured orientation of a ligand to its partner even bind with it in a stable form; moreover, it can predict the binding-conformation of small-molecule ligands to the appropriate binding site.

1.4.1. Docking steps

All the procedures on the ligands NPF or FBN were performed through the same structural-optimization and simulation steps.

1.4.2. Molecular structure optimization

Density functional theory (DFT) was used to optimize the geometric-structure of NPF and FBN without imposing any symmetry constraints, all calculations were realized with the Gaussian 09 package. The exchange functional of Becke and the correlation functional of Lee, Yang and Parr (B3LYP) were employed with 6-311++G(d,p) basis set. Molecular three-dimensional conformation structures of (a) 2NPF, (b) 3NPF, (c) 4NPF, (d) 2FBN, (e) 3FBN and (f) 4FBN are displayed in Figure 48.

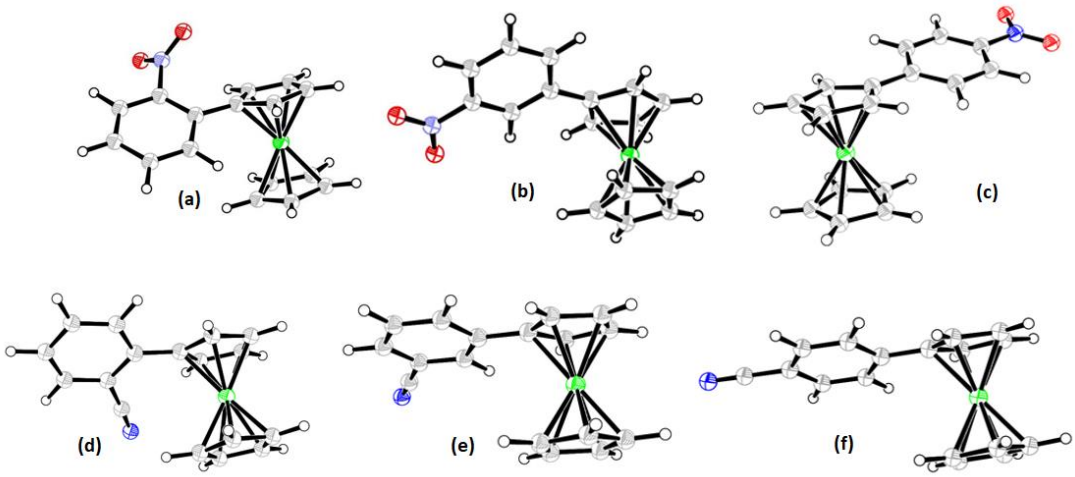

Figure 48: The optimized structures (30% probability ellipsoids) of (a)2NPF, (b)3NPF, (c)4NPF, (d)2FBN, (e)3FBN and (f)4FBN (ORTEP View 03, V1.08); color codes are grey carbon, white hydrogen, blue nitrogen, Green Iron, Red oxygen colour

1.4.3. Molecular docking studies

All semi-flexible docking was carried out using AutoDock 4.2 along with the AutoDock Vina software. The crystal structure of DNA was taken from the protein data bank (http://www.rcsb.org/pdb, PDB ID: 1bna). The PDB file was imported into AutoDock Tools, all hydrogen atoms and gassier charges were added. During all docking process, DNA kept rigid while all the bonds of the ligands were set free. The grid map with 0.375 Å. Lamarckian genetic algorithm was used in the docking running; other parameters were set as default as well as docking processes were conducted in specific grid box coordination with a number of docking runs. The stable conformation that has the lowest binding energy was used for docking analysis.

The free Gibbs energy and binding constant of the docked structure of the NPF and FBN ligands with DNA are listed in Table 10.

Table 10: free Gibbs energy and Binding constant values of docked complexes for DNA-NPF and DNA-FBN obtained from molecular docking calculations

Complexe	K(M^{-1})	-ΔG ($KJ.mol^{-1}$)	The number of runs
DNA-2NPF	2.47×10^{4}	25.08	50
DNA-3NPF	7.14×10^{4}	27.71	47
DNA-4NPF	4.46×10^{4}	26.54	40
DNA-2FBN	3.38×10^{4}	26.20	60
DNA-3FBN	9.21×10^{4}	28.34	45
DNA-4FBN	7.53×10^{5}	27.84	50

In order to determine the DNA-ligand association range by molecular docking study, we can use the magnitude of the negative ΔG to identify the stability and binding affinity of any given DNA–ligand complex; in this regard, the obtained values of binding and binding constants as shown in Table 10 indicated the stability and the high affinity of the obtained complexes. Tow experimental methods with the current theoretical approach; have been used to evaluate the changes in DNA structure in free and bound forms with ligands which gave the same indicators about the binding behaviour of the compounds toward DNA.

The following figure shows the surface-view representations of superimposed complexes NPF-DNA, FBN-DNA, and the target binding sites chosen according to the location of DNA pockets that have higher affinity with ligands.

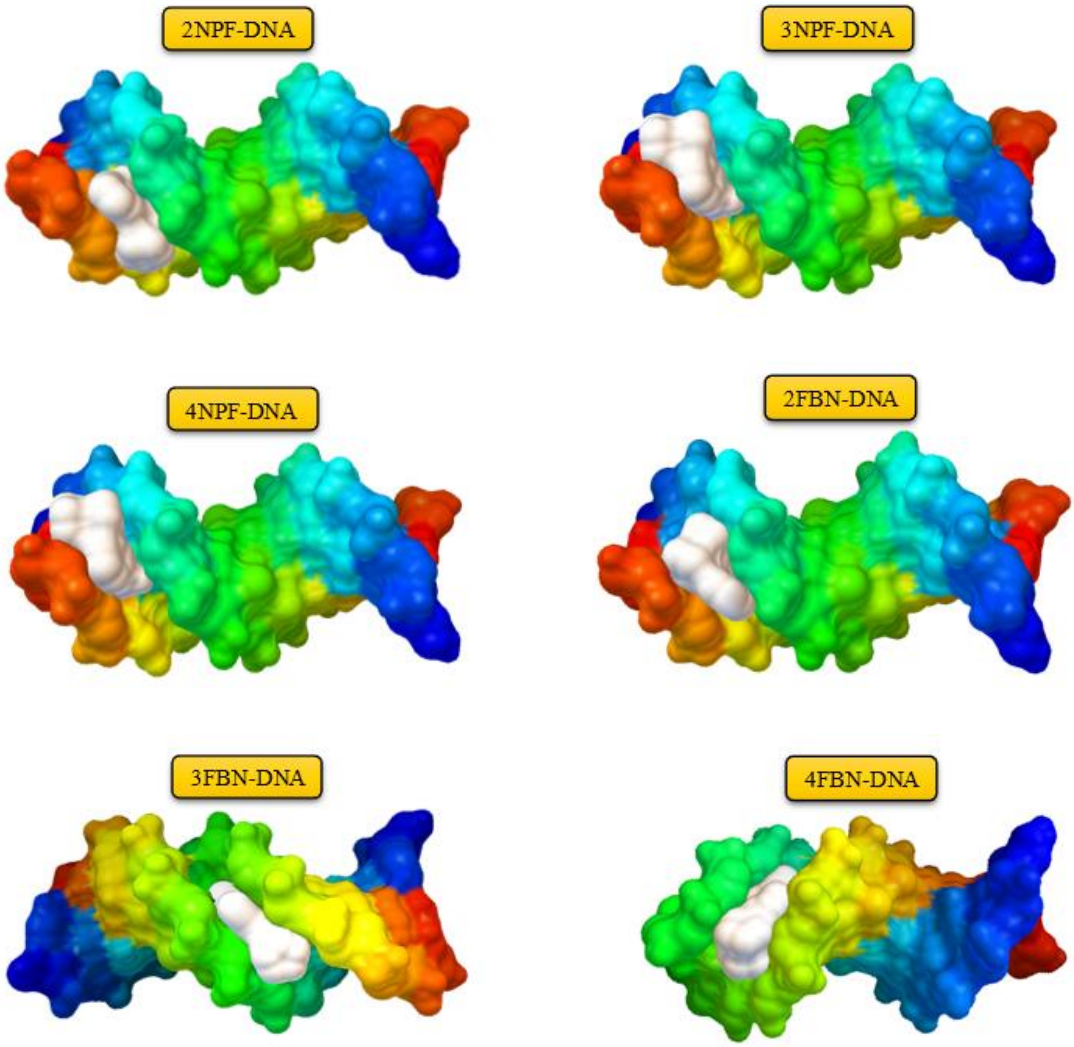

Figure 49: The flexible docking of optimized compounds into potential binding sites at crystal structure of DNA, are represented in surface view. White color is highlighted the ligands in minor groove of DNA

Using the obtained combination of biophysical and biochemical theoretical information with bioinformatics from docking calculations, we can predict the near-native binding poses in the studied complexes. In addition, the docking service attempts to bind the compounds with suitable pockets to mimic the natural path of the interaction of the studied compounds and its receptor by means of the lowest energy value. The visualization of the interactions for all molecules is a helpful manner of understanding the intermolecular binding in a ligand-DNA complex. Many types of fundamental forces are included in the intramolecular association under non-covalent contacts, involving aromatic-aromatic, aromatic-hydrogen, atom-atom and atom-aromatic interactions in the suitable groove by the fundamental role of active functions of two series (nitrile or nitro groups). In the subsequent docking studies, all the studied ferrocene derivatives are situated in the minor groove of DNA.

After visualizing the complexes by Discovery Studio, their interaction poses were highlighted in Figure 50 by stick representation. The interaction of 2NPF with DNA displayed a high-affinity and interposed with the hydrogen bonding interactions amongst the ligand and the double-strand of DNA. Various nucleotides included in the obtained interactions of 2NPF-DNA whether in A or B chain of DNA are represented as a stick with different colors (red, A:DC11), (blue, A:DG10), (yellow, B:DG14), (aqua, B:DG16). The interactions were generated by four hydrogen bonds and π-hydrogen and π-π interaction.

The docking results show the high-affinity between 3NPF with chain A and B of DNA which have been highlighted by stick representation. Tow nucleotides included in the obtained interactions of 3NPF-DNA complex are shown as a stick with different colors (blue, A:DG12), (yellow, B:DG14). The interactions were generated by three hydrogen bonds.

The exploration of the binding performance of 3NPF with DNA appears weak interactions in the target pocket from chain B, which was displayed by stick representation. The leading interaction among ligand and DNA is characterized by π-hydrogen and π-π interaction between the nitro-aromatic ring of 3NPF and hydrogen (22) with the bigger aromatic ring of B:DG14 (labelled by yellow colour).

The significant binding of 2FBN with the active site of DNA in its polynucleotide chains (A and B), were illustrated by stick representation. In this docked complex, there are three nucleotides contributed in the establishment of various bond types and it were highlighted by different colours in stick form (red, A:DG10), (blue, B:DG16), (yellow, A:DC11). The interactions were generated by two hydrogen bonds, π-oxygen and π-π interaction.

Favourable non-covalent contacts between 3FBN and the two strands of DNA were elucidated using a stick model. Four nucleotides attached with 3FBN to form a stable-complex and the colour of nucleotides are: (red, B:DA18), (blue, B:DA17), (yellow, A:DG10), (sky blue, B:DT19). There are all interaction types in the minor groove under the various forms: two hydrogen bonds and two π-anion interactions.

The obtained prominent-interaction in the presence of DNA in bound case with its partner (4FBN) visualized after implementing the docking in stick form. The complex composed of three nucleotides which coloured by (blue, A:AG10), (yellow, A:DG16) and (sky blue, A:DC9). The 4FBN-DNA interaction consists of two hydrogen bonds, π-hydrogen Interaction and π-π interaction.

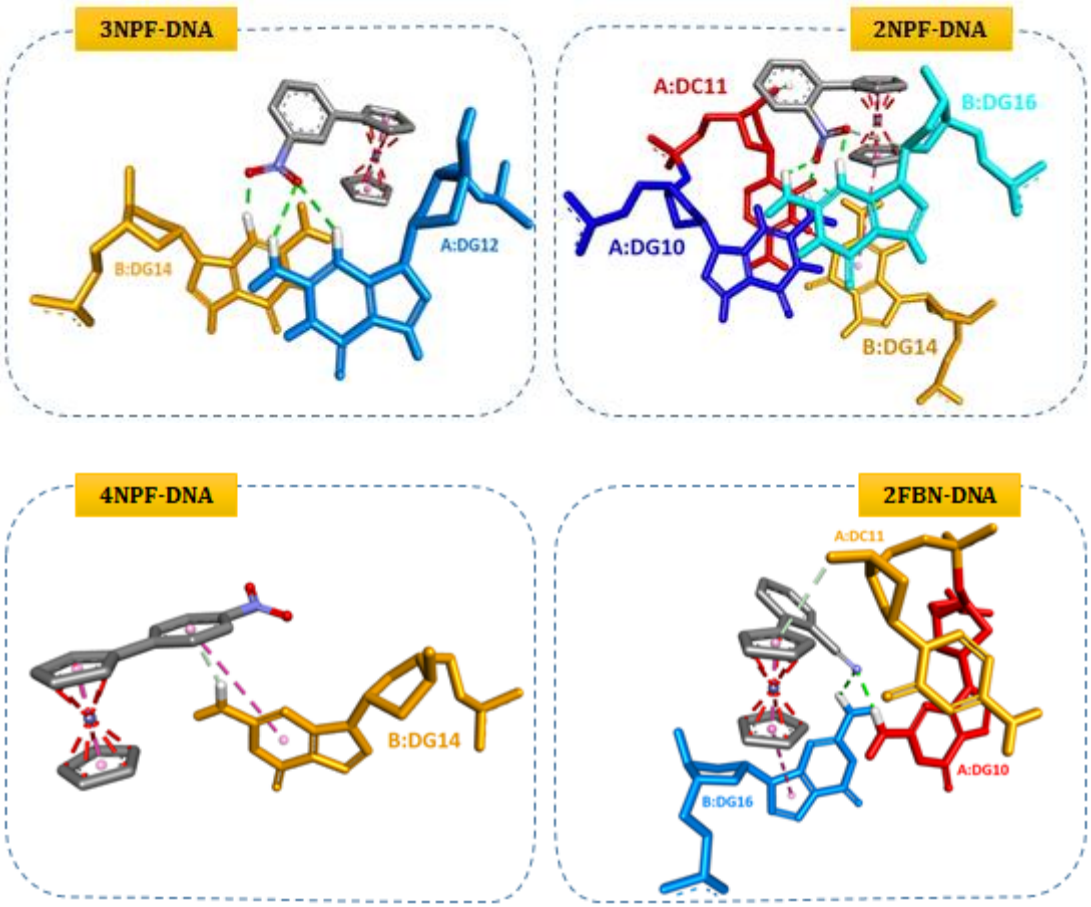

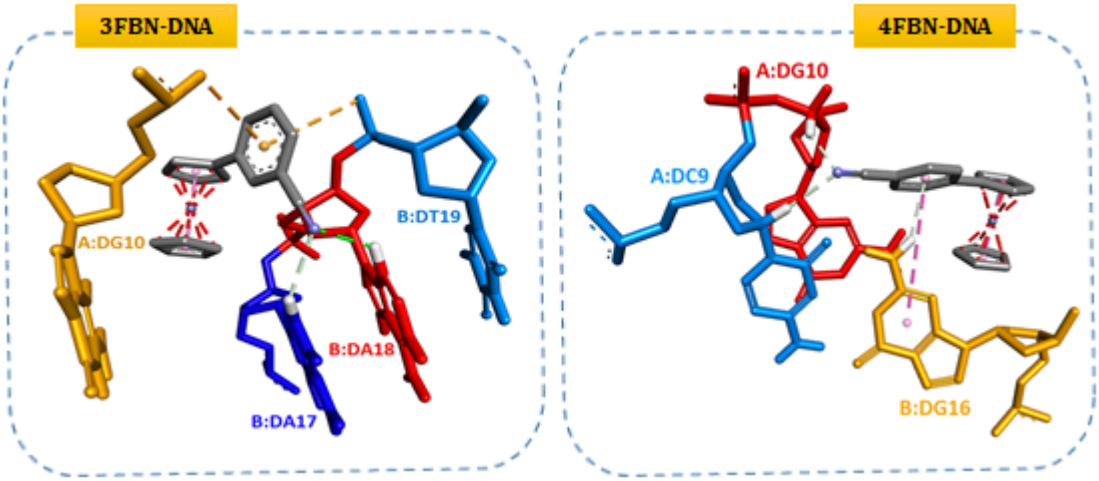

Figure 50: The NPF-DNA and FBN-DNA complexes visualized by stick model

The attachments of FBN and NPF with many residues of DNA have been highly demonstrated in Figure 50 and their distances with interaction types are listed in Table 11.

Table 11: Types and distances of interaction of the ligands to DNA

Complex	H-bond Interaction	Distance (Å)
2NPF-DNA	Ligand-O …H22:B:DG16	2.30
	Ligand-O…H21:A:DG10	1.98
	Ligand-O …H3:B:DG16	1.77
	Ligand-O …C1:B:DG16	2.94
	π -hydrogen Interaction	-
	Ligand …O3:A:DC11	3.84
	π - π Interaction	-
	Ligand … B:DG14	5.69
3NPF-DNA	H-bond Interaction	-
	Ligand-O …H3:A:DG12	2.75
	Ligand-O…H21:A:DG12	2.70
	Ligand-O …H3:B:DG14	1.84
4NPF-DNA	π - hydrogen Interaction	-
	Ligand …H22:B:DG14	2.36
	π - π Interaction	-
	Ligand… B:DG14	5.61
2FBN-DNA	H-bond Interaction	-

	Ligand-N…H_{21}:B:(DG16)	2.26
	Ligand-N…H_{21}:A:(DG10)	2.08
	π -oxygen interaction	-
	Ligand …O3':A: DC11	3.41
	π - π interaction	-
	Ligand …B:DG16	5.12
3FBN-DNA	H-bond Interaction	-
	Ligand-N…H3:B:DC18	2.19
	Ligand-N…H2:B:DG17	2.68
	π -Anion interaction	-
	Ligand…OP1:A:DG10	3.52
	Ligand…OP1:B:DT19	4.43
4CPF-DNA	H-bond Interaction	-
	Ligand-N…H1':A:(DC9)	2.39
	Ligand-N…H 5':A:(DG10)	2.09
	π -hydrogen Interaction	-
	Ligand…H21:B:DG16	2.52
	π - π interaction	-
	Ligand…B:DG16	5.84

The exploited methods in this study are valuable tools in estimating potential interactions of compounds with active sites, and their results indicated a significant convergence between the obtained binding parameter values (k_b and ΔG).

Table 12: Comparison of free Gibbs energy and binding constant values of NPF and FBN interacted with DNA obtained from CV, UV-vis and docking methods

Method	CV		Uv-vis		Docking	
Complex	K (M^{-1})	-ΔG ($KJ.mol^{-1}$)	K (M^{-1})	-ΔG ($KJ.mol^{-1}$)	K (M^{-1})	-ΔG ($KJ.mol^{-1}$)
2NPF-DNA	$5.01x10^{+4}$	26.83	$4×10^4$	26.37	$2.47×10^{+4}$	25.08
3NPF-DNA	$6.76x10^{+4}$	27.54	$6.27×10^4$	27.39	$7.14×10^{+4}$	27.71
4NFP-DNA	$9.12x10^{+4}$	28.28	3.7410^4	26.11	$4.46×10^{+4}$	26.54
2FBN-DNA	$2.63x10^{+4}$	25.23	$4.73×10^4$	26.69	$3.38×10^{+4}$	26.20

3FBN-DNA	$3.39x10^{-4}$	25.86	8.86×10^{4}	28.24	9.21×10^{4}	28.34
4FBN-DNA	$5.37x10^{-4}$	27.00	5.66×10^{4}	27.13	7.53×10^{5}	27.84

2. BSA interaction study

2.1. Cyclic Voltammetric investigation of NPF and FBN interacting with BSA

To completely recognize the overall pharmacokinetic profile of our studied compounds; it is crucial to study the reversible behaviour of NPF and FBN in the presence of BSA. The used mediums for these assays are DMF and 0.1 M 90% DMF/buffer phosphate solution at pH = 7.2. The experiments were performed following the same steps previously mentioned for DNA. The voltammograms of all derivatives were recorded in similar excremental experimental conditions of speed scan (100 $mV.s^{-1}$) and temperature (T=298 K) with supporting electrolyte 0.1 M tetra-n-butylammoniumtetrafluoroborate (Bu_4NBF_4), with and without the increasing concentration of BSA. However, understand and determine the detailed binding information of these bioactive compounds are able to provide essential insights to develop their activity toward BSA [25-26].

2.1.1. Binding constants

Figure 51 shows the effect of increased additions of BSA to the ligands NPF and FBN. The basic electrochemical influences of BSA on ligands voltammograms lead to a decrease in the anodic and cathodic current peak. E_{pa} displaced to the negative direction for all tested NPF and FBN compounds. The obtained results indicated that the interaction mode established between ligands and BSA is by electrostatic forces; this was between a ferrocene moiety which has a positive charge and the polyanionic structure of BSA[27].

The recorded voltammograms also display a clear decreasing in E_{pa} and E_{pc} values. In addition, these decreasing attributed to slow diffusion of the formed adducts BSA-NPF and BSA-FBN.

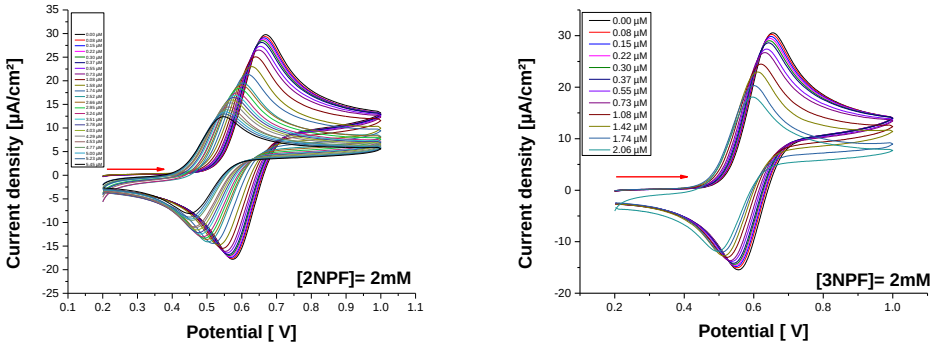

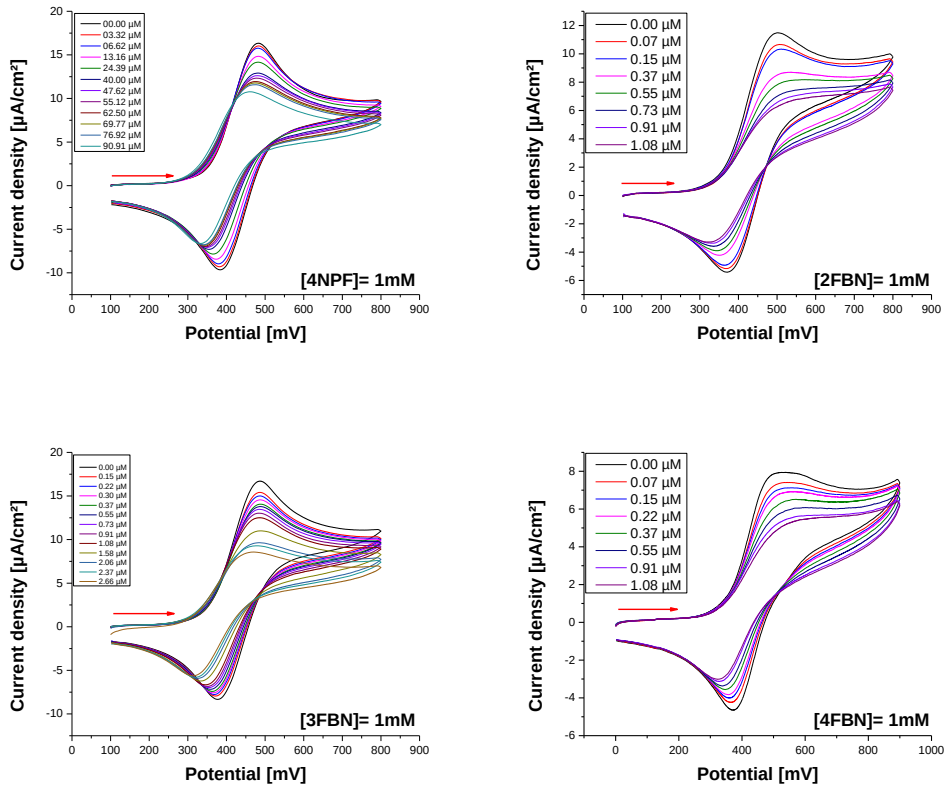

Figure 51: Cyclic voltammograms of NPF and FBN in the absence and presence the increasing concentrations of BSA in 0.1 M 90% DMF/buffer phosphate solution at pH = 7.2 for 2FBN,3FBN,4FBN and 4NPF; In DMF for 2NPF and 3NPF at a scan rate 0.1V s^{-1} on GC disk electrode at 298K with supporting electrolyte 0.1 M Bu_4NBF_4

BSA concentrations were added to NPF and FBN solutions and lead to decreasing in the anodic peak current that obtained after each addition. These responses are employed to determine the binding constant and free Gibbs energy using equation (2.2)[28]; which previously described.

2.1.2. Binding free Gibbs energy

Equation (2.2) was also used to determine the value of binding free Gibbs energy changes. All the calculated binding results of NPF and FBN with corresponding binding parameters (ΔG and k_b) are listed in Table 13.

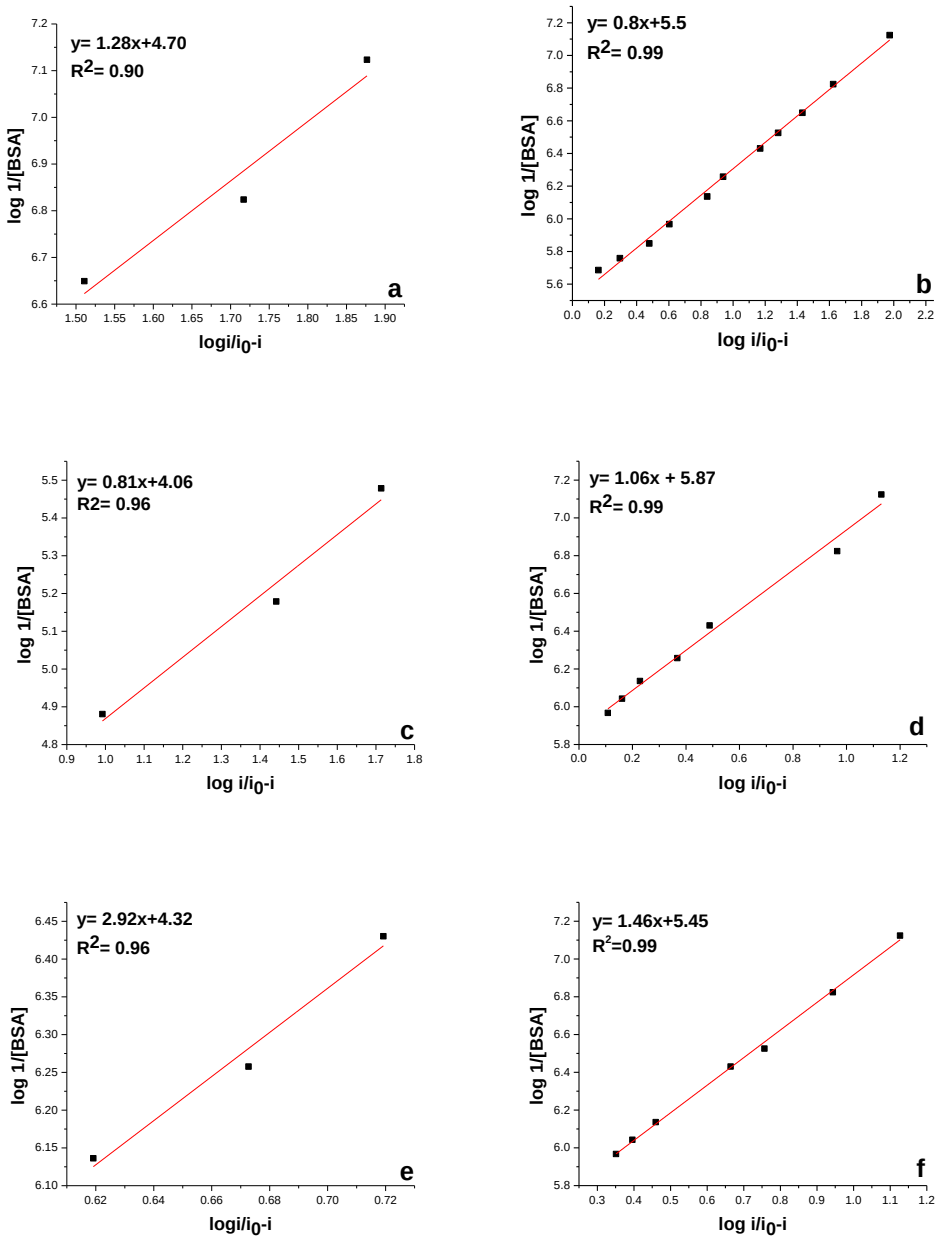

Figure 52: Plots of log 1/([BSA]) versus log1/(1-(i/i_0-i)) used for the calculation the binding constants of ligands NFP and BNF with BSA ((a) 2NPF, (b) 3NPF, (c) 4NPF, (d) 2BNF, (e) 3BNF and (f) 4BNF

Table 13: Binding constant and binding free Gibbs energy values obtained from CV assays of NPF and BNF with BSA at T= 298K

Complex	K(M^{-1})	-ΔG(KJ.mol^{-1})
2NFP-BSA	$4.89x10^4$	26.77
3NFP-BSA	$3.16x10^5$	31.40
4NFP-BSA	$1.15x10^4$	23.18
2BNF-BSA	$7.41x10^5$	33.51

3BNF-BSA	$2.08x10^4$	24.66
4BNF-BSA	$2.96x10^5$	31.11

2.1.3. Diffusion coefficient

To calculate the diffusion coefficients of NPF and FBN in the absence and presence BSA, the voltammograms were obtained at different scan rates for the free and BSA bound ligands. A noticeable change in peak potential with the increase in scan rate was observed. The Randles-Sevcik equation mentioned previously was used to determine the diffusion coefficient values (*D*), (Figure 53).

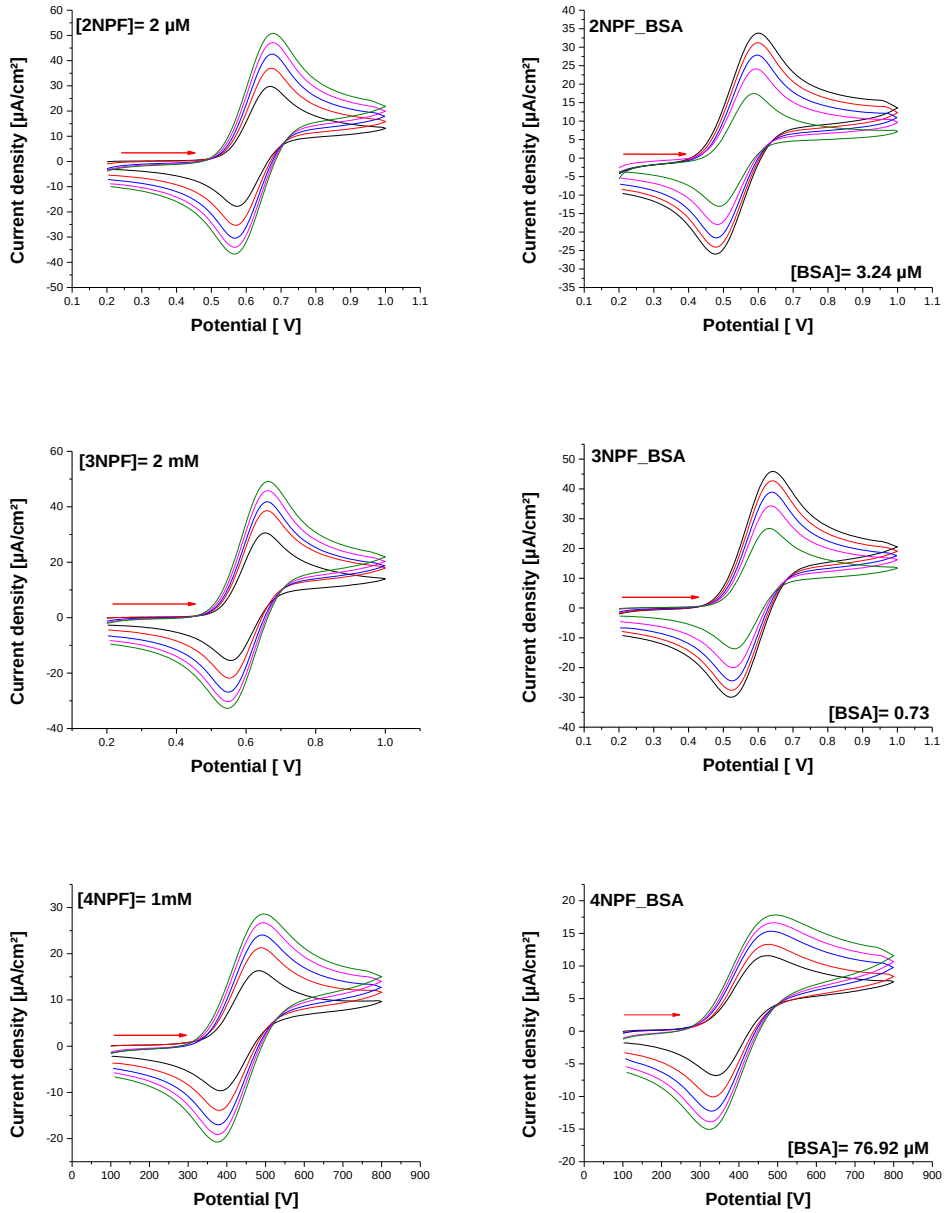

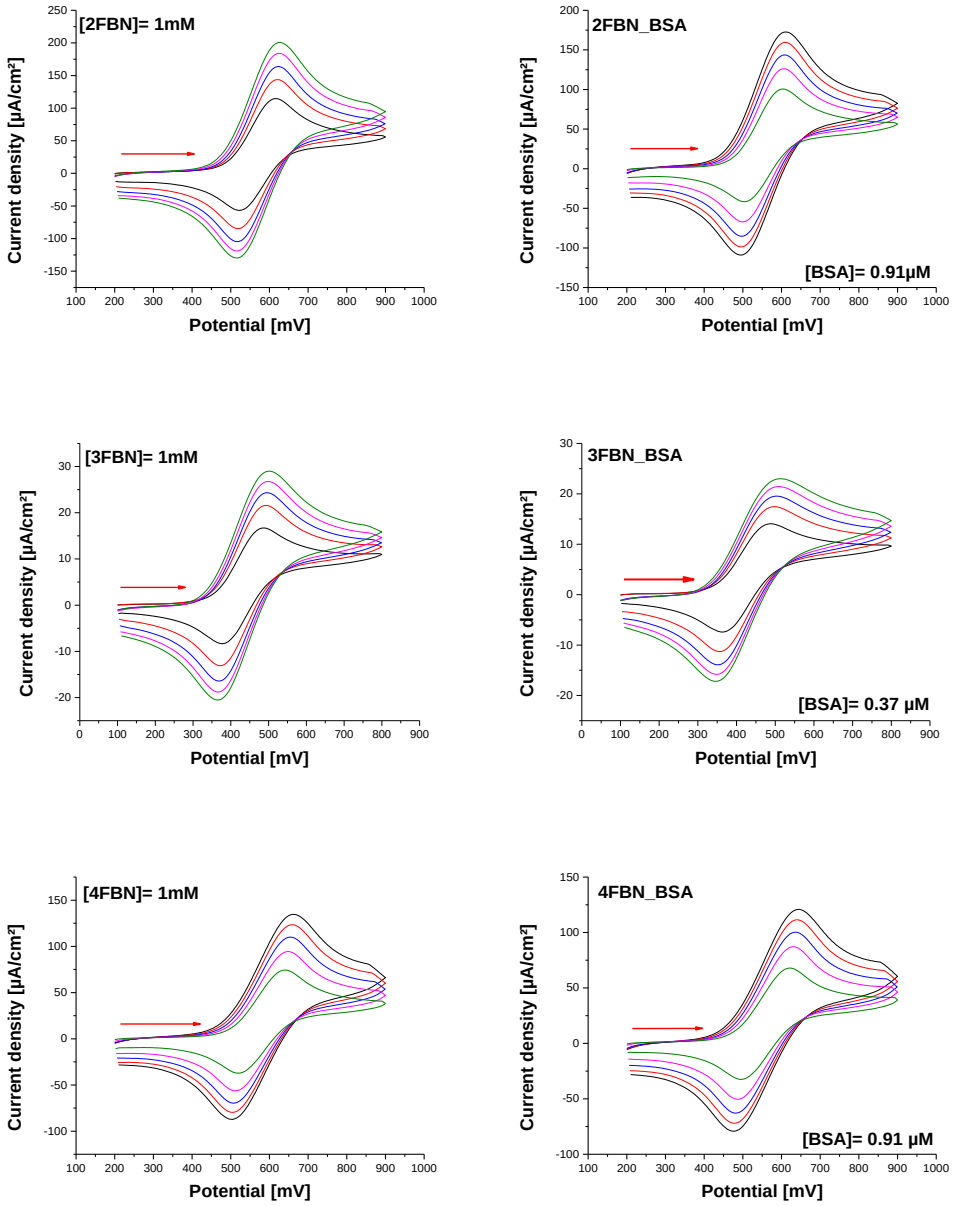

Figure 53: Cyclic voltammetric forms of NPF and FBN in the absence and presence of BSA in 0.1 M 90% DMF/buffer phosphate solution at pH = 7.2 for 2FBN,3FBN,4FBN and 4NPF; in DMF for 2NPF and 3NPF at scan rates 0.1,0.2,0.3,0.4 and 0.5 $v.s^{-1}$ with supporting electrolyte 0.1 M Bu_4NBF_4 on glass carbon electrode

CV measurements of NPF and FBN showed that the anodic peaks and scan rates are increased together in stable and organized behaviour. A straight line was obtained from the plot of anodic peak current versus square root of scan rates. This linear relationship indicated that the process is diffusion-controlled (Figure 54). The diffusion coefficients values are listed in Table 14.

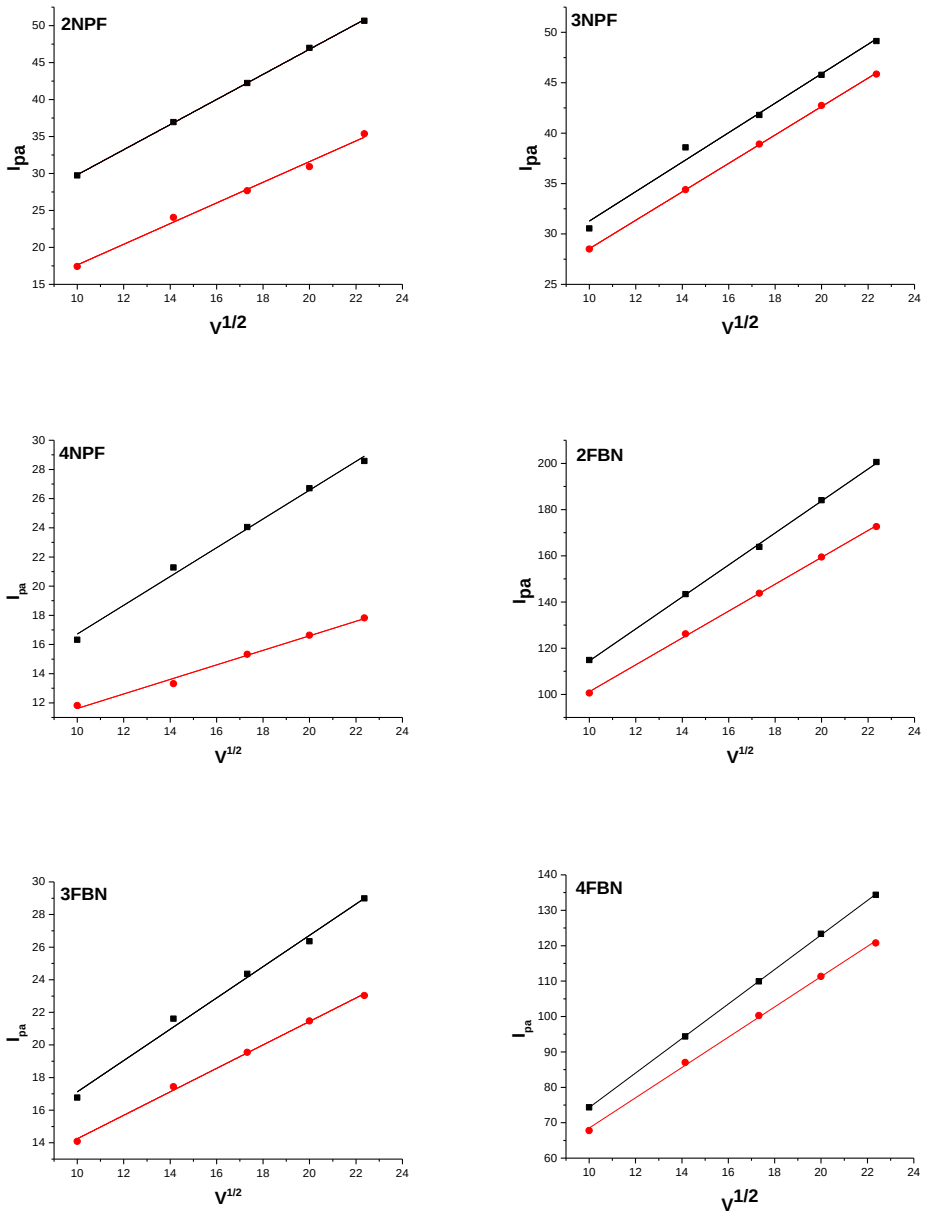

Figure 54: i_{pa} as function with $v^{1/2}$ plots of NPF and FBN in the absence (black lines) and presence of DNA (red lines) at scan rates ranging from 0.1 to 0.5 Vs^{-1} under the used experimental conditions of Figure 53

All diffusion coefficients of the derivatives NPF and BNF with their corresponding adducts NPF-BSA and BNF-BSA are listed in Table 14.

Table 14: Diffusion coefficients of the free and BSA-bound NPF and FBN

Ligand/Complex	Equation	R^2	$D(cm^2.s^{-1})$
2NPF	y = 1.70x + 12.83	0,999	2.36×10^{-7}
2NPF-BSA	y = 1.40x + 3.65	0,992	1.6×10^{-7}
3NPF	y = 1.46x + 16.66	0,986	4.36×10^{-8}
3NPF-BSA	y = 1.41x + 14.44	0,999	4.06×10^{-8}
4NPF	y = 0.97x + 6.85	0,993	7.69×10^{-8}
4NPF-BSA	y = 0.5x + 6.64	0,990	2.04×10^{-9}
2BNF	y = 6.62x+45.28	0,999	3.92×10^{-6}
2BNF-BSA	y = 5.82x+43.03	0,999	2.77×10^{-6}
3BNF	y = 0.97x + 7.38	0,991	7.69×10^{-8}
3BNF-BSA	y = 0.72x + 7.05	0,998	4.24×10^{-8}
4BNF	y = 4.87x+25.55	0,999	1.93×10^{-6}
4BNF-BSA	y = 4.28x+25.72	0,999	1.50×10^{-6}

Table 14 indicated that the free ligands are more diffusing than the BSA bound ligands. Thus, the global behaviour of obtained values can be summarized in the order $D_{ligand} > D_{complex.}$

2.1.4 Ratio of binding constant

To determine the ratio of binding constants of the free to the BSA bound NPF and FBN, the electrochemical behaviour of their reduced and oxidized forms using CV technique at fixed scan rate (100 $V.s^{-1}$) and fixed concentration value was used, Figure 55. The remarkable shift in the anodic and cathodic peak potential values, caused by the addition of BSA, can be used to calculate the K_{ox} /K_{red} values.

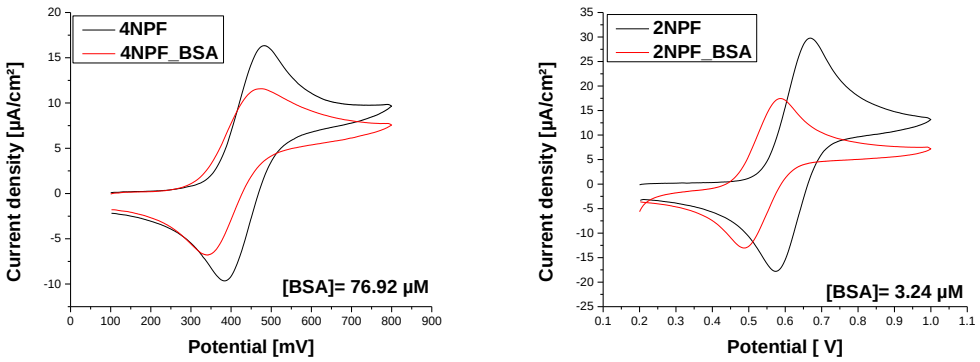

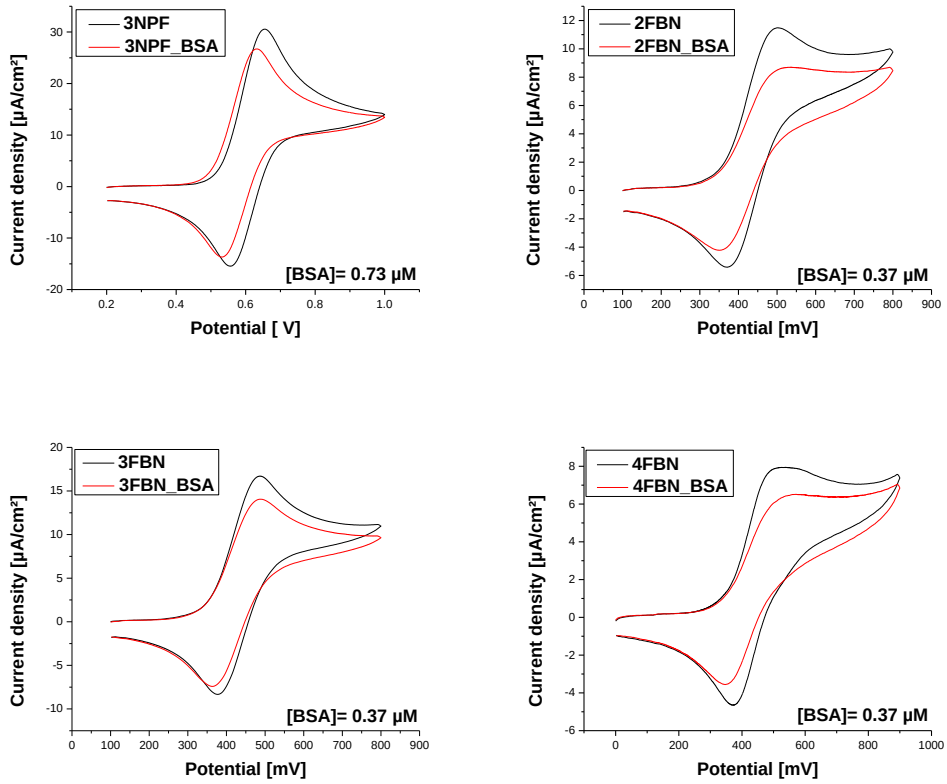

Figure 55: Cyclic voltammograms of NPF and FBN in the absence and presence of BSA in 0.1 M 90% DMF/buffer phosphate solution at pH = 7.2 for 2FBN,3FBN,4FBN and 4NPF; and in DMF for 2NPF and 3NPF at scan rate 100 $mV.s^{-1}$ with supporting electrolyte 0.1 M Bu_4NBF_4 on glass carbon electrode

In such a case, the anodic and cathodic peak potential values are changed according to the increasing additions of BSA; the following equilibrium can be applied[29]:

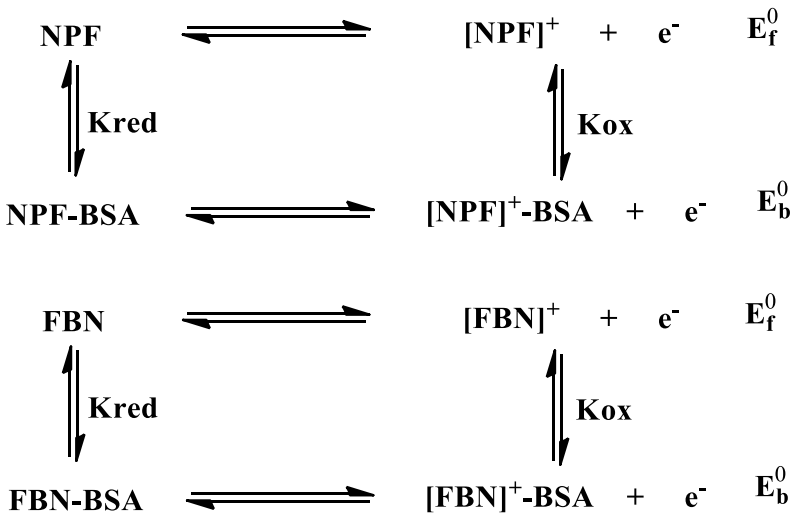

Figure 56: Redox process of the studied compounds with BSA

The application of the Nernst relation to the equilibriums of the redox process is described previously in this chapter. The formal potential shift was calculated based on electrochemical data from the voltammograms in Figure 56 and were summarized in Table 15

Table 15: Electrochemical data of the free and BSA bound NPF and FBN used for calculation the ratio of the binding constants

Ligand/complex	E_{pa}	E_{pc}	E°(mV)	ΔE°(mV)	K_{ox}/K_{red}
2NPF	668	574	621	85.5	28.5
2NPF-DNA	585	486	535.5		
3NPF	656	554	605	22.15	2.41
3NPF-DNA	634	531	582.5		
4NPF	480	385	432.5	27.2	2.92
4NPF-DNA	469	341	405		
2FBN	502	369	435.5	3.5	0.88
3FBN-DNA	527	351	439		
3FBN	486.29	376.92	431.59	5.29	1.22
3FBN-DNA	489.69	362.92	426.31		
4FBN	538	374	456	4	1.17
4FBN-DNA	572	348	460		

The calculated ratios of the binding constants indicate that the oxidized species of all ligands react slightly more potent to BSA than their reduced spices except the compound 3FBN.

2.2. UV visible spectroscopic investigation of NPF and FBN interacting with BSA

Currently, ultra-violet visible spectroscopy technique is among the best methods for studying the interactions between macro-biomolecules (BSA) with bioactive compounds. The goal of this study is monitoring the slight decreasing in the absorption of studied compounds as function of the change in their wavelengths. Two important parameters can be obtained: free Gibbs energy (ΔG) and binding constant (K). The non-covalent contacts of FBN and NPF with BSA were exanimated using this technique. The aim of this investigation is the validation of the obtained binding parameters from cyclic voltammetry. The experimental measurements of studied derivatives were conducted in 0.1 M 90% DMF/buffer phosphate solution at pH = 7.2

for 2FBN, 3FBN, 4FBN and 4NPF and in DMF for 2NPF and 3NPF. The obtained results are shown in Figure 57.

In the visible region, the compounds of 2NPF, 3NPF, 4NPF, 2FBN and 4FBN possess only one absorption band situated in the range from 410 to 460 nm. The absorption peak of 3FBN was found in the near UV region at 270 nm. The behaviours of all the exanimated compounds have the same pattern and a similar response in the ultraviolet-visible spectrum. The absorption bands of the studied compounds which appeared in the visible region are caused by $\pi \rightarrow \pi^*$ transitions of the conjugated system of the phenyl ring. A strong peak in the ultra-violet region at 270 nm is due to $n \rightarrow \pi^*$ transition.

Hypochromicity denotes weak-binding among the studied ligands with specific homology domain (I, II, III) of bovine serum albumin.

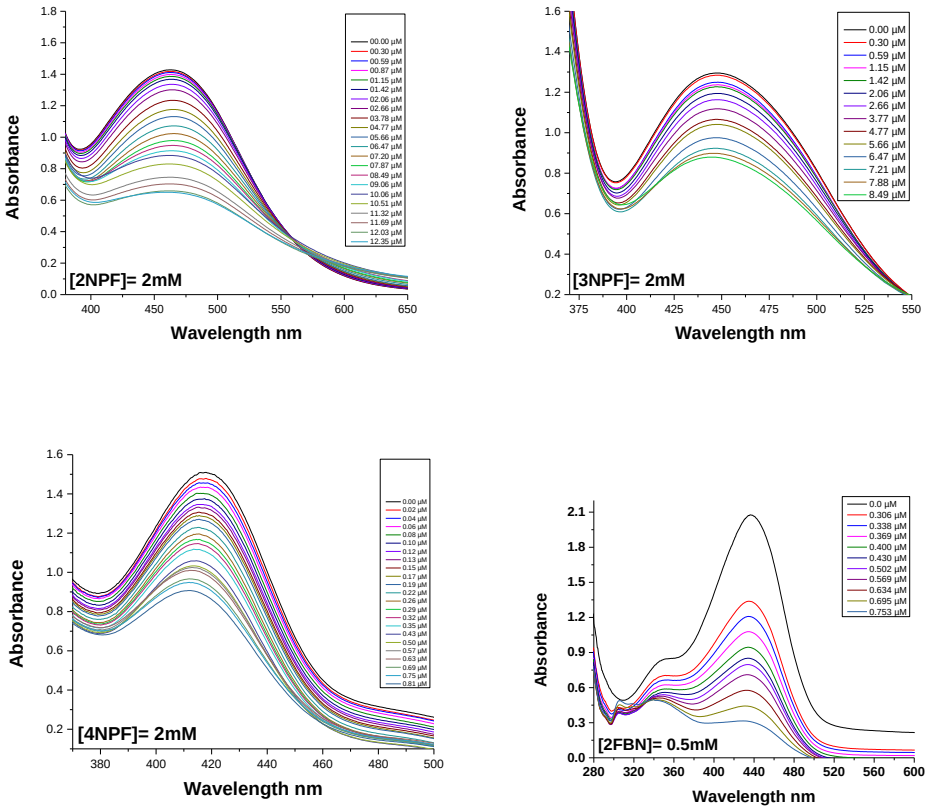

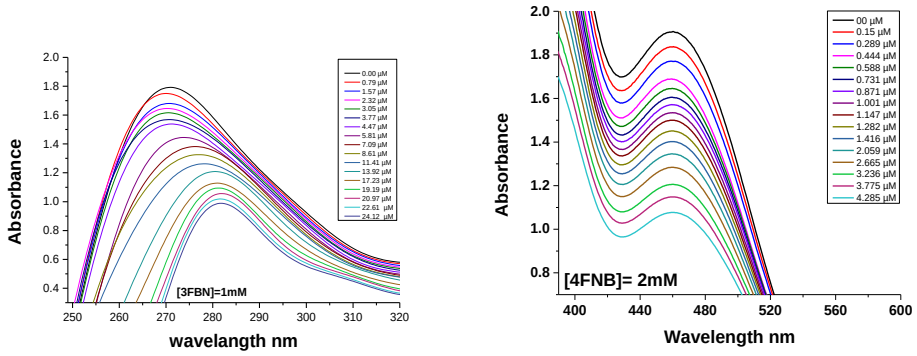

Figure 57: UV-visible absorption spectrums of NPF and FBN in the presence of increasing concentrations of BSA in 0.1 M 90% DMF/buffer phosphate solution at pH = 7.2 for 2FBN, 3FBN, 4FBN and 4NPF and in DMF for 2NPF and 3NPF at 298K

2.2.1. Binding constant

Ligands NFP and FBN interact with BSA binding sites, the equilibrium between the free and bound compounds has been used to calculate the binding constant (k_b) using the equation (2.2) described previously at the beginning of this chapter. Figure 58 represents the intercept to slope ratio of the plots of $A_0/(A-A_0)$ versus $1/[BSA]$ used for determination k_b values used for determination ΔG values[30-31].

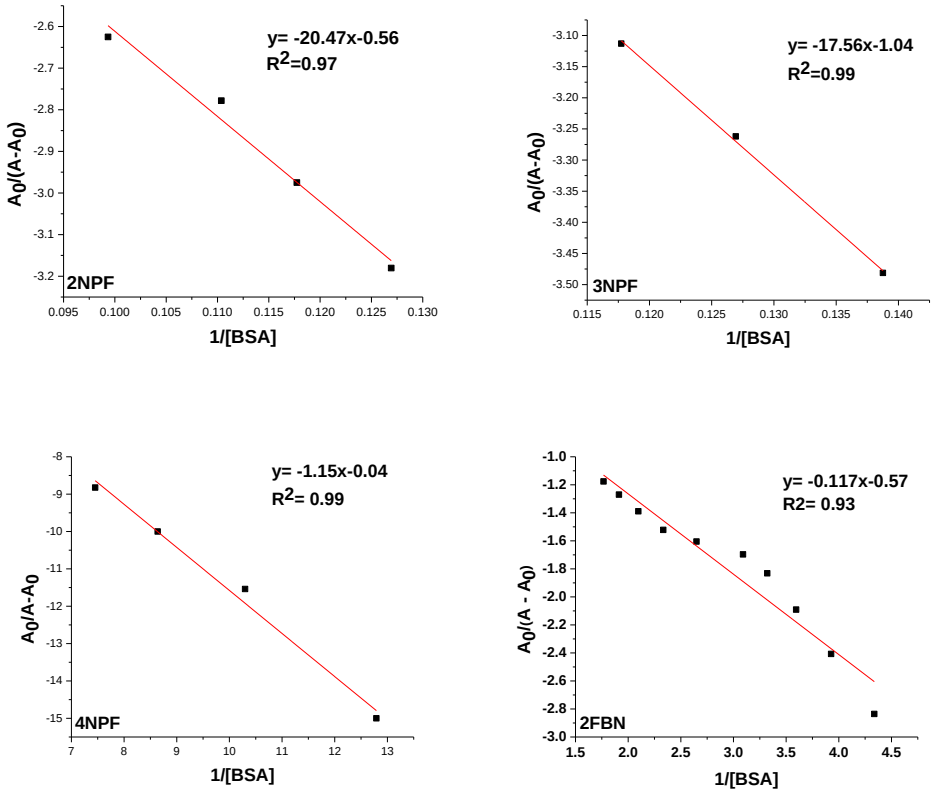

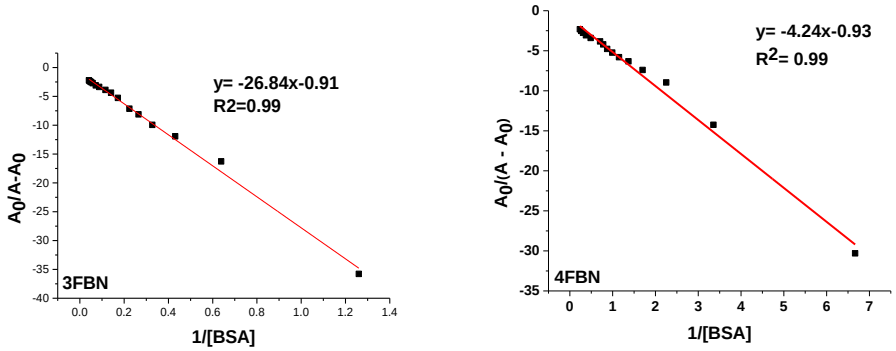

Figure 58: Typical plots of $A_0/(A-A_0)$ as a function with 1/ [BSA] employed for calculation of the binding constants of ligands NPF and FBN with BSA

2.2.2. Binding free Gibbs energy

The kind of binding mode and the value of binding free Gibbs energy change were determined by applying the Equation (2.2). Table 16 summarized the obtained ΔG and k_b values[23].

Table 16: The binding parameters of NPF and FBN obtained from the electronic spectroscopic data at T= 298 K

Complex	K_b (M^{-1})	-ΔG ($KJ.mol^{-1}$)
2NPF-BSA	2.73×10^4	25.33
3NPF-BSA	5.92×10^4	27.39
4NPF-BSA	3.48×10^4	25.93
2FBN-BSA	2.03×10^5	30.32
3FBN-BSA	3.39×10^4	25.83
4FBN-BSA	2.19×10^5	30.49

2.3. Docking study on BSA-Ligand interactions

Molecular docking studies of BSA with ferrocene derivatives have become increasingly crucial in pharmacochemistry and are commonly utilized as a key stage in medicinal compounds designing. The simulation researches in this field provide complementary information for BSA-binding experiments. All the ligands were docked with the crystalline structure of BSA obtained from (http://www.pdb.org) with the ID code: 4f5s[32]. The visualization of the interaction resulted from the docking processes were generated with Protein Ligand Interaction Profiler web (PLIP) server[33].

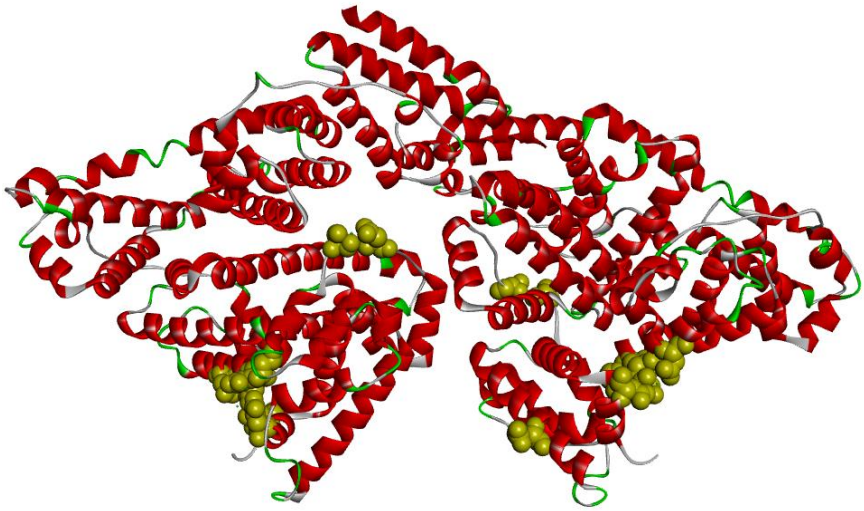

Figure 59: 3D structure of Bovine Serum Albumin in space fill model and their active sites highlighted by carbon presentation (yellow color).

The flexible docking experiments were carried out employing a multistep docking protocol previously described at the begging of this chapter; visualizations of non-covalent contacts between the studied compounds and BSA can be performed at the end of computational docking process with PLIP web server. Also, we can use the obtained data for highlighting the binding poses inside the complex.

The binding parameters ΔG and K_b related to the complexes BSA-NPF and BSA-FBN are calculated and listed in Table 17.

Table 17: Binding free energy and binding constant values of NPF and FBN with BSA

Complex	K (M^{-1})	-ΔG ($KJ.mol^{-1}$)	The number of runs
BSA-2NPF	4.53×10^4	26.58	55
BSA-3NPF	5.56×10^4	27.09	34
BSA-4NPF	1.28×10^4	25.54	40

BSA-2FBN	5.77×10^{5}	31.68	100
BSA-3FBN	1.65×10^{4}	24.16	60
BSA-4FBN	2.99×10^{5}	31.64	100

The compounds FBN and NPF and their calculated binding parameters are summarized in the Table 17, indicating high affinities between all compounds and BSA. The magnitude of negative free Gibbs energy and the significant value of the binding constant denoted the high stability of the formed complex. These binding results and target pockets in BSA can be exploited to prepare new bio-compounds with high performance during a binding mechanism.

The representation of surface view is an *in silico* simulation tool used to highlight the attachments between the potential drugs and target proteins. The results of docked conformations help to interpret the interaction mechanism among BSA-cavities and ferrocene derivatives. In addition, these docking results confirmed the formation of macromolecular complexes involving BSA and studied ligands. The represented findings in Figure 60, and Table 18 indicated that ligands could interact with the BSA by low binding energy ranging from 26 to 31 ($KJ.mol^{-1}$). All the ligands being surrounded by various forces when to exist in the target pocket of BSA.

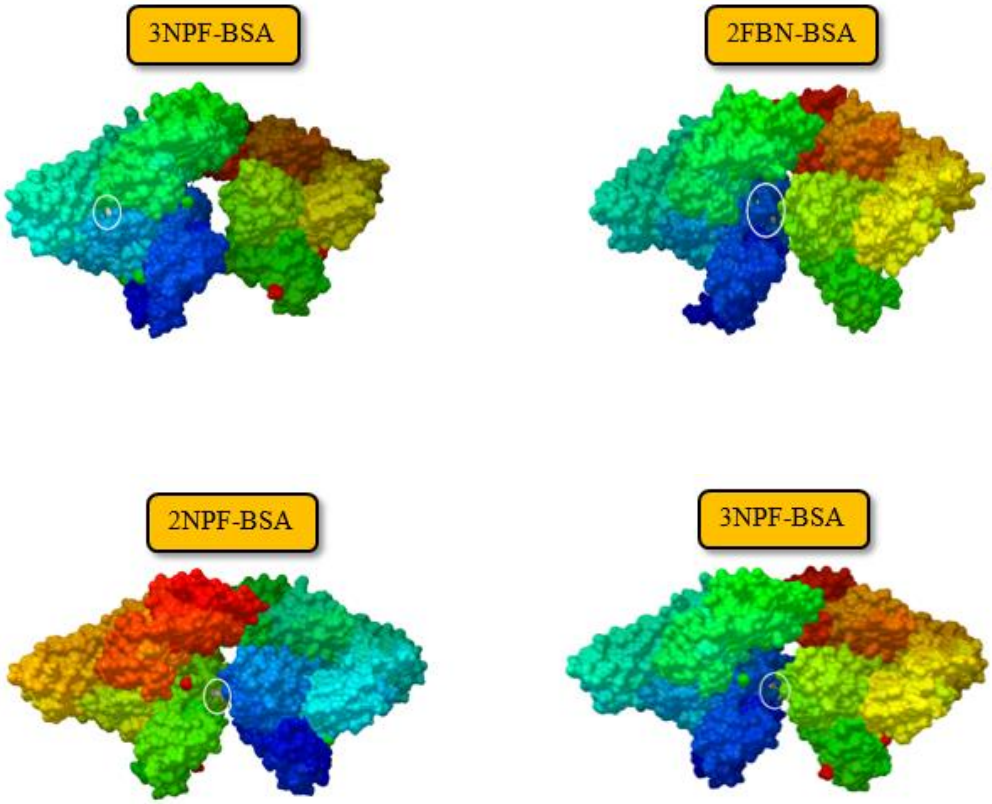

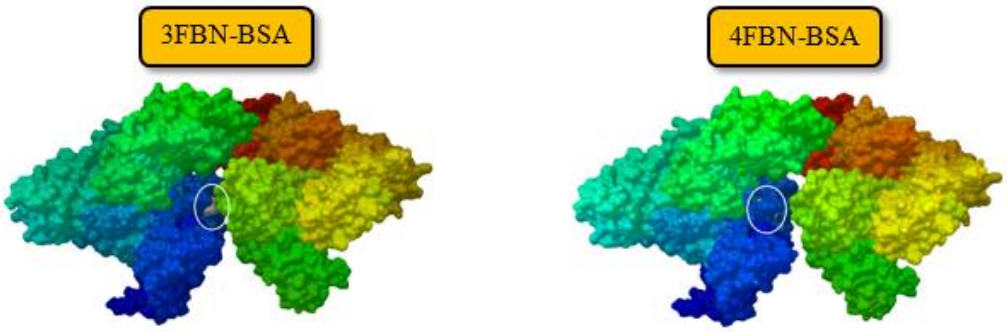

Figure 60: Best docking poses of ligands (white color within a circle) NPF and FBN with BSA

Results from molecular docking suggest that hydrogen bonding, hydrophobic forces and π-stacking interaction are involved in the binding process. All the visualizations in Figure 60 illustrate the interaction of NPF and FBN with the nearby residues in the target active site of the BSA structure. The interacting residues, distances, and type of interactions are summarized in Tables 18, 19 and 20.

Table 18: Hydrophobic interactions between the ligands NPF and FBN with BSA

Sample code	Residue	Amino acid	Distance (Å)
2NPF	122B	LEU	3.83
	125B	GLU	3.85
	133B	PHE	3.21
	136B	LYS	3.29
	136B	LYS	3.81
	136B	LYS	3.45
	137B	TYR	3.90
	140B	GLU	3.50
3NPF	133A	PHE	3.23
	136A	LYS	3.45
	136A	LYS	3.59
	136A	LYS	2.97
	140A	GLU	3.49
	160A	TYR	3.92
4NPF	197A	LEU	3.26
	213A	TRP	2.84
	213A	TRP	2.58
	346A	LEU	3.54

	480A	LEU	2.98
	480A	LEU	3.18
	480A	LEU	3.08
	480A	LEU	2.70
	483A	ARG	3.67
	483A	ARG	3.11
2FBN	115A	LEU	3.41
	117A	PRO	3.41
	122A	LEU	2.92
	136A	LYS	3.37
	136A	LYS	3.83
	137A	TYR	3.98
	137A	TYR	3.82
	137A	TYR	3.42
	140A	GLU	3.59
	160A	TYR	3.30
3FBN	115A	LEU	3.96
	115A	LEU	3.45
	117A	PRO	3.72
	137A	TYR	3.38
	160A	TYR	3.81
	115A	LEU	3.96
4FBN	115A	LEU	3.10
	122A	LEU	3.02
	136A	LYS	3.15
	136A	LYS	3.07
	137A	TYR	3.39
	137A	TYR	3.67
	137A	TYR	3.44
	140A	GLU	3.47
	141A	ILE	3.28
	160A	TYR	3.50

Table 19: Hydrogen bonds between ligands NPF, FBN and BSA

Sample code	Residue	Amino acid	Distance H-A (Å)	Distance D-A (Å)
2NPF	136B	LYS	2.19	3.09
3NPF	132A	LYS	1.79	2.79
	136A	LYS	3.26	3.85
4NPF	201A	SER	2.33	3.20
4FBN	185A	ARG	2.09	3.01

Table 20: π-stacking interactions between ligands NPF, FBN and BSA

Sample code	Residue	Amino acid	Distance H-A (Å)
2FBN	133A	PHE	3.81
	160A	TYR	5.24
4FBN	133A	PHE	3.91

The studied derivatives of 3NPF, 4NPF, 2FBN, 3FBN, 4FBN attached with BSA via chain A; while 2NPF is attached via chain B.

The compound 2NPF formed one hydrogen bond between the amino acid residues lys-136 as a donor and the polar group of the ligand (nitro group). The same ligand interacted through hydrophobic interactions with the residues Glu140, lys-136, Tyr-160, Phe-133, (Figure 61.a).

The nitro function of 3NPF attached with amino groups of residues Lys-132 and Lys-136 via two hydrogen bonds and the global structure of 3NPF interacted with the residues Glu140, lys-136, Tyb-130, Phe-133 via hydrophobic forces (Figure 61.b).

The studied ligand 4NPF binds with BSA at the residue Ser-201 by one hydrogen bond. Furthermore, 4NPF linked with charged residues Trp -213, Leu-346, Ser-201, Leu-197, Arg-483, Leu-480 by hydrophobic interactions (Figure 61.c).

The conformation 2FBN-BSA established in the presence of two forces; π-stacking formed between polar residues Phe-133 and Tyr-160 with benzene and cyclopentadienyl rings are also contributing to hydrophobic forces. The target residues are: Pro-117, Leu-115, Glu-140,Lys-136, Leu-122, Tyr-160, Tyr-137 and the charged locations of 2FBN (Figure 61.d).

The complex 3FBN-BSA formed by only hydrophobic binding force between residues Tyr-160, Pro-117, Leu-115, Tyr-137 and the studied ligand (Figure 61.e).

The high affinity of 4FBN toward the specific binding pocket of BSA was generated by three kinds of force: (1) hydrophobic interactions between 4FBN and the residues Leu -115, Glu-140, Ile-141, lys-136, Tyr-160, Tyr-137, Leu-122; (2) hydrogen bonding between the residues Arg-185 and nitrile group of 4FBN, (3) π-stacking force among the ring of Phe-133 and cyclopentadienyl ring of 4FBN (Figure 61.f).

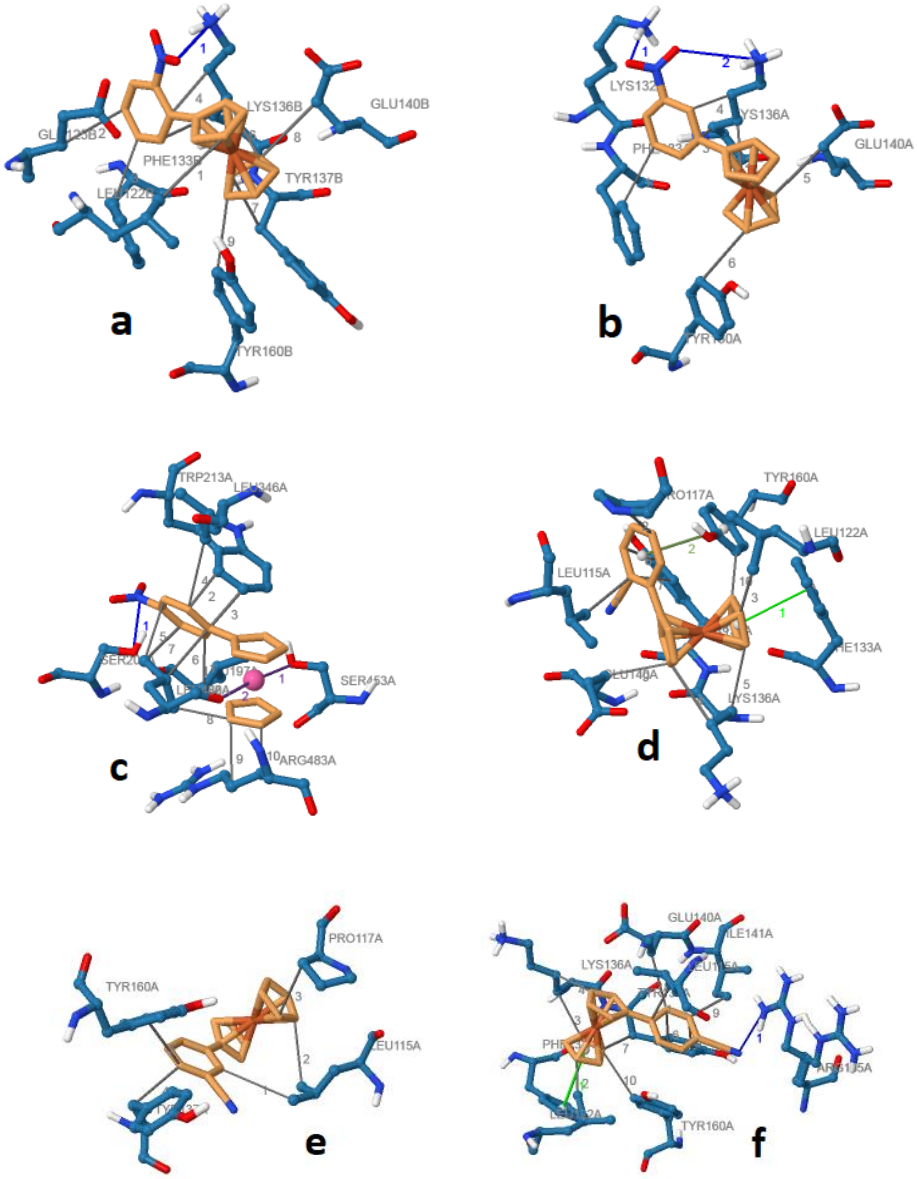

Figure 61: Best docking poses for (a) 2NPF-BSA, (b) 3NPF-BSA (c) 4NPF-BSA (e) 2FBN-BSA (f) 3FBN-BSA and (g) 4FBN-BSA generated with PLIP web server

Elements colors: hydrogen, oxygen, nitrogen, and iron are represented in white, red, blue and brown reflectively. **Color code:** Hydrogen bonds: Bleu lines, Hydrophobic interaction: Gay lines, π-Cation Interaction beige line.

All the adduct attachments of NPF-BSA and FBN-BSA are highly elucidated in Figure 61 using PLIP and also gave a good representation for non-covalent interactions surrounding the ligands NPF and FBN.

Table 21: Binding parameters (k and ΔG) of NPF and FBN compounds obtained from CV, UV-vis and docking methods

Method	CV		Uv-vis		Docking	
Complex	$K(M^{-1})$	$-\Delta G\ (KJ.mol^{-1})$	$K(M^{-1})$	$-\Delta G\ (KJ.mol^{-1})$	$K(M^{-1})$	$-\Delta G\ (KJ.mol^{-1})$
2NPF-BSA	4.89×10^{4}	26.77	2.73×10^{4}	25.33	4.53×10^{4}	26.58
3NPF-BSA	3.16×10^{5}	31.40	5.92×10^{4}	27.39	5.56×10^{4}	27.09
4NFP-BSA	1.15×10^{4}	23.18	3.48×10^{4}	25.93	1.28×10^{4}	25.54
2FBN-BSA	7.41×10^{5}	33.51	2.03×10^{5}	30.32	5.77×10^{5}	31.68
3FBN-BSA	2.08×10^{4}	24.66	3.39×10^{4}	25.83	1.65×10^{4}	24.16
4FBN-BSA	2.96×10^{5}	31.11	2.19×10^{5}	30.49	2.99×10^{5}	31.64

Table 21 clearly displays that the molecular docking results are in good agreement with the results obtained from the experimental assays.

Chapter 6

Antioxidant activity evaluation

1. Antioxidant activity study

1.1. $O_2^{-\cdot}$ free radical scavenging assay

This investigation focused on estimating the antioxidant capacity of our studied compounds NPF and FBN and determining their binding parameters against $O_2^{-\cdot}$ (ΔG, k_b, IC_{50} and k_{ox}/k_{red}). The obtained results from the present study can provide new information about the chemical effect of the nitro and nitrile functions and their positions through the reactions of the ligands with $O_2^{-\cdot}/O_2$ redox couple. Also, the cyclic voltammetric method has been essentially used to give the binding characterizations of the basic form of studied ligands. Many papers related to the antioxidant capacity evaluation of compounds based ferrocene showed high antioxidant potency against the generated free radical ($O_2^{-\cdot}$).

1.1.1. Cyclic voltammetric investigation

When adding NPF or FBN to the saturated solution by oxygen, the anodic and cathodic potential values of $O_2^{-\cdot}/O_2$ redox couple are shifted toward more negative values. This shift indicated the formation of a complex between the studied compounds and $O_2^{-\cdot}/O_2$ redox couple. Furthermore, a significant decreasing in the anodic current peak was also noticed following the addition of the studied samples. This decrease in anodic current peak was used to calculate the binding parameters. Both compounds NPF and FBN are attached to $O_2^{-\cdot}$ by electrostatic forces. The obtained findings of half-maximal inhibitory concentration (IC_{50}) with calculated binding factors guide us to know the compound with higher antioxidant activity and which one must be enhanced to improve their antioxidant capacity. Figure 62 represents the voltammograms of electrochemical assays of superoxide anion radical for 2FBN, 3FBN, 4FBN, 2NPF, 3NPF and 4NPF in DMSO solution at a fixed scan rate[34-35].

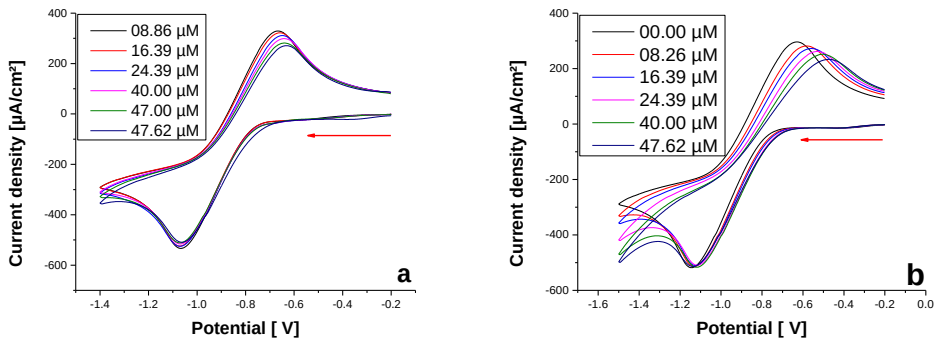

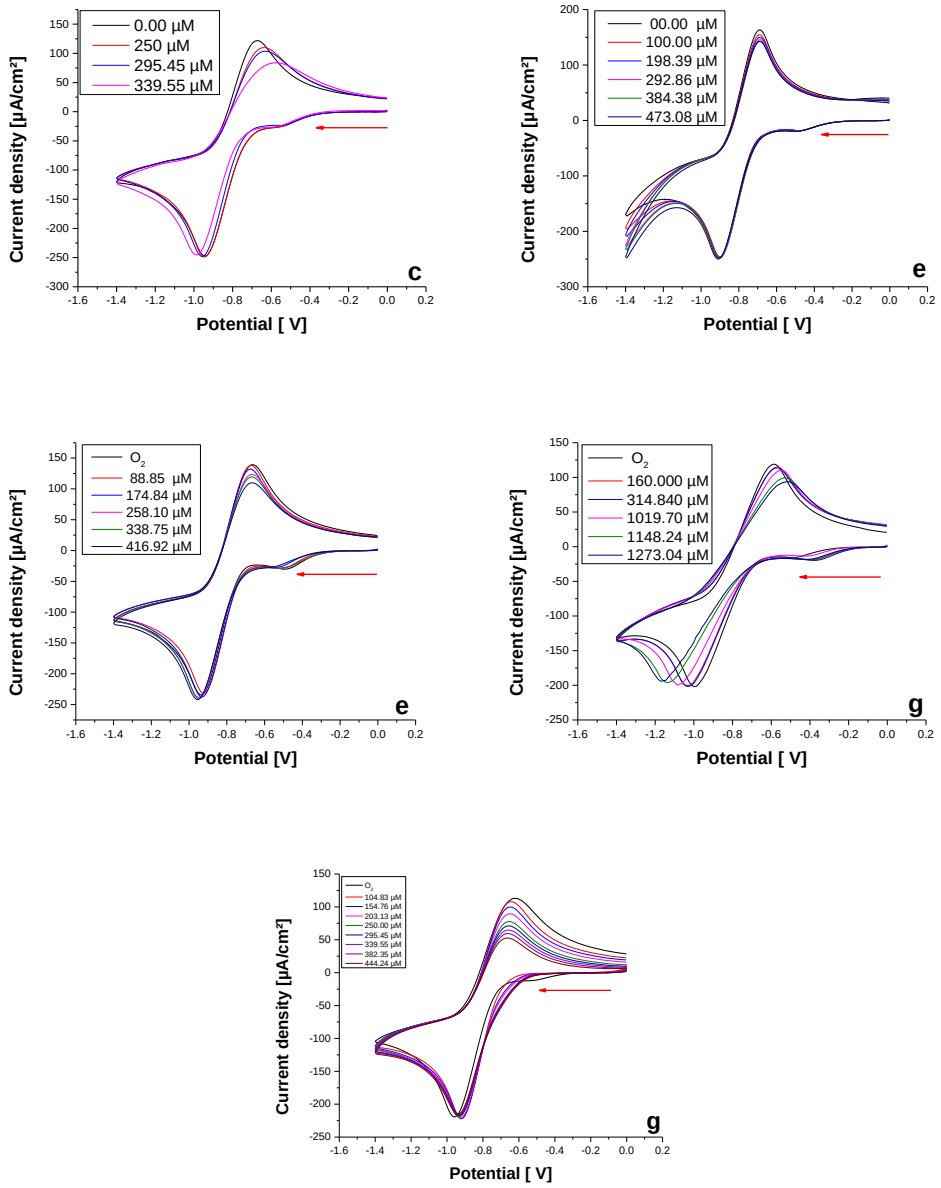

Figure 62: Cyclic voltammograms of $O_2^{-\cdot}$ with 0.18 M of 2NPF(a), 3NPF(b), 4NPF(c) , 2FBN(c) , 3FBN(c), 4NPF(d) and acid gallic (g) measured at a scan rate 0.1V s^{-1} on GC disk electrode at 298K with supporting electrolyte 0.1 M Bu_4NBF_4

The experimental data of all the studied compounds showed a remarkable diminution in the anodic peak current [36]. Meanwhile, their antioxidant capacities are shown in Figure 62 and could be due to presence of the nitro and nitrile groups in the ferrocene moiety.

1.1.1.1. Binding constant

The concentrations of NPF and FBN added to the saturated solution by oxygen gave rise to making up the complexes NPF_$O_2^{-\cdot}$ and FBN_$O_2^{-\cdot}$. The kinetic behaviours of studied compounds are affected by this formation furthermore their obtained anodic peak current values were employed to calculate the k_b.

The application of the following equation gave the binding parameter mentioned above [37].

$$log\frac{1}{C} = logk + log\frac{i}{i_0 - i} \qquad (2.10)$$

Where C represents the concentration of studied ligand (mol.L^{-1}), k is the binding constant in L.mol^{-1}, i_0 and i are the anodic peaks current density in the free and $O_2^{-\cdot}$ bound compounds. All the plots of NPF and FBN are represented in Figure 63.

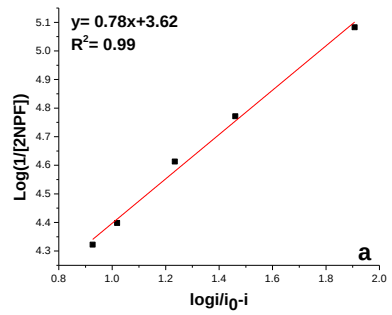

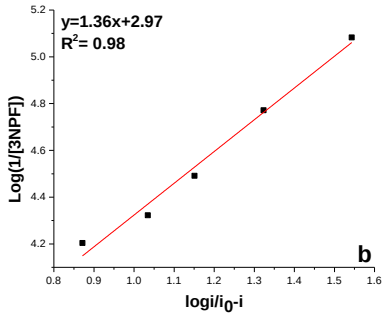

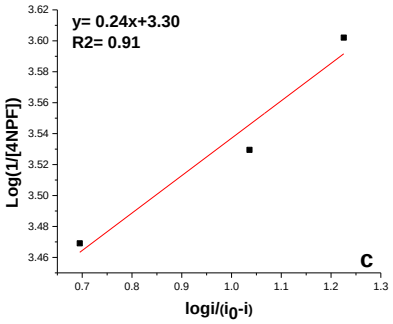

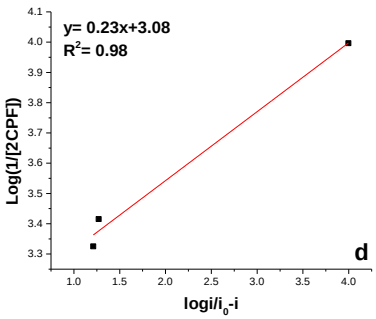

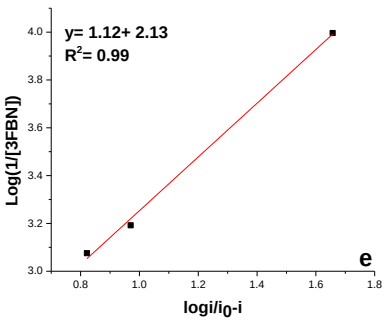

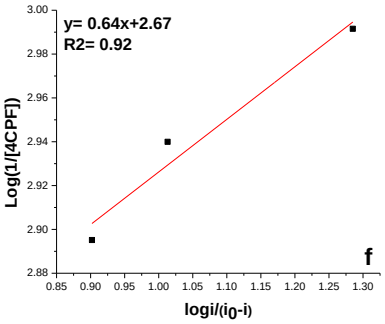

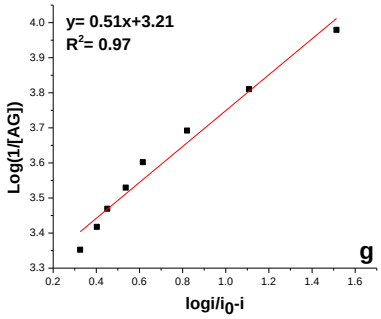

Figure 63: Plots of log 1/[C] versus log1/(1-(i/i_0-i)) used to calculate the binding constants of ligands NFP and BNF with $O_2^{-\cdot}$ ((a) 2NPF, (b) 3NPF, (c) 4NPF, (d) 2BNF, (e) 3BNF, (f) 4BNF and (g) GA.

1.1.1.2. Binding free Gibbs energy

The thermodynamic value ΔG was also calculated using the equation (2.11)[38]:

The values of ΔG and k have been obtained by the application of equation (2.11) with the resulted electrochemical data of the studied ligands and Gallic acid in coupled with superoxide ions.

Table 22: k_b and ΔG values of compounds NPF and FBN with $O_2^{-\cdot}$ obtained from CV assay at T=298 K

Complex	K(M-1)	-ΔG (KJ.mol-1)
2NFP- O_2^{-}	4.17×103	20.67
3NFP- O_2^{-}	9.33×102	16.96
4NFP- O_2^{-}	2.0×104	18.83
2BNF- O_2^{-}	1.2×103	17.58
3BNF- O_2^{-}	1.35×102	12.16
4BNF- O_2^{-}	4.68× 102	15.24
GA_ O_2^{-}	1.74×103	18.50

1.1.1.3. Ratio of binding constants

The decrease in shift anodic current peak (i_{pa}) of NPF and FBN in the presence of $O_2^{-\cdot}$ being accompanied by a shift in anodic potential peak (E_{pa}) to more negative potential values (Figure 76). The constant binding ratio was calculated depending on this electrochemical behavior.

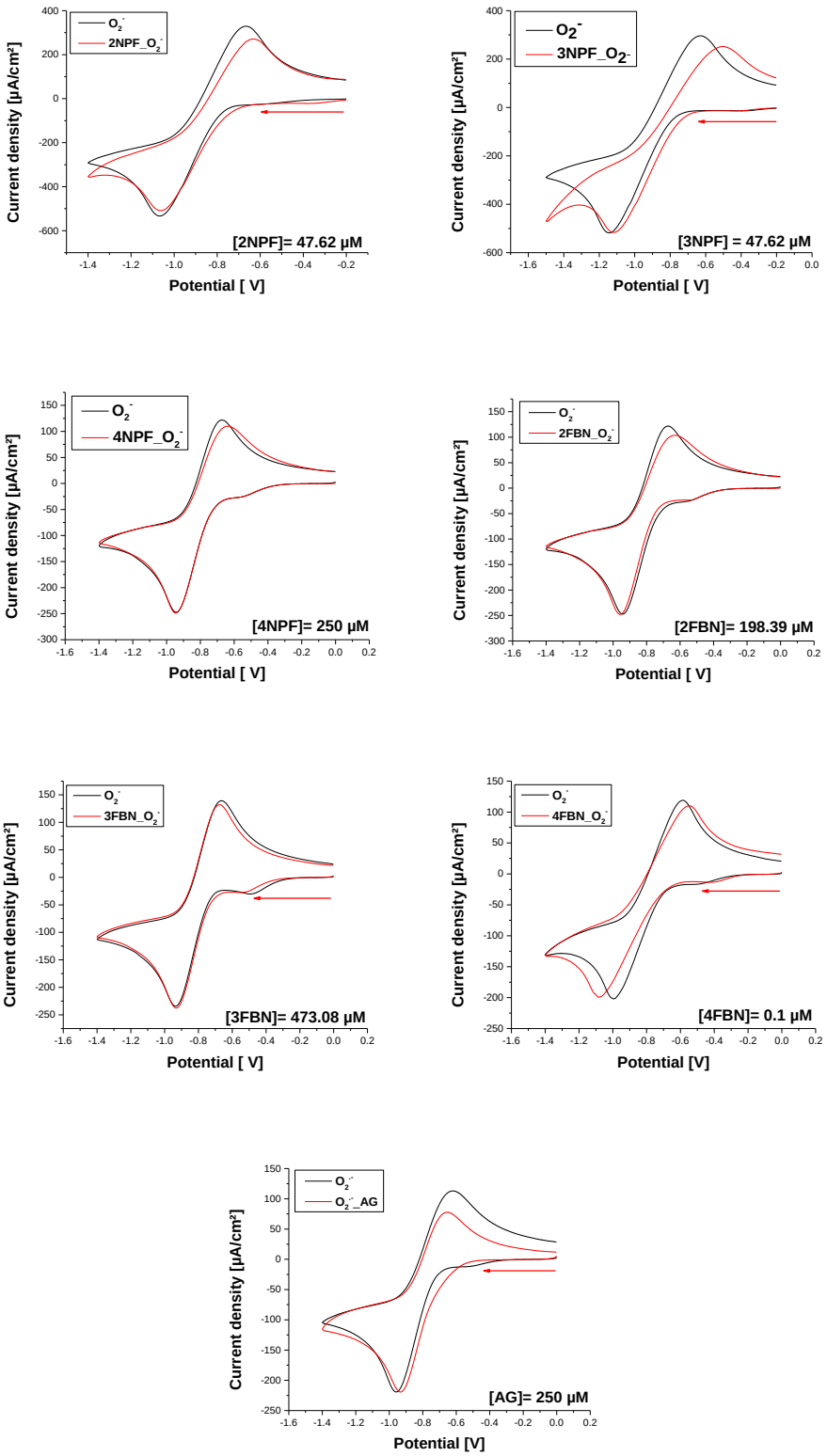

Figure 64: Cyclic voltammograms of $O_2^{-\cdot}$ in the absence (black line) and presence (red line) of 2NPF, 3NPF, 4NPF, 2FBN, 3FBN and 4FBN, 4FBN and GA in DMSO solution at scan rate100 mV.s-^{1} with supporting electrolyte 0.1 M TBATFB on glass carbon electrode

Both values of shift peak potential of NPF and FBN are shifted upon the addition of the studied compound to a saturated solution of O_2 in DMSO; the following equilibriums can be applied,

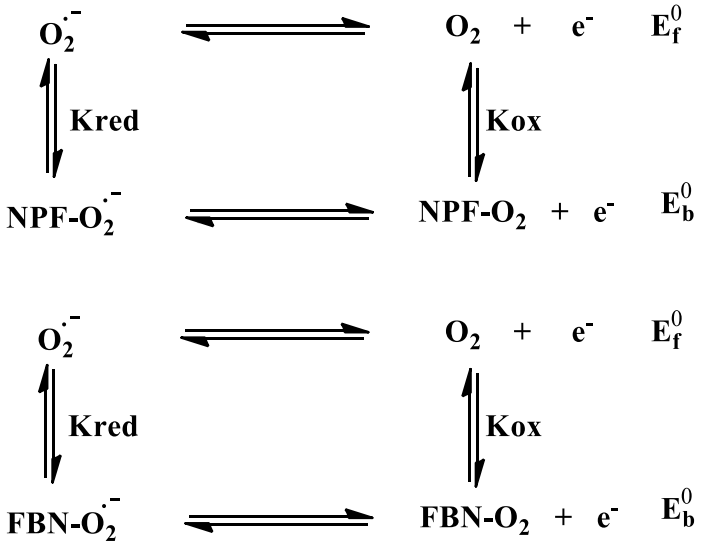

Figure 65: Redox process of $O_2^{-\cdot}$ with the studied compounds

The application of the Nernst relation to the equilibriums of Figure 71 gave the following equations (1,2)[39]:

$$\Delta E^0 = E_f^0 - E_b^0 = E^0(O_2^{-\cdot}) - E^0(O_2^{-\cdot} - NPF) = 0.061\frac{k_{ox}}{k_{red}} \qquad (2.12)$$

$$\Delta E^0 = E_f^0 - E_b^0 = E^0(O_2^{-\cdot}) - E^0(O_2^{-\cdot} - FBN) = 0.061\frac{k_{ox}}{k_{red}} \qquad (2.13)$$

$E_f^0 and E_b^0$ are respectively the formal potentials of the free and O_2 and $O_2^{-\cdot}$ bound compounds. The ΔE^0 estimated depending on the obtained data from the voltammograms in figure 64, and their results are summarized in Table 23. The binding constants ratios were determined using equation (2.12) and (2.13) by replacing ΔE^0 from Table 23.

Table 23: Electrochemical potential data of the free and bound O_2 with NPF and FBN utilized for determination the ratio of the binding constants

Ligand/complex	E_{pa}	E_{pc}	E°(mV)	ΔE°(V)	Kox/Kred
O2-	-0.671	-1.065	-0.868	-0.0105	0.99
2NPF- O2-	-0.637	-1.078	-0.8575		
O2-	-0.631	-1.145	-0.888	-0.09	0.99
3NPF- O2-	-0.476	-1.12	-0.798		

O2-	-0.67	-0.94	-0.805	0.025	0.38
4NPF- O2-	-0.57	-0.99	-0.78		
O2-	-0.7	-0.91	-1.61	-0.0359	0.50
2FBN- O2-	-0.6871	-0.887	-1.5741		
O2-	-0.66	-0.94	-0.8	0.0035	1.15
3FBN- O2-	-0.651	-0.956	-0.8035		
O2-	-0.59	-0.99	-0.79	0.055	8.55
4FBN- O2-	-0.52	-1.17	-0.845		
O2-	-0.62	-0.96	-0.79	0.005	0.82
GA-O2-	-0.655	-0.93	-0.793		

The obtained ratios of the binding constants indicate that both species of $O_2^{-\cdot}/O_2$ redox couple react with 2NPF and 3NPF in similar reactivity. Ligands 4NPF and 2FBN bind slightly stronger with superoxide ion than the oxygen molecule. Furthermore, the calculated K_{ox}/K_{red} values in Table 23 indicated that the oxygen is bound stronger with 3FBN and 4FBN than its reduced form.

1.1.1.4. Diffusion coefficient

Diffusion coefficients can be determined using the Randles-Sevcik Equation (2.5) at T= 298 in the same manner as described in chapter 5.

The electrochemical essays were carried out using the CV method at various scan rates from 0.1 to 0.5 $v.s^{-1}$. Their recorded cyclic voltammograms are represented in Figure 66.

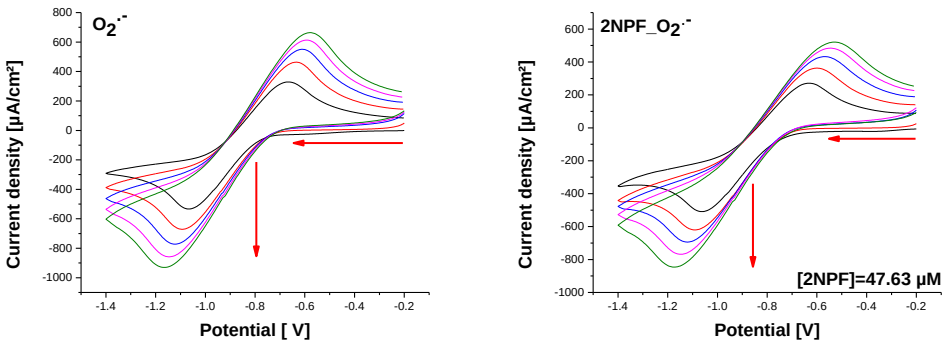

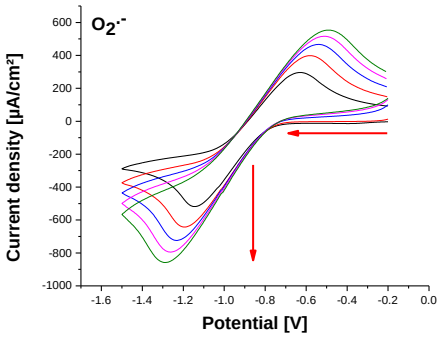
$O_2^{\cdot-}$
Current density [µA/cm²]
Potential [V]

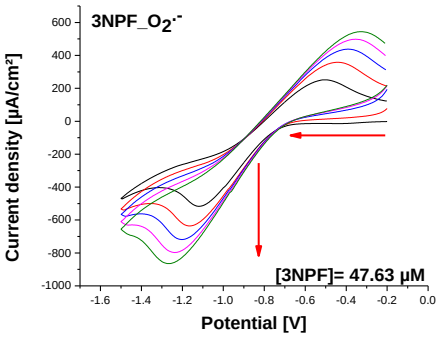
3NPF_$O_2^{\cdot-}$
[3NPF]= 47.63 µM
Current density [µA/cm²]
Potential [V]

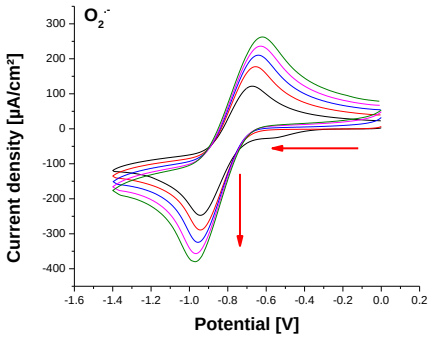
$O_2^{\cdot-}$
Current density [µA/cm²]
Potential [V]

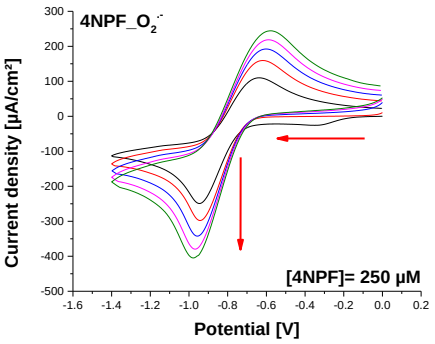
4NPF_$O_2^{\cdot-}$
[4NPF]= 250 µM
Current density [µA/cm²]
Potential [V]

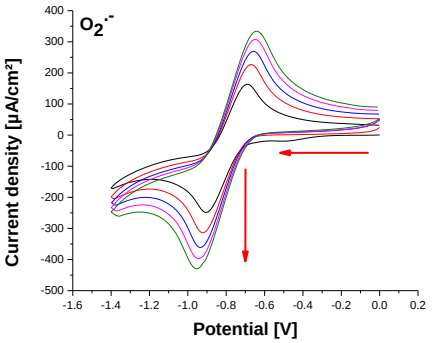
$O_2^{\cdot-}$
Current density [µA/cm²]
Potential [V]

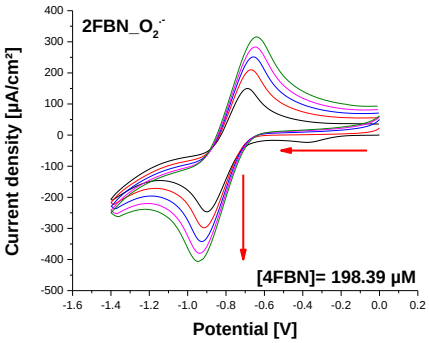
2FBN_$O_2^{\cdot-}$
[4FBN]= 198.39 µM
Current density [µA/cm²]
Potential [V]

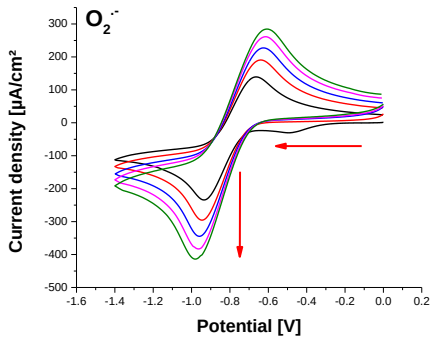
$O_2^{\cdot-}$
Current density [µA/cm²
Potential [V]

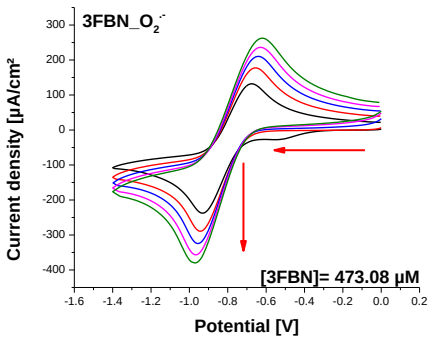
3FBN_$O_2^{\cdot-}$
[3FBN]= 473.08 µM
Current density [µA/cm²
Potential [V]

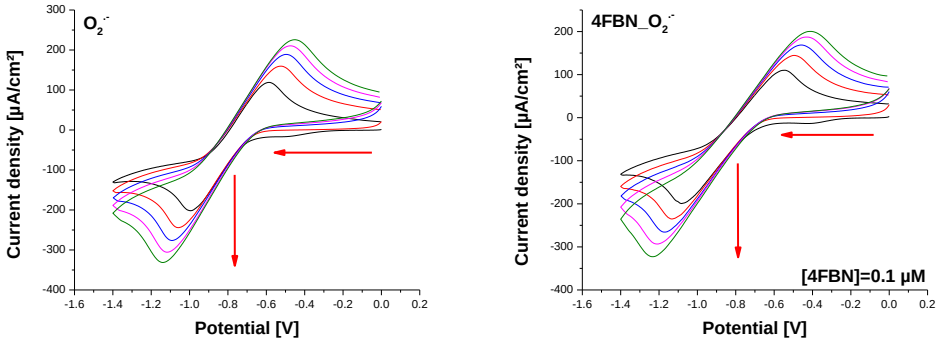

Figure 66: Cyclic voltammograms of $O_2^{-\cdot}$ in the absence and presence of increasing concentrations of NPF and FBN in DMSO at scan rates 100,200,300,400 and 500 mV.s-1 with supporting electrolyte 0.1 M TBATFB on GC electrode

The values of anodic and cathodic currents of NPF and FBN increased according to the scan rates that have been used to monitor the diffusion phenomena. The change in anodic peaks and scan rates are increased together in a stable and organized electrochemical behaviour. Straight lines were obtained on plotting the anodic current peak values versus square root of scan rates. This linear relationship indicates that the electrochemical process is diffusion-controlled reaction (Figure 67); the diffusion coefficients values are listed in Table 24.

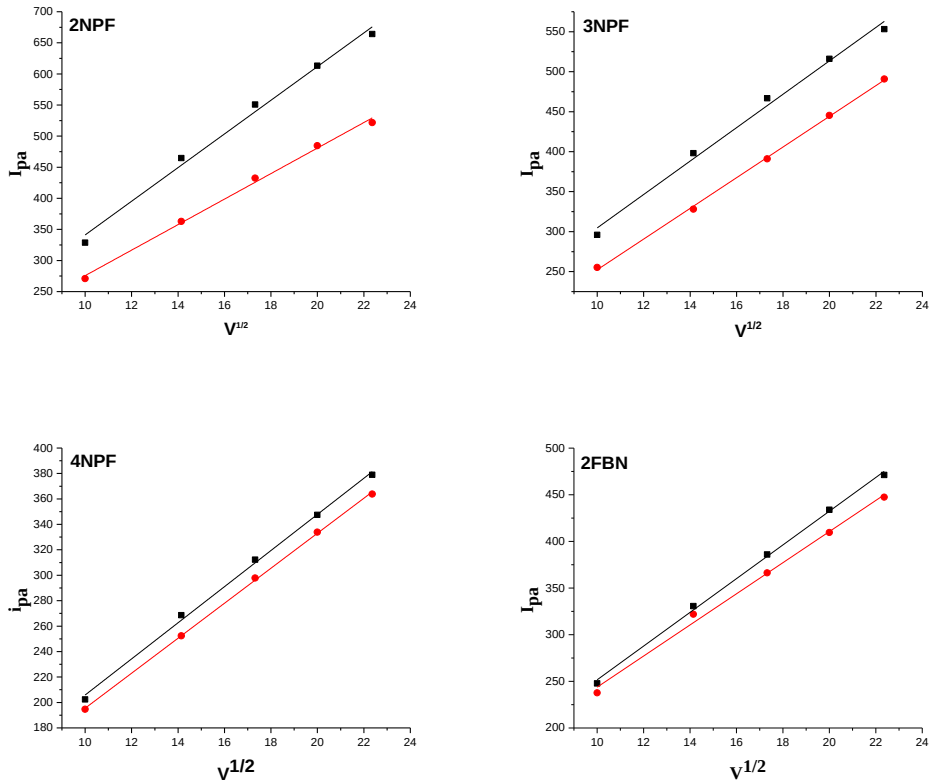

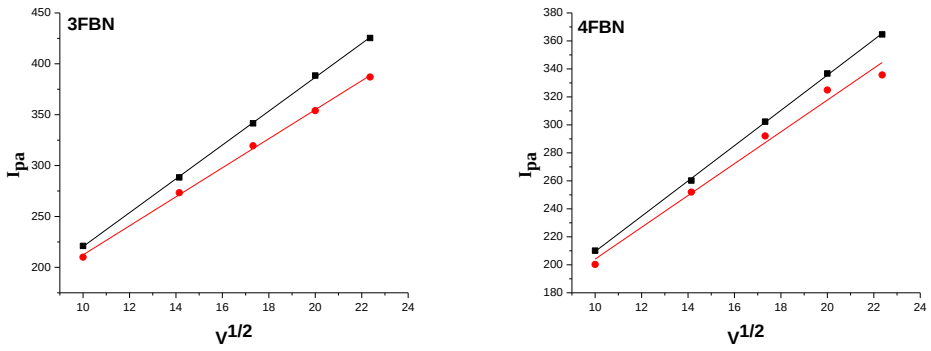

Figure 67: I_{pa} as function with $v^{1/2}$ plots of $O_2^{-\cdot}$ in the absence (black lines) and presence of NPF and FBN (red lines) at scan rates ranging from 0.1 to 0.5 Vs^{-1} under the same conditions of Figure 66

All diffusion coefficients of the derivatives NPF and BNF with their corresponding complexes NPF-$O_2^{-\cdot}$ and BNF-$O_2^{-\cdot}$ are listed in Table 24.

Table 24: Diffusion coefficients of the free and bound cases of $O_2^{-\cdot}$ with NPF and FB

$O_2^{-\cdot}$ / ligand_$O_2^{-\cdot}$	Equation	R^2	D(cm2.s-1)
$O_2^{-\cdot}$	y = 27.07x + 70.50	0,99	5.99×10^{-5}
2NPF-$O_2^{-\cdot}$	y = 20.51x + 70.49	0,99	3.44×10^{-5}
$O_2^{-\cdot}$	y = 20.89x + 95.74	0,99	3.57×10^{-5}
3NPF-$O_2^{-\cdot}$	y = 19.19x + 60.41	0,99	3.01×10^{-5}
$O_2^{-\cdot}$	y = 14.20x + 63.88	0,99	1.65×10^{-5}
4NPF-$O_2^{-\cdot}$	y = 13.75x + 57.96	0,99	1.54×10^{-5}
$O_2^{-\cdot}$	y = 18.07x + 70.91	0,99	2.67×10^{-5}
2BNF-$O_2^{-\cdot}$	y = 16.68x + 76.98	0,99	2.28×10^{-5}
$O_2^{-\cdot}$	y = 16.63x + 54.14	0,99	2.26×10^{-5}
3BNF-$O_2^{-\cdot}$	y = 14.26x + 69.64	0,99	$1,66\times10^{-5}$
$O_2^{-\cdot}$	y = 12.60x + 83.50	0,99	1.30×10^{-5}
4BNF-$O_2^{-\cdot}$	y = 11.37x + 90.45	0,99	$1,06\times10^{-5}$

As general observation, the comparison between the diffusion values of $O_2^{-\cdot}$ and $O_2^{-\cdot}$ -ligand can be summarized in the order $D_{(O_2^{-\cdot})} > D_{(O_2^{-\cdot}\_ligand)}$.

1.1.1.5. half-maximal inhibitory concentration (IC_{50})

In vitro assays, the value IC_{50} represents the concentration (mg/mL) of the examined bio-compound that having a potential to inhibit 50 % of the active oxygen ($O_2^{-\cdot}$) that existed initially in the studied meduim[40].

The shift in anodic current peaks of the free and $O_2^{-\cdot}$ bound compounds were used to determine the IC_{50} values. The equation (2.14) was used to plot I % versus different ligand concentrations.

$$\%\ O_2^{-\cdot} radical\ scavenging\ activity = \frac{i_{pa_0} - i_{pa}}{i_{pa_0}} x100 \qquad (2.14)$$

Where $i_{pa_0} and\ i_{pa}$ are respectively the anodic current peaks of active oxygen the absence and present of increasing concentrations of studied ligands. The equations obtained from the linear calibration graph in the studied concentration range for NPF, FBN are summarized in Table 25. Linear regression of all studied compounds and their plots are represented in Figure 74. The IC_{50} values and the equations of NPF and FBN are also listed in Table 25.

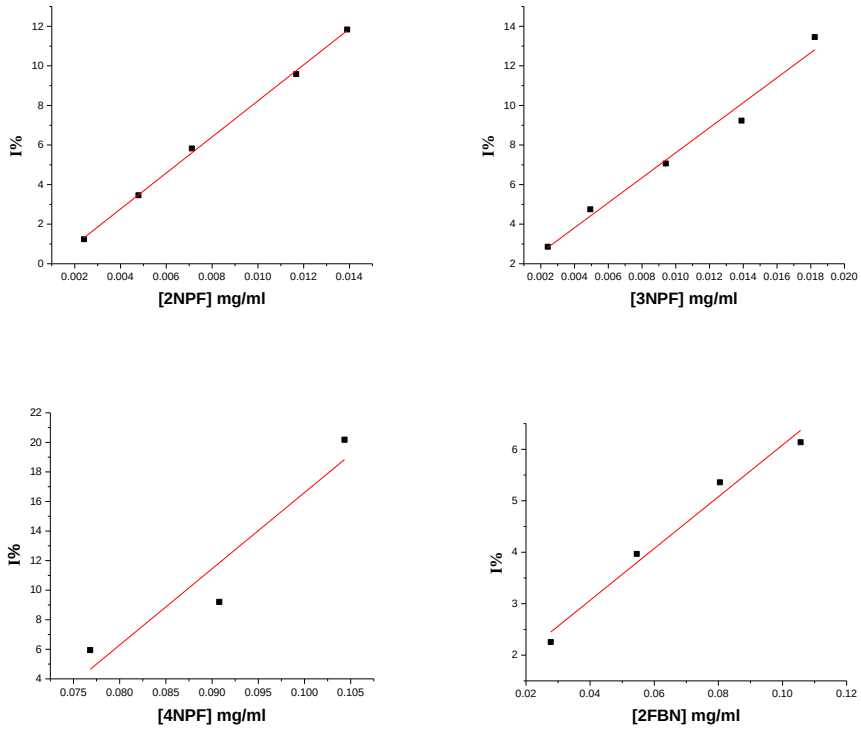

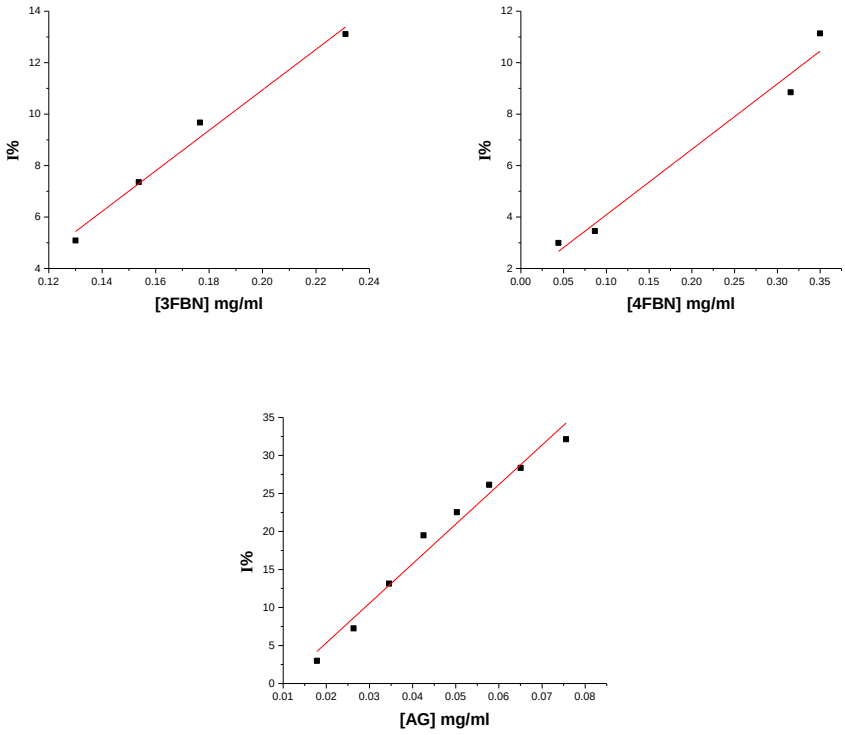

Figure 68: Typical plots of I% as a function of C (mg/ml) used for calculation the IC_{50} values of ligands NPF and FBN with $O_2^{-\cdot}$

Table 25: IC_{50} values of the studied compounds and AG

Compound	Equation	R2	IC_{50} [mg/ml]
2NPF	y = 910.88x -0.88	0.99	0.06
3NPF	y = 631.85x +1.29	0.99	0.08
4NPF	y = 543.02x -34.974	0.81	0.16
2FBN	y = 50.3x +1.05	0.97	0.97
3FBN	y = 78.66x-4.79	0.98	0.70
4FBN	y = 25.45x+1.54	0.96	1.90
GA	y=520.42x-5.06	0.97	0.11

The analysis of obtained IC_{50} values from the $O_2^{-\cdot}$ scavenging activity assays indicated that all the studied compounds have an excellent antioxidant effect; which were in the order 2NPF > 3NPF > GA > 4NPF > 3FBN> 2FBN> 4FBN, thus, these compounds represent strong candidates as antioxidant agents.

1.2. DPPH free radical scavenging assay

After evaluating the antioxidant capacity of NPF and FBN using the electrochemical assays, the antioxidant properties were also measured using spectroscopic assays. In this regard, DPPH has been used. Moreover, the gradual increase in compounds concentrations led to decrease of DPPH absorption with a slight shift in their wavelengths; these observations were exploited to calculate the binding parameters ΔG, k_b and IC_{50}.

1.2.1. Uv-visible investigation

The spectra-forms in Figure 75 have been recorded according to the increasing additions of studied compounds with reference compound (DPPH) in a quartz cell. Also, the same figure shows a large decrease in the shift absorption values of studied ligands, which clearly indicates their high reactivity with DPPH radical [41].

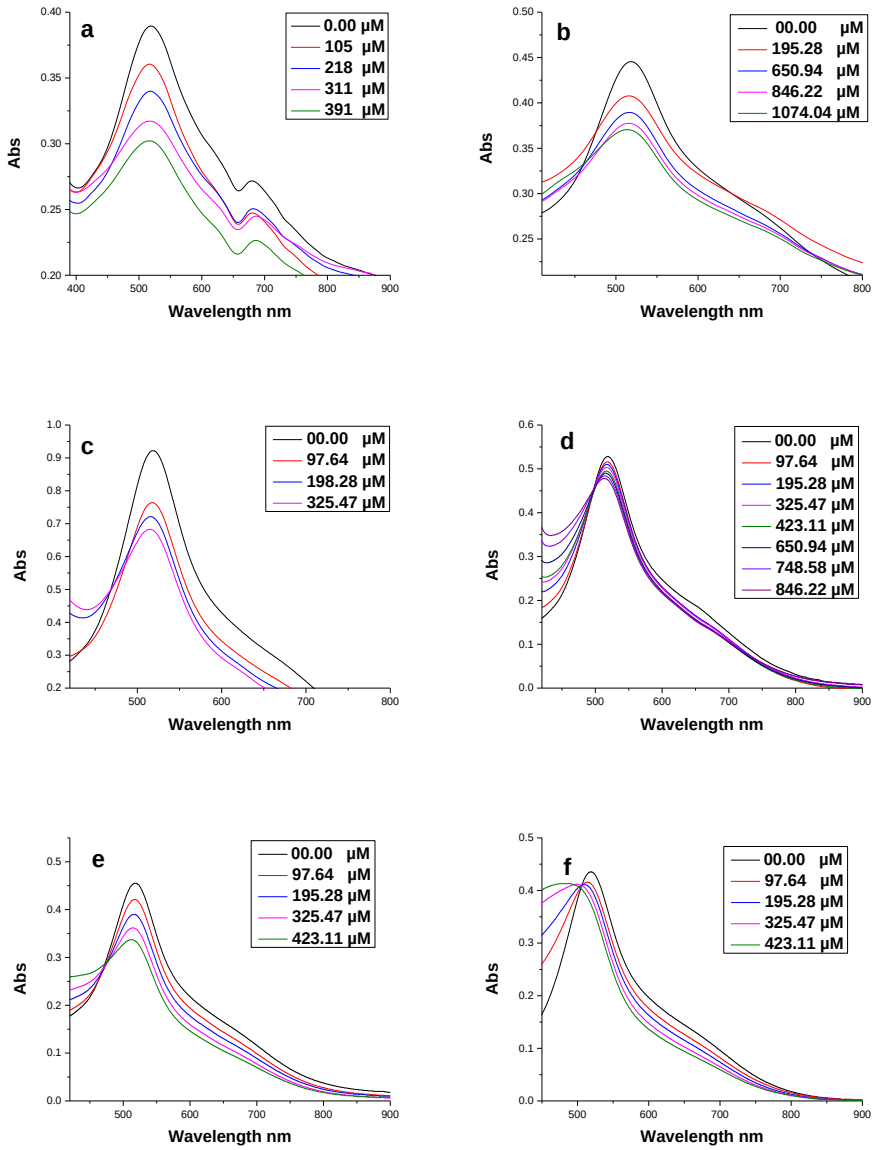

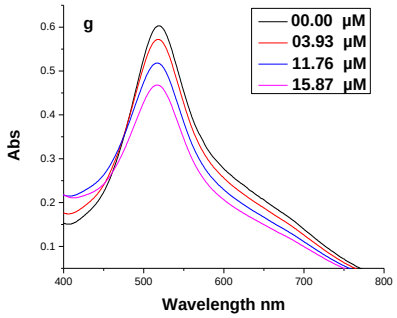

Figure 69: UV-visible spectrums of DPPH solution in the absence and presence increasing concentrations of 2NPF (a), 3NPF (b), 4NPF (c), 2FBN (d), 3FBN (e) 4FBN (f) and GA (g) in acetonitrile at room temperature: 298 K

1.2.1.1. Binding constant

The shift absorption values obtained from the increased additions of NPF and FPN were used to determine the intrinsic binding constant by applying the following equation [42].

$$\frac{A_0}{A-A_0} = \frac{\varepsilon_G}{\varepsilon_{H-G}-\varepsilon_G} + \frac{\varepsilon_G}{\varepsilon_{H-G}-\varepsilon_G}\frac{1}{K_b[C]} \qquad (2.15)$$

Where K_b represents the binding constant; C is the concentration of the studied compounds; ε_G *and* ε_{H-G} are the extinction coefficients of DPPH and DPPH-ligand solutions respectively; A_0 and A are DPPH absorption in the absence and presence NPF and FBN respectively. K_b was obtained from the intercept to slope ratio of the plot of $A_0/A\text{-}A_0$ as function with 1/[**C**], Figure 70.

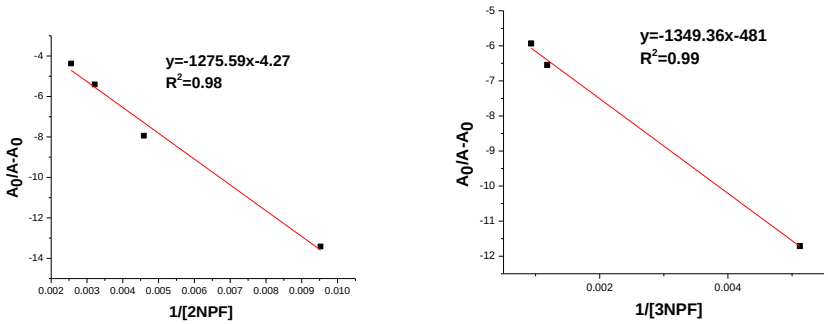

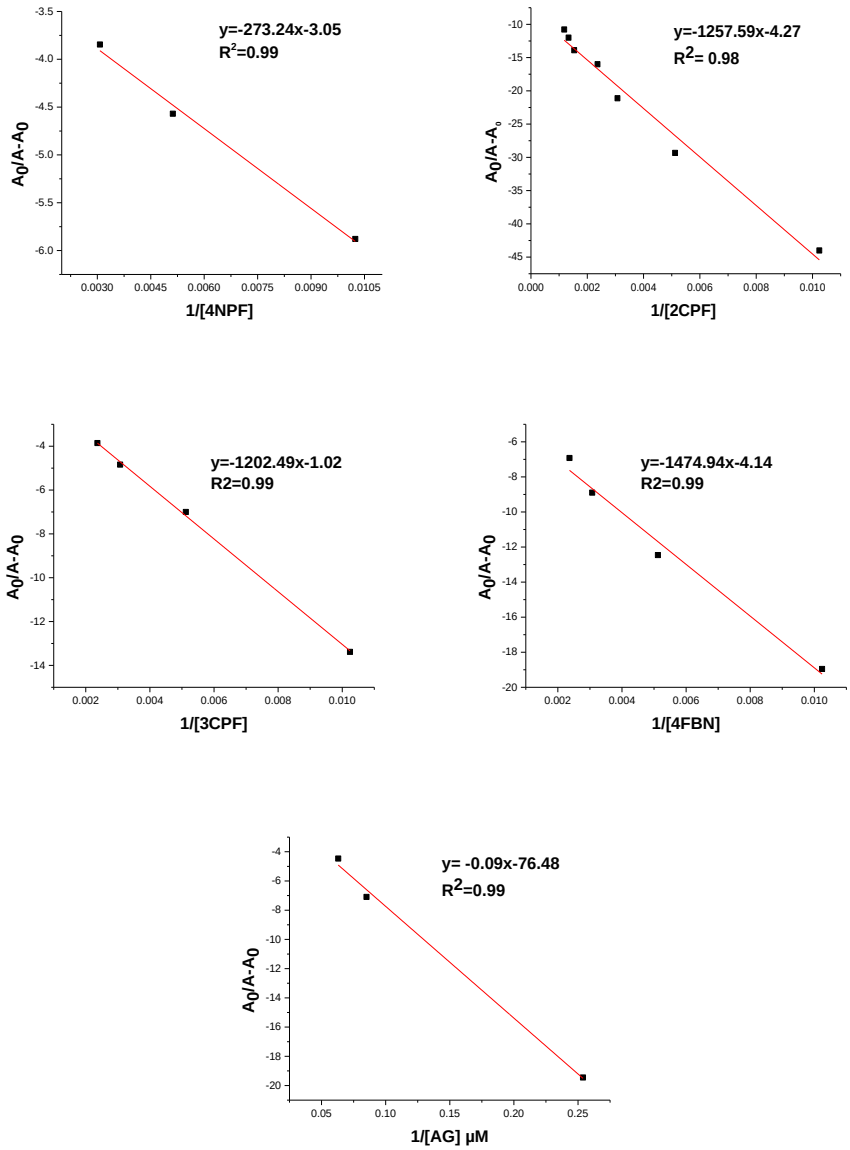

Figure 70: Plots of $A_0/A\text{-}A_0$ versus 1/[C] used for the calculation of binding constants of ligands NFP and BNF with DPPH

1.2.1.2. Binding free Gibbs energy

The values of ΔG were determined using equation (2.2), previously applied in chapter 5, the calculated binding free Gibbs energy values are listed in the following table.

Table 26: k_b and ΔG values of compounds NPF and FBN with DPPH obtained from spectroscopic assays at T= 298 K

Complex	K(M^{-1})	-ΔG(KJ.mol^{-1})
2NFP_DPPH	1.13×10^3	17.43
3NFP_DPPH	3.56×10^3	20.28
4NFP_DPPH	1.1×10^4	23.06
2FBN_DPPH	2.21×10^3	19.10
3FBN _DPPH	8.48×10^2	16.72
4FBN _DPPH	2.8×10^3	19.69
GA_DPPH	1.18×10^3	17.53

The results shown in Table 26 confirm the spontaneity of the reaction between ligands and DPPH.

1.2.1.3. Half-maximal inhibitory concentration (IC_{50})

The obtained experimental data from DPPH scavenging activity assays of NPF and FBN were also used to access their IC_{50}values. Based on equation (2.16), the maximum absorption values obtained from kinetic curves against the different compound concentrations were utilized to estimate IC_{50}values of the studied ligands.

$$\%\, DPPH radical scavenging activity = \frac{A_0 - A}{A_0} \text{x} 100 \qquad (2.16)$$

Where A_0 and A represent DPPH absorbance in the absence and presence NPF and FBN respectively.

The IC_{50} values and the equations obtained from the linear calibration graph of NPF and FBN are shown in Figure 77.

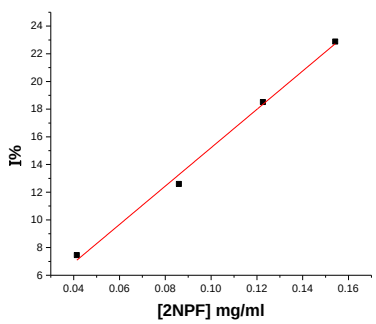

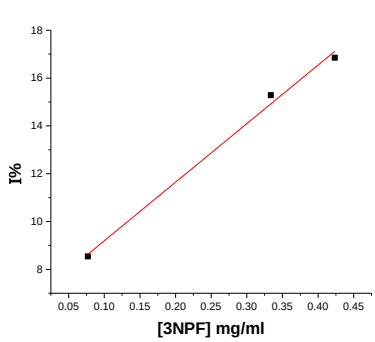

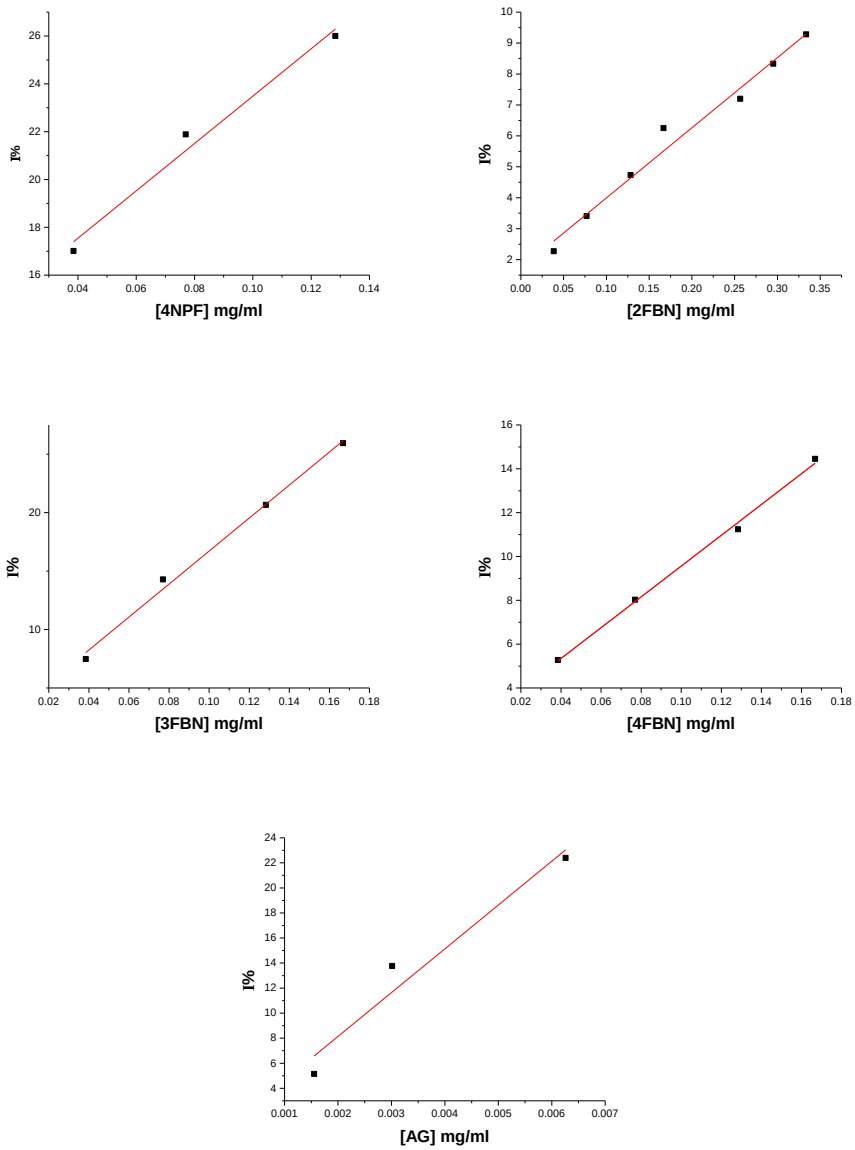

Figure 71: Typical plots of I% as a function of C (mg/ml) used for calculation the IC_{50} values of ligands NPF and FBN with DPPH

Table 27: IC_{50} values of the studied compounds and GA

Compound	Equation	R^2	IC_{50} [mg/ml]
2NPF	y = 138.63x+1.35	0.99	0.35
3NPF	y = 24.5x+6.75	0.98	1.77
4NPF	y = 99.02x+13.58	0.97	0.37
2FBN	y=22.67x+1.73	0.98	2.13
3FBN	y=141.13x+2.60	0.99	0.34
4FBN	y=70.25x+2.60	0.99	0.68
GA	y=3497.70x+1.14	0.91	0.01

As denoted in Table 27, the order of the antioxidant efficacy is GA> 3FBN > 2NPF > 4NPF > 4FBN > 3NPF > 2FBN. It is observed that compound 3FBN has the best reactivity against DPPH radical in these two series.

1. Ali, S., Din, I.U., Kamal, S., & Altaf, A.A. (2013). DNA interaction, antibacterial and antifungal studies of 3-nitrophenylferrocene. Journal of the Chemical Society of Pakistan, 35(3), 923-929.2. Lanez, T.; Pauson, P. L., Ferrocene derivatives. Part 25. Their use in the synthesis of 5H-cyclopenta[c]quinolines and 5,6-dihydro-5-azabenz[e]azulenes. Journal of the Chemical Society, Perkin Transactions 1 1990, (9), 2437-2442.
3. Chérifa, B., Abdehamid, K., Belgacem, T., & Touhami, L. (2015). Synthesis and Electrochemical Properties of N-(Ferrocenylmethyl)Aminobenzonitrile and N-(Ferrocenylmethyl)Nitroaniline Derivatives. International Letters of Chemistry, Physics and Astronomy, 49, 27-34.
4. T. Lanez, Synthesis of pyridine and cyclopent[c] azepine derivatives by photochemical and acid- catalyzed degradation of substituted ferrocenes, thèse de doctorat, university of Strathclyde, (1989).
5. Deweese, Joseph E., and Neil Osheroff. "The DNA cleavage reaction of topoisomerase II: wolf in sheep's clothing." Nucleic acids research 37.3 (2009): 738-748.
6. Gagne, R. R.; Koval, C. A.; Lisensky, G. C., Ferrocene as an internal standard for electrochemical measurements. *Inorganic Chemistry* **1980,***19* (9), 2854-2855.
7. Hussain, R. A.; Badshash, A.; Sohail, M.; Lal, B.; Altaf, A. A., Synthesis, chemical characterization, DNA interaction and antioxidant studies of ortho, meta and para fluoro substituted ferrocene incorporated selenoureas. *Inorganica Chimica Acta* **2013,***402*, 133-139.
8. Sai Krishna, A. D.; Panda, G.; Kondapi, A. K., Mechanism of action of ferrocene derivatives on the catalytic activity of topoisomerase IIα and β—Distinct mode of action of two derivatives. *Archives of Biochemistry and Biophysics* **2005,***438* (2), 206-216.
9. Carpi, F. M.; Di Pietro, F.; Vincenzetti, S.; Mignini, F.; Napolioni, V., Human DNA extraction methods: patents and applications. *Recent patents on DNA & gene sequences* **2011,***5* (1), 1-7.
10. Mardan-Nik, M.; Saffar Soflaei, S.; Biabangard-Zak, A.; Asghari, M.; Saljoughian, S.; Tajbakhsh, A.; Meshkat, Z.; Ferns, G. A.; Pasdar, A.; Ghayour-Mobarhan, M., A method for improving the efficiency of DNA extraction from clotted blood samples. *J Clin Lab Anal* **2019,***33* (6), e22892-e22892.
11. Price, C. W.; Leslie, D. C.; Landers, J. P., Nucleic acid extraction techniques and application to the microchip. *Lab on a chip* **2009,***9* (17), 2484-94.
12. Boom, R.; Sol, C. J.; Salimans, M. M.; Jansen, C. L.; Wertheim-van Dillen, P. M.; van der Noordaa, J., Rapid and simple method for purification of nucleic acids. *Journal of clinical microbiology* **1990,***28* (3), 495-503.
13. Vijayalakshmi, R.; Kanthimathi, M.; Subramanian, V.; Nair, B. U., DNA cleavage by a chromium (III) complex. *Biochemical and biophysical research communications* **2000,***271* (3), 731-734.
14. Shah, A.; Qureshi, R.; Janjua, N. K.; Haque, S.; Ahmad, S., Electrochemical and spectroscopic investigations of protonated ferrocene-DNA intercalation. *Analytical Sciences* **2008,***24* (11), 1437-1441.
15. Pešić, M.; Bugarinović, J.; Minić, A.; Novaković, S. B.; Bogdanović, G. A.; Todosijević, A.; Stevanović, D.; Damljanović, I., Electrochemical characterization and estimation of DNA-binding capacity of a series of novel ferrocene derivatives. *Bioelectrochemistry* **2020,***132*, 107412.
16. Hussain, R. A.; Badshah, A.; Sohail, M.; Lal, B.; Akbar, K., Synthesis, chemical characterization, DNA binding and antioxidant studies of ferrocene incorporated selenoure. *Journal of Molecular Structure* **2013,***1048*, 367-374.

17. Lal, B.; Badshah, A.; Altaf, A. A.; Khan, N.; Ullah, S., Miscellaneous applications of ferrocene-based peptides/amides. *Applied Organometallic Chemistry* **2011,***25* (12), 843-855.
18. Aslanoğlu, M.; Öge, N., Voltammetric, UV absorption and viscometric studies of the interaction of norepinephrine with DNA. *Turkish Journal of Chemistry* **2005,***29* (5), 477-485.
19. Shah, A.; Zaheer, M.; Qureshi, R.; Akhter, Z.; Nazar, M. F., Voltammetric and spectroscopic investigations of 4-nitrophenylferrocene interacting with DNA. *Spectrochimica Acta Part A: Molecular and Biomolecular Spectroscopy* **2010,***75* (3), 1082-1087.
20. Ismail, M. B.; Booysen, I. N.; Akerman, M. P., Oxorhenium (V) complexes with bidentate carbohydrazide Schiff bases: synthesis, characterization and DNA interaction studies. *Transition Metal Chemistry* **2017,***42* (5), 405-412.
21. Husain, M. A.; Sarwar, T.; Rehman, S. U.; Ishqi, H. M.; Tabish, M., Ibuprofen causes photocleavage through ROS generation and intercalates with DNA: a combined biophysical and molecular docking approach. *Physical Chemistry Chemical Physics* **2015,***17* (21), 13837-13850.
22. Terenzi, A.; Barone, G.; Silvestri, A.; Giuliani, A. M.; Ruggirello, A.; Liveri, V. T., The interaction of native calf thymus DNA with FeIII-dipyrido [3, 2-a: 2′, 3′-c] phenazine. *Journal of inorganic biochemistry* **2009,***103* (1), 1-9.
23. Lanez, E.; Bechki, L.; Lanez, T., Computational molecular docking, voltammetric and spectroscopic DNA interaction studies of 9N-(ferrocenylmethyl) adenine. *Chemistry & Chemical Technology, 1 (13), 2019* **2019,** (1), 11-17.
24. Sirajuddin, M.; Ali, S.; Badshah, A., Drug–DNA interactions and their study by UV–Visible, fluorescence spectroscopies and cyclic voltametry. *Journal of Photochemistry and Photobiology B: Biology* **2013,***124*, 1-19.
25. Arshad, N.; Abbas, N.; Bhatti, M. H.; Rashid, N.; Tahir, M. N.; Saleem, S.; Mirza, B., Synthesis, crystal structure, DNA binding and in vitro biological studies of Ni(II), Cu(II) and Zn(II) complexes of N-phthaloylglycine. *Journal of Photochemistry and Photobiology B: Biology* **2012,***117*, 228-239.
26. Lanez, T.; Benaicha, H.; Lanez, E.; Saidi, M., Electrochemical, spectroscopic and molecular docking studies of 4-methyl-5-((phenylimino) methyl)-3H-and 5-(4-fluorophenyl)-3H-1, 2-dithiole-3-thione interacting with DNA. *Journal of Sulfur Chemistry* **2018,***39* (1), 76-88.
27. Sun, L.; Zhang, J.; Liu, K., Electrochemical investigation of ascorbic acid interacting with bovine serum albumin. *Analytical letters* **2007,***40* (16), 3050-3059.
28. Khennoufa, A.; Bechki, L.; Lanez, T.; Lanez, E.; Zegheb, N., Spectrophotometric, voltammetric and molecular docking studies of binding interaction of N-ferrocenylmethylnitroanilines with bovine serum albumin. *Journal of Molecular Structure 1224*, 129052.
29. Correa, R. S.; de Oliveira, K. M.; Delolo, F. G.; Alvarez, A.; Mocelo, R.; Plutin, A. M.; Cominetti, M. R.; Castellano, E. E.; Batista, A. A., Ru (II)-based complexes with N-(acyl)-N′, N′-(disubstituted) thiourea ligands: synthesis, characterization, BSA-and DNA-binding studies of new cytotoxic agents against lung and prostate tumour cells. *Journal of inorganic biochemistry* **2015,***150*, 63-71.
30. Chu, X.; Shen, G.-L.; Jiang, J.-H.; Kang, T.-F.; Xiong, B.; Yu, R.-Q., Voltammetric studies of the interaction of daunomycin anticancer drug with DNA and analytical applications. *Analytica chimica acta* **1998,***373* (1), 29-38.
31. Ramadevi, P.; Singh, R.; Jana, S. S.; Devkar, R.; Chakraborty, D., Ruthenium complexes of ferrocene mannich bases: DNA/BSA interactions and cytotoxicity against A549 cell line. *Journal of Photochemistry and Photobiology A: Chemistry* **2015,***305*, 1-10.

32. Suryawanshi, V. D.; Walekar, L. S.; Gore, A. H.; Anbhule, P. V.; Kolekar, G. B., Spectroscopic analysis on the binding interaction of biologically active pyrimidine derivative with bovine serum albumin. *Journal of Pharmaceutical Analysis* **2016,***6* (1), 56-63.
33. Sebastian Salentin, Sven Schreiber, V. Joachim Haupt, Melissa F. Adasme, Michael Schroeder, PLIP: fully automated protein–ligand interaction profiler, Nucleic Acids Research, Volume 43, Issue W1, 1 July 2015, Pages W443–W447.
34. Wani, T. A.; Bakheit, A. H.; Ansari, M. N.; Al-Majed, A.-R. A.; Al-Qahtani, B. M.; Zargar, S., Spectroscopic and molecular modeling studies of binding interaction between bovine serum albumin and roflumilast. *Drug Des Devel Ther* **2018,***12*, 2627-2634.
35. Manjushree, M.; Revanasiddappa, H. D., A Diversified Spectrometric and Molecular Docking Technique to Biophysical Study of Interaction between Bovine Serum Albumin and Sodium Salt of Risedronic Acid, a Bisphosphonate for Skeletal Disorders. *Bioinorganic Chemistry and Applications* **2018,***2018*, 6954951.
36. Lanez, T.; Henni, M.; Hemmami, H., DEVELOPMENT OF CYCLIC VOLTAMMETRIC METHOD FOR THE STUDY OF THE INTERACTION OF ANTIOXIDANT STANDARDS WITH SUPEROXIDE ANION RADICALS CASE OF [alpha]-TOCOPHEROL. *Scientific Study & Research. Chemistry & Chemical Engineering, Biotechnology, Food Industry* **2015,***16* (2), 161.
37. Lanez, T.; Henni, M., Antioxidant activity and superoxide anion radical interaction with 2-(ferrocenylmethylamino) benzonitrile and 3-(ferrocenylmethylamino) benzonitrile. *Journal of the Iranian Chemical Society* **2016,***13* (9), 1741-1748.
38. Ahmed, S.; Shakeel, F., Antioxidant activity coefficient, mechanism, and kinetics of different derivatives of flavones and flavanones towards superoxide radical. *Czech Journal of Food Sciences* **2012,***30* (2), 153-163.
39. Lanez, Elhafnaoui, Lazhar Bechki, and Touhami Lanez. "Antioxidant Activities, Binding Parameters, and Electrochemical Behavior of Superoxide Anion Radicals Twords 1-Ferrocenylmethylthymine and 1-Ferrocenylmethylcytosine." Current Physical Chemistry 10.1 (2020): 10-22.
40. Carter, M. T.; Rodriguez, M.; Bard, A. J., Voltammetric studies of the interaction of metal chelates with DNA. 2. Tris-chelated complexes of cobalt (III) and iron (II) with 1, 10-phenanthroline and 2, 2'-bipyridine. *Journal of the American Chemical Society* **1989,***111* (24), 8901-8911.
41. Lanez, T.; Henni, M., Determination of binding parameters of 2-(Ferrocenylmethylamino) Benzonitrile and 3-(Ferrocenylmethylamino) Benzonitrile WITH 1, 1-Diphenyl-2-Picrylhydrazyl free radical. *Journal of Fundamental and Applied Sciences* **2016,***8* (1), 176-181.
42. Shao, J.; Zhao, T.; Ma, H.-P.; Jia, Z.-P.; Jing, L.-L., Synthesis, Characterization, and Antioxidant Activity of 8-Hydroxygenistein. *Natural Product Communications* **2020,***15* (1), 1934578X20901399.

Experimental

Chemicals and reagents

The aprotic solvent, dimethyl sulfide (DMSO) analytical grade from Sigma-Aldrich, acetonitrile (ACN) HPLC-grade from Sigma-Aldrich, N,N-dimethylformamide (DMF) analytical grade from PROLABO; were employed as solvents without further purification for cyclic voltammetry and absorption spectroscopic experiments. All other common laboratory chemicals are analytical grade.

Molecular oxygen was provided from a cylinder (research grade (99.99%) from the company Linde gas Algérie. BSA was obtained from Merck and used as received, while its concentration was determined by the extinction coefficient of 44300 M^{-1} cm^{-1} at 280 nm. DNA was isolated from chicken blood by salting out procedure and stored at 4 °C until use.

2,2-diphenyl-1-picrylhydrazyl (DPPH) (99 %) purchased from Alfa Aesar, tetrabutylammoniumtetrafluoroborate (Bu_4NBF_4) (electrochemical grade (99 %)) Sigma-Aldrich) was employed as supporting electrolyte and its concentration was kept 0.1 M. Ferrocene (98%) was purchased from Fluka. Ortho, Para and Meta amino-benzonitriles (95%) purchased from Alfa Aesar. Sodium nitrite ($NaNO_2$) (99%) and Magnesium sulfate ($MgSO_4$) were purchased from commercial provider.

Melting points were determined using a melting point apparatus (obtained from Gallenkamp) and are uncorrected.

Instrument and Methods

3.2. Cyclic voltammetry assays

All electrochemical assays were conducted using a PGZ301 voltammeter running on VoltaMaster 4 V 7.08 software (Radiometer Analytical SAS, France). The supporting electrolyte concentration was kept at 0.1 M for all measurements, which were conducted under an inert atmosphere by bubbling nitrogen gas through the studied medium. Experiments were run with a one-compartment three-electrode system containing a glassy carbon (GC) working electrode with a geometric area of 0.013 cm^2, a platinum wire as a counter (auxiliary) electrode and Hg/Hg_2Cl_2 paste covered wire as a reference electrode.

Both studies the binding affinity of ferrocene derivatives towards DNA and BSA were carried out in similar voltammetric manipulation steps, firstly, before adding DNA or BSA, the electrochemical behaviours of all ligands were recorded in fixed scan rate (100 mV/s) and a chosen concentration of ligands ranging from 10^{-1} to 10^{-3} M, additionally, the studied medium

containing NPF and FBN was also recorded in various scan rates: 200, 300,400,500 $mV.s^{-1}$. Secondly, solutions of ligands were subjected to increasingly additions of DNA or BSA concentrations, each addition was followed by recording the voltammograms at the same scan rates ranging from 100 to 500 mV/s. The experimental data obtained from free or DNA-bound and BSA-bound ligands were utilized to estimate the following binding parameters K_b, ΔG, K_{ox}/K_{red}, D, IC_{50}.

In the section of binding capacity evaluation for ferrocene derivatives against a superoxide anion, the testing solution inside the three electrochemical cell has been bubbled by high-purity commercial oxygen for 15 min. A initial stage, the voltammogram of ($O_2^{-\cdot}/O_2$) couple was recorded in 100, 200, 300, 400 and 500 mV/s scan rate, after that, the addition of each concentration of studied ligand into the studied medium led to the decrease in shift anodic current peaks of obtained voltammograms and have been recorded with the scan rates which are mentioned above.

3.3. UV-Visible assays

Absorption spectra measurements were conducted on a UV-Vis spectrometer, (Shimadzu 1800, Japan), using the cell of length 3 cm.

Experimental kinetic monitoring was achieved with a Pentium IV (CPU 4.0 GHz and RAM 2 Gb) microcomputer by means of UV probe software version 2.34 (Shimadzu). The mathematical relationship between variables can be summarized in specific equations conducted by OriginLab software version 2.0 (Integral Software, France). Kinetic characterization assays of each designed compound were carried out in a particular concentration and all of them dissolved in DMSO at ambient temperature.

Both binding titration assays of DNA or BSA with ferrocene derivatives series were exploited to record their electronic UV-VIS behaviours in free and bound states. The obtained experimental data from the spectrums in two states were utilized to determine the binding parameters: Kb, ΔG.

In vitro evaluation of antioxidant ferrocene derivatives capacities with DPPH radical were studied in the same experimental conditions:

C_{DPPH}= 3.17x10^{-4} M and T= 298 k. The UV-VIS response of DPPH either obtained in the absence or presence studied ferrocene ligands were employed to calculate the spectroscopic binding parameters (K_b, ΔG, IC_{50}) that obtained from the application of the following (x, y)

variables: (1) $A_0/A-A_0$ versus 1/[C], (2) I % versus$[C]_{mg/ml}$; the first variables used for calculating the values of binding constants and binding free gibbs energy as well as the second one utilized for determination IC_{50} values.

Geometry optimization and docking setup

The structures of the two series FBN and NPF were geometrically optimized by Gaussian 09 program package, by means of density functional theory (DFT) and the B3LYP level of theory with 6-311++G(d,p) basis set. The molecular semi-docking calculations were performed using AutoDock 4.2 docking software; also, all theoretical procedures were executed on a Pentium 2.20 GHz and RAM 4.00 Go microcomputer MB memory with windows 10 operating system.

The crystalline structure codes of DNA and BSA are (PDB ID: 1bna and 4f5s), they were provided from Protein Data Bank (http://www.pdb.org). For the docking section, Lamarckian genetic algorithms enclosed the target part from protein (DNA or BSA) in specific grid points. Their coordination are listed in Table A, and B as well as a point number separated by 1.000 Å and the grid spacing is 0.3751 Å, the typical sizes (x,y,z) of the grid boxes set and also summarized in Table A and B. Docking experiments are flexibility conducted in various docking number-runs (Table A and B) with 150 random individuals and the maximum number of energy evaluation is 2,500,000; the other parameters were left without changing, and a step size of 0.375 centred on the binding sites of two proteins, the best-docked complexes were chosen based on the lower value of binding docking energy. After completing the docking calculations, different ΔG values are being accompanied by ligand-DNA or ligand-BSA adducts. The best poses of ligands attached with target protein pockets were used for intramolecular attachments analysis.

Table A. Coordination and parameters for BSA docking simulations

Compound code	Coordination of Grid Centre			Grid size (Å)		
	X	Y	Z			
2NPF	14.78	20.976	8.807	50	90	100
3NPF	14.78	20.976	8.807	60	80	100
4NPF	34.015	13.966	47.484	60	60	60
2FBN	34.89	23.99	98.76	126	70	100
3FBN	26.774	28.605	96.09	40	40	40
4FBN	34.892	23.991	98.761	126	70	100

Table B. Coordination and parameters for DNA docking simulations

Compound code	Coordination of Grid Centre			Grid size (Å)		
	X	Y	Z			
2NPF	14.78	20.976	21.143	40	40	40
3NPF	14.78	20.976	8.807	50	60	90
4NPF	14.78	20.976	8.807	80	80	80
2FBN	14.166	20.109	-1.090	50	50	50
3FBN	14.78	20.976	8.807	100	80	100
4FBN	14.78	20.976	8.807	80	80	80

PLIP is a visualization web server and currently plays a key step in many modelling interactions studies as well as it has an extraordinary performance with docked complexes additionally the interacting information that can be provided from this procedure follows: binding types, (1) hydrogen bonds, (2) water bridges, (3) salt bridges, (4) halogen bonds, (5) hydrophobic interactions, (6) π-stacking, (7) π-cation interactions.

(It represented in different colours); bond length (between a target residue and studied ligand); Amino acid identifications: name, number code and chain (A or B in BSA).

Experimental Procedures

Our interest is to evaluate a series of ferrocene derivatives that may help chemical scientists find out strong candidates having high efficacy against various types of human diseases.

1- Para-ferrocenylbenzonitril

Para-ferrocenylbenzonitril (4FBN) was readily synthesized based upon the method of Lanez et al[3]. and its electrochemical and spectroscopic characterizations are summarized in the following table:

Table C. Electrochemical and spectroscopic parameters obtained from CV and UV-vis essays of 4FBN

Compound	CV characteristics						
4FBN	**I_{pa}(µA)**	**I_{pc}(µA)**	**$\lvert I_{pa}/I_{pc} \rvert$**	**$E_{1/2}$**	**E_{pa} (mV)**	**E_{pc}(mV)**	**E_{pa}-E_{pc}**
	32.99	-31.6	1.04	582.635	619.69	545.58	74.11
	UV-vis characteristics						
	λ_{max}		**Abs**		**Transition type**		

	460	1.74	n⟶π*

2- Ortho-ferrocenylbenzonitril

Ortho-ferrocenylbenzonitril (2FBN) was readily prepared based on the method of Lanez et al[3], and its electrochemical and spectroscopic characterizations are summarized in the following Table D.

Table D. Electrochemical and spectroscopic parameters obtained from CV and UV-vis essays of 2FBN

Compound	CV characteristics						
2FBN	**I_{pa}(µA)**	**I_{pc}(µA)**	**$\lvert I_{pa}/I_{pc}\rvert$**	**$E_{1/2}$**	**E_{pa} (mV)**	**E_{pc}(mV)**	**E_{pa}-E_{pc}**
	3.93	-3.78	1.04	397.66	435.33	359.99	75.34
	UV-vis characteristics						
	λ_{max}		**Abs**		**Transition type**		
	437		2.08		n⟶π*		
	350		0.84		π⟶π*		

3- Meta-ferrocenylbenzonitril

The electrochemical and spectroscopic information are listed in following table.

Table E. Electrochemical and spectroscopic parameters obtained from CV and UV-vis essays of 3FBNCompound

	CV characteristics						
3FBN	**I_{pa}(µA)**	**I_{pc}(µA)**	**$\lvert I_{pa}/I_{pc}\rvert$**	**$E_{1/2}$**	**E_{pa} (mV)**	**E_{pc}(mV)**	**E_{pa}-E_{pc}**
	6.74	-7.14	0.94	396.76	443.36	350.16	93.2
	UV-vis characteristics						
	λ_{max}		**Abs**		**Transition type**		
	300		2.59		π⟶π*		

Conclusion

Binzonitrilferrocene derivatives (2FBN, 3FBN, 4FBN) have been successfully prepared by the arylation of ferrocene with the diazonium salts of the corresponding cyanoaniline. In addition, all the prepared compounds have been characterized by electrochemical and spectroscopic techniques.

The antioxidant and anticancer investigations have been concerned for a clear evaluation of the binding ability of two series NPF and FBN with DNA and BSA.

The antioxidant activity of binzonitrilferrocenes and nitropenylferrocnes were evaluated by $O_2^{-\cdot}$ and DPPH free radical scavenging assays. The obtained electrochemical parameters (ΔG, K_b, D) indicated that the superoxide anion radical attached with NPF and FBN by electrostatic forces. The IC_{50} values ranging from 0.06 to 1.9, the least value was for 2NPF. Furthermore, the obtained spectroscopic parameters (ΔG, K_b) indicated the spontaneity of the reaction between $DPPH^{\cdot}$ with NPF and FBN, the range of IC_{50} values obtained from spectroscopic assays was from 0.34 to 2.16, the least value was for 3FBN. In addition, the anticancer activity of NPF and FBN were studied through the increasing concentrations of DNA and BSA using cyclic voltammetry and UV-visible spectroscopic methods. The obtained binding parameters from CV investigation indicated that the nature of the interaction of ferrocene derivatives with DNA and BSA were by non-covalent forces. Furthermore, diffusion coefficients of the free ligands were higher than that of the bound ligand. UV-visible investigation revealed a significant affinity between the studied ligands and DNA, BSA. Molecular docking results further confirmed the interaction of the studied compounds with the targets (DNA, BSA) and also allowed the visualizations of the resulted interactions of ligand-DNA and ligand-BSA complexes.

In this work, two series of NPF and FBN have been successfully evaluated and greatly supports the efforts of researchers to prepare new antioxidant and anticancer drugs that possess more effectively behaviours towards cancer and oxidative stress diseases. In addition, this

would open up the possibility of extending the research to other ferrocene derivatives. Also further studies can be carried out to look at their effects on human organs like cytotoxicity investigations.

Publications

J. Electrochem. Sci. Eng. **10(4)** (2020) 335-346; http://dx.doi.org/10.5599/jese.861

Open Access: ISSN 1847-9286
www.jESE-online.org

Original scientific paper

BSA-binding studies of 2- and 4-ferrocenylbenzonitrile: voltammetric, spectroscopic and molecular docking investigations

Hacen Benamara, Touhami Lanez✉ and Elhafnaoui Lanez

University of El Oued, Chemistry Department, VTRS Laboratory, B.P.789, 39000, El Oued, Algeria

Corresponding author: ✉lanezt@gmail.com; Tel.: +213-661655550

Received: May 29, 2020; Revised: June 11, 2020; Accepted: June 15, 2020

Abstract

The binding affinity of 2-ferrocenylbenzonitrile (2FBN) and 4-ferrocenylbenzonitrile (4FBN) with bovine serum albumin (BSA) has been investigated by cyclic voltammetry, absorption spectroscopy and molecular modelling techniques. The results indicated that both of the two derivatives could bind to BSA and cause conformational changes with the order 2FBN > 4FBN. The voltammetric behavior of 2FBN and 4FBN before and after the addition of BSA suggests that the electrochemical reaction is kinetically controlled by the diffusion step and demonstrated that diffusion coefficients of 2FBN-BSA and 4-FBN-BSA complexes are lower than that of free compounds. Molecular docking suggested that the binding mode of the two compounds to BSA is of hydrophobic and hydrogen bond interactions, moreover the ligand 2FBN additionally show a π-cation interaction.

Keywords

Cyclic voltammetry; ferrocene derivatives; binding constant; interactions; modelling; in silico; in vitro

Introduction

Nitriles and cyanides are compounds containing a -CN functional group in their molecular structure. In nitriles the -CN functional group is attached to an organic structure [1], but in cyanides, it is attached to an inorganic compound [2]. Cyanides are toxic because they denote the highly toxic inorganic salts of hydrogen cyanide, while nitriles are not toxic because they do not release cyanide ions [3,4]. The non-toxic properties of nitriles encouraged researchers to study their pharmaco-chemistry as potential drugs. The prevalence of nitrile-containing drugs shows the biocompatibility of the nitrile functionality [5,6]. Recently many pharmaceuticals drugs containing nitriles are either prescribed for many different types of diseases or are in clinical trial [6].

Nitrile groups are usually known as hydrogen bond acceptors [7-9], many studies show the formation of hydrogen bonding between the nitrogen atom of the nitrile group and amino acids of

protein backbone [10-13]. The bonds are often established between the nitrile and the expected hydrogen bond of the donor serine or arginine amino acids.

Serum albumin is the most important protein in blood plasma and plays a vital role in the transport and distribution of metals, fatty acids, hormones, and renders toxins harmless by transporting them to disposal sites. In addition, BSA binds to variety drugs at multiple sites in the body vascular system [14-16].

BSA interactions with small molecules have become increasingly important in pharmacochemistry and are commonly used as key steps in the construction of medicinal compounds [17-21]. The research in this field provides strong support for BSA-binding studies and a deeper understanding of the way medicaments target and bind receptors [22,23]. BSA interactions with small molecules also help in understanding the toxicity, pharmacokinetics, biochemistry, pharmacodynamics, and distribution of molecules in the organism. Thus, the investigation of BSA interactions with small molecules has been an important analysis in medicinal chemistry and clinical medicine [24].

The pharmacochemistry of ferrocene derivatives has attracted the attention of many scientists, and their study has been encouraged by potential biological applications [25-27]. Many ferrocene derivatives that have been studied in the last decade show important biological activities, such as cytotoxic [28-30], antimicrobial [31,32] and antitumor [33-38] activities.

The incorporation of the ferrocenyl moiety into the structure of biologically active molecules may lead to the increase of their biological activities, based on the fact that nitriles-containing ferrocenes are expected to be more pharmacologically active than free nitriles. In this context the present study surveys the interaction of two nitrile-containing ferrocene with BSA by focusing on the roles of the -CN functional groups. The study was carried out in 0.1 M 90 % DMF/buffer phosphate solution at pH 7.4 using voltammetric, spectroscopic and molecular docking techniques.

Experimental

Synthesis

2-ferrocenylbenzonitrile (2FBN) and 4-ferrocenylbenzonitrile (4FBN) addressed in this work are shown in Figure 1a and 1b, and were synthesised by the coupling reaction between ferrocene and the diazonium salts of the corresponding cyanoaniline, as reported previously by our group [39]. The crystal structure of BSA was taken from protein databank (https://www.rcsb.org/, PDB ID: 4f5s) (Figure 1c).

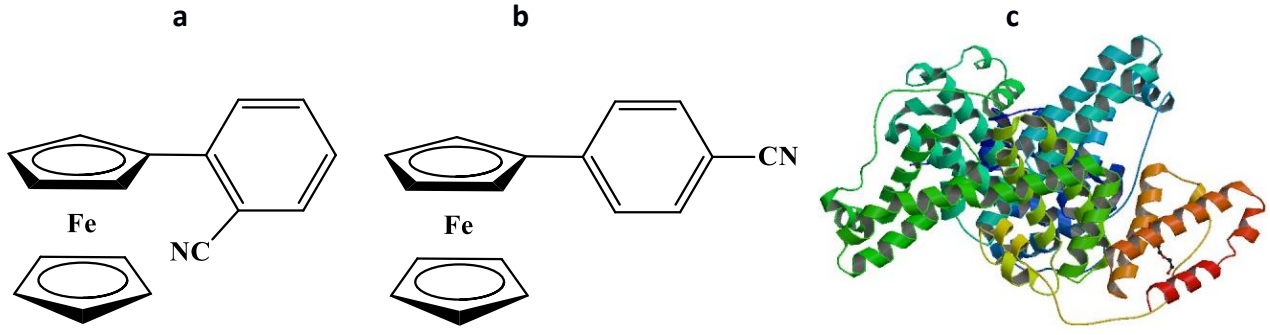

Figure 1. *Chemical structures of (a) 2-ferrocenylbenzonitrile, (b) 4-ferrocenylbenzonitrile and (c) structure of BSA (ID: 4f5s)*

Chemicals

All reagents and solvents were of analytical grade and obtained from commercial sources and used without further purification. BSA was obtained from Merck and used as received, while its

concentration was determined by the extinction coefficient of 44300 M^{-1} cm^{-1} at 280 nm [40]. All stock solutions were used within 5 days after preparation and stored at 4 °C until use. The phosphate buffer solution was prepared using sodium dihydrogen phosphate and disodium hydrogen phosphate (Sigma Aldrich) and double-distilled water. The physiological pH (pH 7.4) was maintained by this phosphate buffer. N,N-Dimethylformamide (DMF) (HPLC-grade; Sigma-Aldrich) was used as the solvent in voltammetric and spectroscopic assays. Tetrabutylammonium tetra-fluoroborate (Bu_4NBF_4) (electrochemical grade 99 %; Sigma-Aldrich) was used as the supporting electrolyte. Nitrogen gas was provided from a cylinder (research grade (99.99 %); Linde gaz Algérie).

Materials and measurements

Voltammetric assays were performed using a PGZ301 voltammeter running on VoltaMaster 4 V 7.08 software (Radiometer Analytical SAS, France). The concentration of the supporting electrolyte was kept at 0.1 M all time. The air was removed from the solution by bubbling nitrogen gas through it. Experiments were run in a three-electrode electrochemical cell containing a glassy carbon (GC) working electrode with a geometric area of 0.013 cm^2, a platinum wire as counter (auxiliary) electrode and Hg/Hg_2Cl_2 paste covered wire as reference electrode.

Absorption spectra measurements were conducted on a UV-Vis spectrometer, (Shimadzu 1800, Japan), using the cell of length 1 cm.

Chemical structures of 2FBN and 4FBN were optimized by Gaussian 09 program package [41], using density functional theory (DFT) and the B3LYP level of theory [42,43] with 6-311++G(d,p) basis set.

The molecular docking studies were done using AutoDock 4.2 docking software [44,45], all docking studies were executed on a Pentium 2.20 GHz and RAM 4.00 Go microcomputer MB memory with windows 10 operating system.

Results and discussion

Cyclic voltammetric study

BSA-2FBN and BSA-4FBN complexes in 0.1 M 90 % DMF/buffer phosphate solution at pH 7.4 were used. Various concentrations of BSA were added into 12 ml solution of 100 µM of the ligand solutions, and the voltammograms were recorded in the potential range of 0.1 to 0.8 V *vs.* Hg/Hg_2Cl_2 at 28 ± 1 °C.

Many studies on the interaction of BSA with small molecules in this potential range have been carried out using cyclic voltammetry techniques, and all these studies have shown that BSA does not show any adsorption on the bare electrode surface at this potential range [46-50]. Adsorption of BSA can only appear at negative potential [51].

The cyclic voltammograms (Figure 2) of 2FBN and 4FBN at different concentrations of BSA show respectively oxidation and reduction maximums in a reversible electrochemical process. Addition of an increasing amount of BSA solution results in a decrease in peak current height with a positive shift in peak potential position. This decrease in anodic peak current height is exploited for the calculation of the binding parameters.

The binding constant, K_b, was calculated from the observed cyclic voltammetry data, using the following equation [52]:

$$\log\frac{1}{c_{BSA}} = \log K_b + \log\frac{i}{i_0 - i} \quad (1)$$

where C_{BSA} is BSA concentration, K_b represents the binding constant, while i_0 and i indicate the anodic peak current density of the free and BSA-bound compounds, respectively.

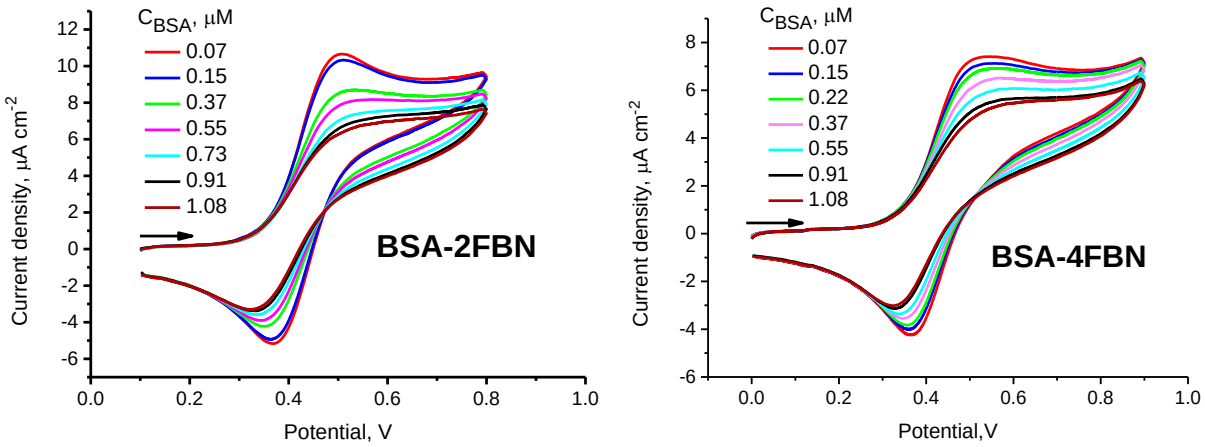

Figure 2. *Cyclic voltammograms of BSA–2FBN and BSA–4FBN complexes at different concentration of BSA. 2FBN and 4FBN concentrations were kept at 100 µM*

Obviously, K_b can be determined from the intercept of the plot of log $(1/C_{BSA})$ *vs.* log $(i/(i_0-i))$. These plots are for 2FBN and 4FBN represented in Figure 3, from which the values of binding constants were determined as 7.05×10^5 M^{-1} for 2FBN and 3.44×10^5 M^{-1} for 4FBN. The binding free energy changes calculated using the equation $\Delta G = -nRT \ln K_b$ are found equal to -33.94 and -32.14 kJ mol^{-1}, respectively. The order of magnitude and the sign of the obtained binding free energy indicate respectively the electrostatic mode and the spontaneity of interactions between the compounds and BSA.

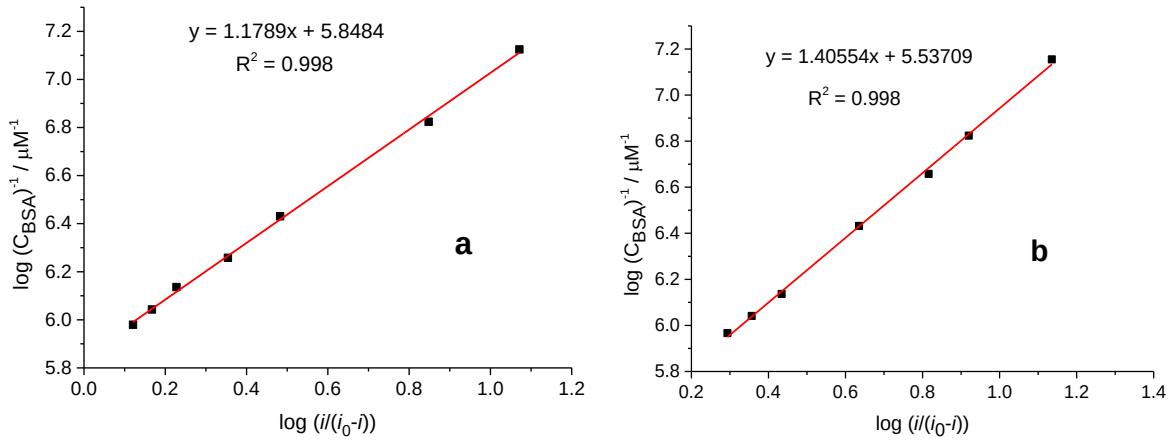

Figure 3. *Plots of log $(C_{BSA})^{-1}$ vs. log $(i/(i_0-i))$ used to calculate BSA binding constants: (a) 2FBN, (b) 4FBN*

Ratio of binding constants

The ratio of the binding constants of the reaction of the reduced form FBN (FBN represents 2FBN or 4FBN) with BSA to that of the oxidized form $[FBN]^+$, could be calculated from the voltammograms of Figure 4, which represent the cyclic voltammograms of 100 µM solution of 2FBN and 4FBN in the absence and presence of 0.37 µM of BSA. The shift in the anodic and cathodic peak potential values caused by the addition of BSA can be used to calculate the ratio of binding constants [53].

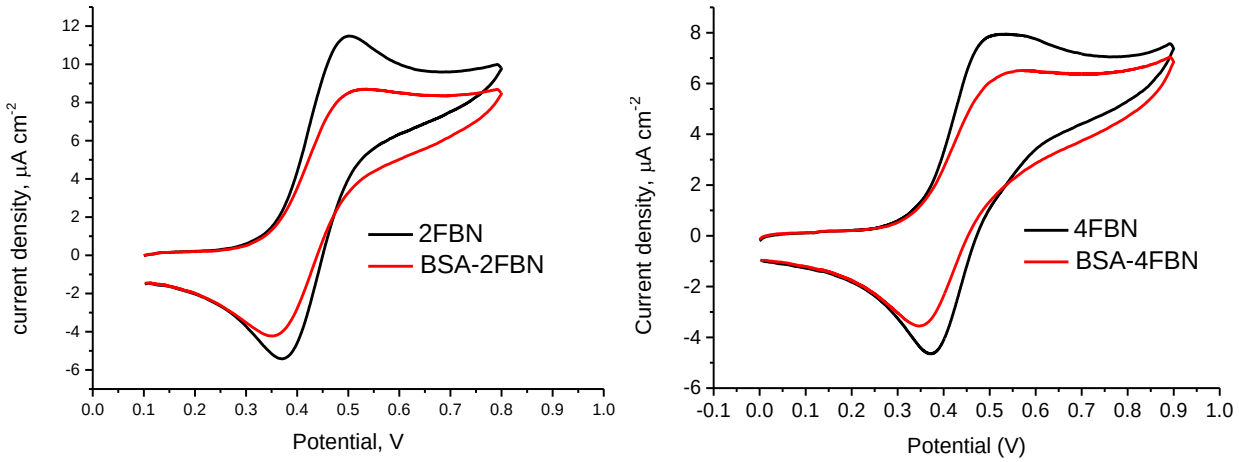

Figure 4. *Cyclic voltammograms of the free compounds (100 µM) and their BSA complexes (0.37 µM), scan rate 100 mV s^{-1}*

In such case when both the anodic and cathodic peak potential values are shifted upon the addition of BSA, the following equilibriums can be applied [54]:

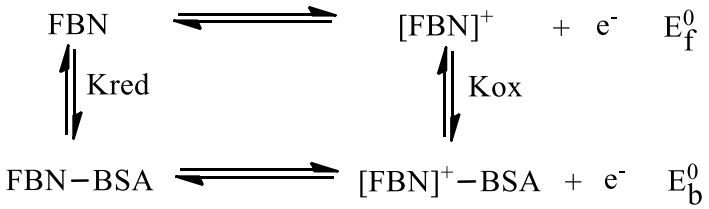

Figure 5. *Redox process of studied compounds with BSA, FBN represents 2FBN or 4FBN.*

The application of the Nernst relation to the equilibriums of Figure 5 produces the following equation:

$$\Delta E^0 = E_b{}^0 - E_f{}^0 = E^0(\text{FBN-BSA}) - E^0(\text{FBN}) = 0.06 \log \frac{K_{red}}{K_{ox}} \quad (2)$$

In equation (2), $E_f{}^0$ and $E_b{}^0$ are the formal potentials of the FBN^+/FBN couple of free and BSA-bound compounds, respectively. The formal potential shift ΔE^0 calculated on the basis of the voltammograms of Figure 4, are summarized in Table 1. The ratios of the binding constants were calculated from equation (2) by replacing ΔE^0 taken from Table 1.

Table 1. *Electrochemical data of free and BSA-bound 2FBN and 4FBN used to calculate the ratio of the binding constants.*

Sample code	E_{pa} / V	E_{pc} / V	E^0 / V	ΔE^0/ mV	K_{red} / K_{ox}
2FBN	0.502	0.369	0.4355	3.5	1.14
2FBN-BSA	0.527	0.351	0.439		
4FBN	0.538	0.374	0.456	4.0	1.16
4FBN-BSA	0.572	0.348	0.46		

The obtained ratios of the binding constants indicate that the reduced form of both 2FBN and 4FBN bind slightly stronger to BSA than their oxidized forms.

Diffusion coefficients

The diffusion coefficients of the free and BSA-bound 2FBN and 4FBN compounds were obtained from their electrochemical behavior represented in Figures 6 and 7. These cyclic voltammograms were obtained by varying the potential scan rates of 100 µM of the free compounds in the absence

and presence of 0.91 µM of BSA. All the voltammograms present well-defined stable redox peaks attributed to the redox process of 2FBN and 4FBN.

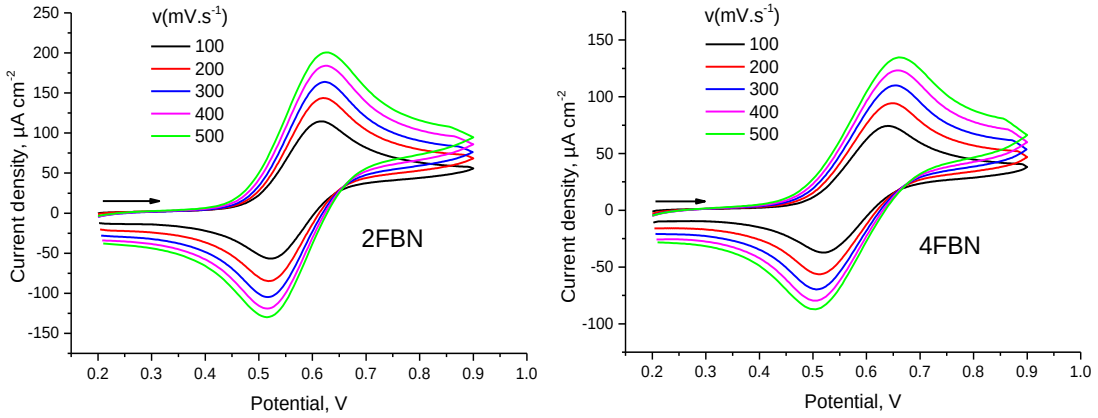

Figure 6. *Cyclic voltammetric behavior of 100 µM of 2FBN and 4FBN in 0.1 M 90 % DMF/buffer phosphate solution at different scan rates.*

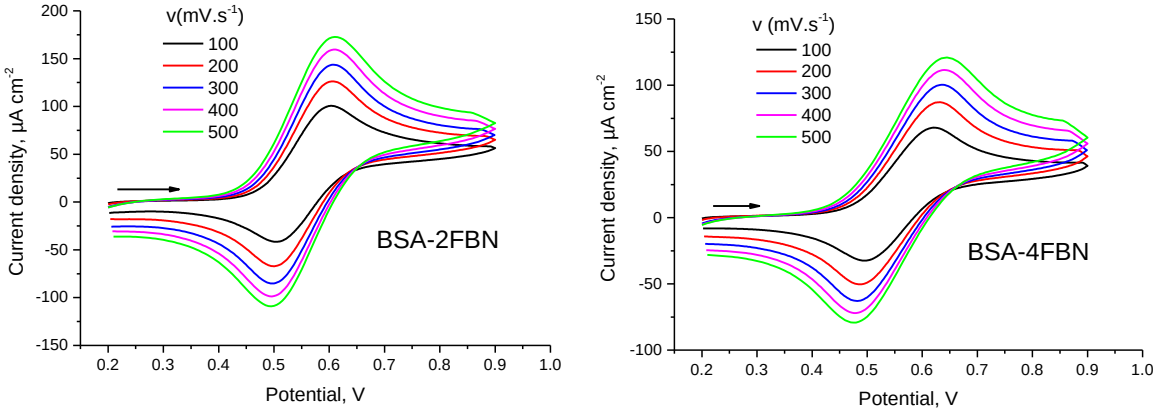

Figure 7. *Cyclic voltammetric behavior of 0.91 µM of BSA-2FBN and BSA-4FBN in 0.1 M 90 % DMF/buffer phosphate solution at different scan rates*

Diffusion coefficients of FBN-BSA in the solution with an excess of BSA were calculated from the voltammograms of Figures 6 and 7 using the following Randles–Ševčik equation [55]:

$$i_{pa} = 2.69 \times 10^5 n^{\frac{3}{2}} S C D^{\frac{1}{2}} v^{\frac{1}{2}} \quad (3)$$

In equation (3), i_{pa} represents the anodic peak current (A), n is the number of electrons participated in the oxidation process, S is the surface of the working electrode (cm^2), C is the concentration of the electroactive compounds (mol cm^{-3}), D is the diffusion coefficient ($cm^2\ s^{-1}$), and v is the scan rate (V s^{-1}). The plots of i_{pa} *vs*. $v^{1/2}$ in Figure 8 suggest that the oxidation reaction is diffusion controlled. The diffusion coefficients of the free and BSA-bound compounds were calculated from the slopes of linear regressions of the plots of i_{pa} *vs*. $v^{1/2}$. The lower diffusion coefficients of the bound compounds as compared to the free once, further confirm the interaction between the studied compounds and BSA (Table 2).

Table 2. *Diffusion constant values of the free and BSA bound form of 2FBN and 4FBN.*

Sample code	Equation	R^2	$D \times 10^6$/ $cm^2\ s^{-1}$
2FBN	y = 6.94x + 44.25	0.999	3.94
2FBN-BSA	y = 5.78x + 42.97	0.999	2.73
4FBN	y = 4.89x + 24.63	0.999	1.96
4FBN-BSA	y = 4.22x + 26.40	0.999	1.46

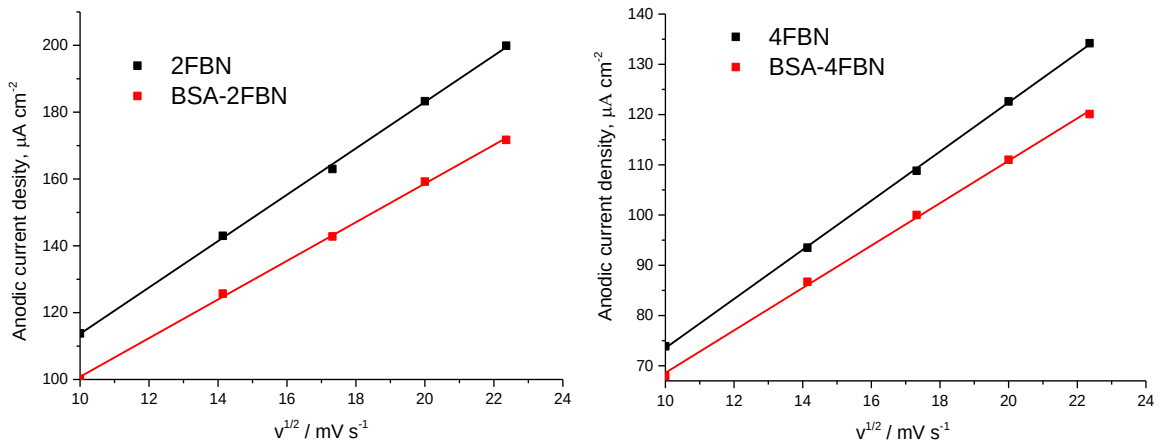

Figure 8. *i_{pa} vs. $v^{1/2}$ plots of 100 µM 2FBN and 4FBN in the absence and in presence of 0.91 µM BSA based on voltammograms in Figures 6 and 7.*

Absorption spectroscopic studies

The interactions of 2FBN and 4FBN with BSA were also studied by absorption spectroscopic titration. The purpose of this study was to validate the results obtained from cyclic voltammetry assays. The experiments were carried out with 0.1 M 90 % DMF/buffer phosphate solution of pH 7.4. Incremental portions of BSA solution from 0.34 to 0.70 µM for 2FBN and from 0.15 to 2.67 µM for 4FBN were added to the same solution containing 0.5 mM of 2FBN and 2 mM of 4FBN. The obtained mixture was scanned in the range of 300–600 nm. BSA does not show any absorption at this wavelength, while the strong peak which appeared at 434.5 nm (due to π→π* transition in the conjugated ring of ferrocene moiety) lowered in intensity upon continuous addition of BSA to 2FBN and 4FBN (Figure 9).

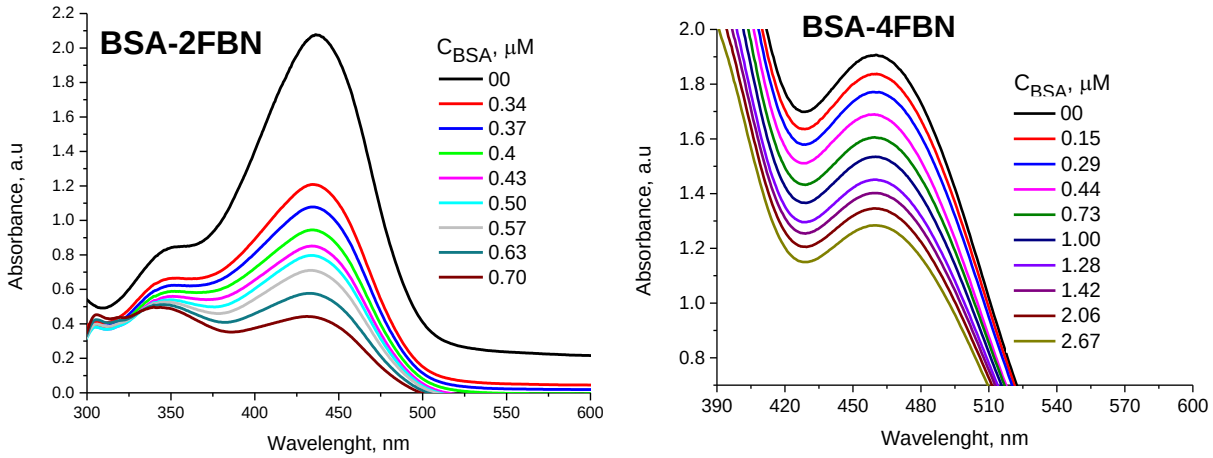

Figure 9. *Absorbance spectra of 2FBN-BSA and 4FBN-BSA complexes. 2FBN and 4FBN concentrations were kept respectively at 0.5 and 2 mM*

The binding constant K_b was evaluated from the absorption data according to Benesi-Hildebrand equation [56]:

$$\frac{A_0}{A-A_0} = \frac{\varepsilon_f}{\varepsilon_b-\varepsilon_f} + \frac{\varepsilon_f}{\varepsilon_b-\varepsilon_f}\frac{1}{K_b C_{BSA}} \quad (4)$$

In equation (4), A_0 and A are absorbencies of the ligands and their complexes with BSA, respectively, while ε_f and ε_b are their extinction coefficients. The plot of $A_0/(A_0\text{-}A)$ *vs.* $1/C_{BSA}$ gave a

slope of $\varepsilon_f/(\varepsilon_b - \varepsilon_f)K_b$, and intercept equal to $\varepsilon_f/(\varepsilon_b - \varepsilon_f)$, where K_b is the ratio of the slope to the intercept (Figure 10). The value of K_b has been determined to be 7.18×10^5 for 2FBN-BSA and 2.79×10^5 M^{-1} for 4FBN-BSA. The corresponding free binding energies calculated using the equation $\Delta G = -nRT \ln K_b$ were equal to -33.77 and -31.40 kJ mol^{-1}, respectively. These values are in good agreement with those obtained from cyclic voltammetry experiments.

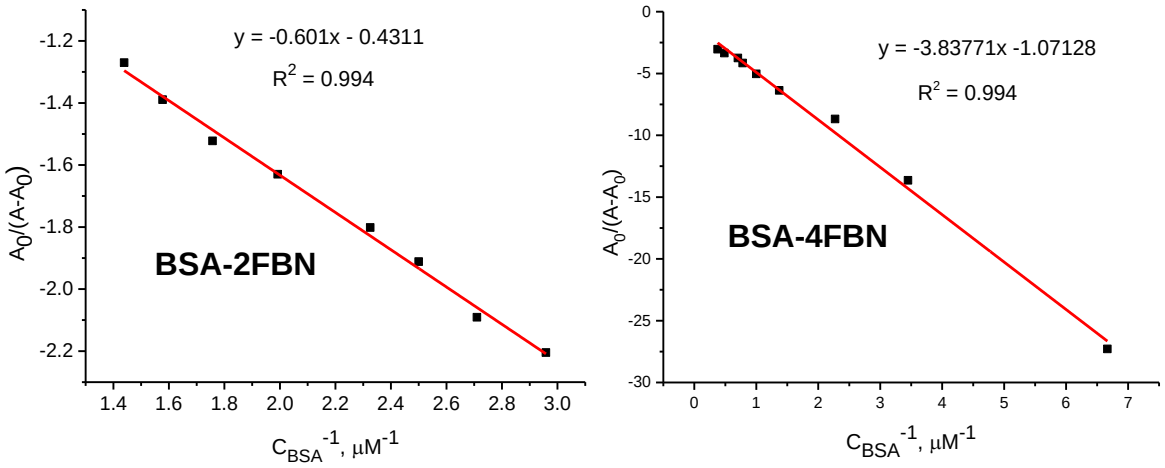

Figure 10. *Plots of $A_0/(A_0-A)$ vs. C_{BSA}^{-1} used to calculate the binding constants of BSA-2FBN and BSA-4FBN*

Docking setup

Geometry optimization

Density functional theory (DFT) was used for the optimisation without imposing any symmetry constraints and calculations were realized with the Gaussian 09 package. The exchange functional of Becke, and the correlation functional of Lee, Yang and Parr (B3LYP) were employed with 6-311++G(d,p) basis set. The optimized structures of the compounds are depicted in Figure 11.

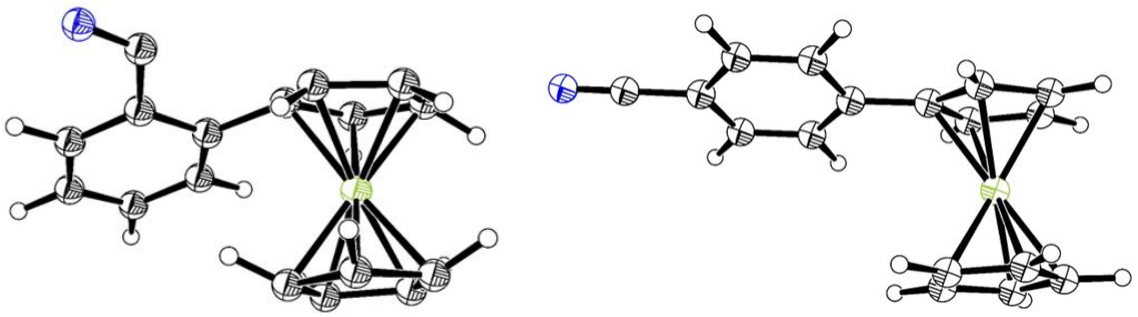

Figure 11. *The optimized structures of 2FBN and 4FBN (ORTEP View 03, V1.08); color codes are carbon (grey), hydrogen (white), nitrogen (blue), iron (green).*

Molecular docking studies

In order to confirm and interpret the results of cyclic voltammetric and spectrophotometric measurements and recognize the way in which 2FBN and 4FBN bind to BSA, semi flexible docking was carried out using AutoDock 4.2 along with the AutoDock Vina software. The crystal structure of BSA was taken from the protein databank (https://www.rcsb.org/, PDB ID: 4f5s). The PDB file was imported into AutoDock Tools, all hydrogen atoms and gassier charges were added. During all docking process, BSA kept rigid while all the bonds of the ligands were set free. The grid map with 0.375 Å spacing and 126×70×100 points were generated. The docking experiment comprised of 100 docking

runs with 150 individuals and 2.500.000 energy evaluations. Lamarckian genetic algorithm was used in the docking, and other parameters were set as default. The stable conformation which corresponds to the lowest binding energy was used for docking analysis. The visualization of the interaction was generated with PLIP web service (protein Ligand Interaction Profiler).

Results from molecular docking suggest that hydrogen bonding, hydrophobic forces and π-cation interaction are involved in the binding process. Figure 12 illustrates the interaction of 2FBN and 4FBN with the nearby residues in the active site of BSA.

The interacting residues, distances, and type of interactions are summarised in Tables 3 and 4.

Table 3. *Hydrophobic interactions between the ligands 2FBN and 4FBN with BSA.*

Interaction type	Residue	Amino acid	Distance, Å
BSA-BSA	80A	LEU	2.85
	81A	ARG	3.45
	88A	ALA	3.72
BSA-4FBN	115B	LEU	3.99
	115B	LEU	3.57
	122B	LEU	3.14
	136B	LYS	3.94
	137B	TYR	3.15
	140B	GLU	3.68
	141B	ILE	3.58
	160B	TYR	3.96

Table 4. *Hydrogen bonds between the ligands 2FBN and 4FBN and BSA.*

Interaction type	Residue	Amino acid	Distance H-A, Å	Distance D-A, Å
2FBN-BSA	81A	ARG	3.00	3.45
	82A	GLU	2.04	3.05
	82A	GLU	3.22	3.71
4FBN-BSA	137B	TYR	2.38	3.32

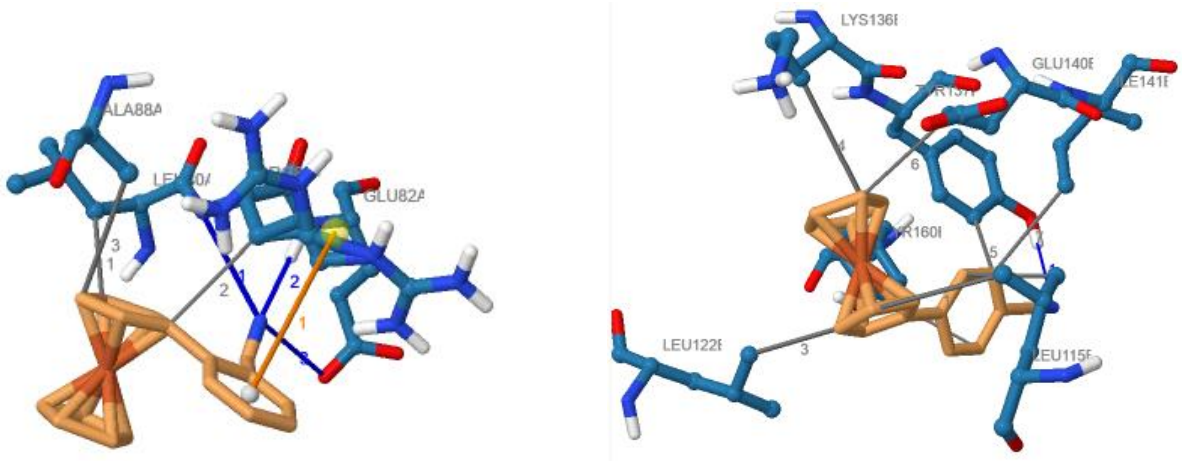

BSA-2FBN BSA-4FBN

Figure 12. *Best docking poses for BSA-2FBN and BSA-4FBN generated with PLIP web service illustrating the hydrophobic and H-bons interactions. Elements colors: hydrogen, oxygen, nitrogen, and iron are represented in white, red, blue and brown, respectively Color code: Hydrogen bonds: bleu lines, hydrophobic interactions: gray lines, π-Cation interactions: beige lines.*

The compound 2FBN formed three hydrogen bonds between amino acid residues Arg-81 and Glu-82 as donors and the polar groups of the ligand – nitrile group. 4FBN formed only one hydrogen bond between the residue Tyr-137 as acceptor and the nitrogen of the 4FBN as a donor, table 4. The distances in table 4 are between hydrogen and the receptor atoms (H-A), and between donor and receptor atoms (D-A). Furthermore, for the complex 2FBN-BSA, molecular docking results also suggested a π-cation interaction between the positively charged amino acid residue Arg-81 and the benzene ring within a distance of 5.01 Å.

The ligand 4FBN interacted through hydrophobic interactions with the residues Leu-115, Leu-122, Lys-136, Tyr-137, Glu-140, Ile-141, and Tyr-160,

The binding free energy of the docked structure of 2FBN and 4FBN ligands with BSA was found to be -32.89 and -31.26 kJ mol^{-1}, respectively. The binding constant K_b calculated using the equation $\Delta G = -nRT \ln K_b$ was found to be 5.77×10^5 and 2.99×10^5 mol^{-1}, respectively. These results are supported by the absorption spectroscopy and cyclic voltammetry experiments. Overall, molecular docking results are in good agreement with the data obtained from experimental assays.

Conclusions

In the present work, we applied experimental and theoretical methods for the determination of binding proprieties of two nitrile-containing ferrocenes with BSA. Binding free energies for the interaction of 2FBN and 4FBN with BSA, obtained from voltammetric experiments, were respectively -33.95 and -32.14 kJ mol^{-1}, and these values are in good agreement with those obtained from adsorption spectroscopic assays (-33.77 and -31.40 kJ mol^{-1}). The low diffusion coefficient values of the BSA-bound 2FBN and 4FBN as compared to the corresponding free 2FBN and 4FBN, further confirm the formation of the complexes 2FBN-BSA and 4FBN-BSA which diffuses more slowly compared to the free compounds due to their higher molecular weight. Molecular docking study further confirms the obtained experimental results and allows the visualisation of interactions and determination of bonds length formed between the ligands and the amino acid residues of BSA.

***Acknowledgements**: The authors are grateful to the Algerian Ministry of Higher Education and Research for financial support (project code: B00L01UN390120150001).*

References

[1] *Compendium of Polymer Terminology and Nomenclature, IUPAC Recommendations 2008,* R. G. Jones, J. Kahovec, R. Stepto, E. S. Wilks, M. Hess, T. Kitayama, W. Val Matanomski (Eds.). With advice from A. Jenkins and P. Kratochvil, The Royal Society of Chemistry, Cambridge, UK, 2009, p. 98.

[2] *Nitriles - MeSH - NCBI*, (n.d.). https://www.ncbi.nlm.nih.gov/mesh/68009570 (accessed April 22, 2020).

[3] J. Wit, H. Van Genderen, *Biochemical Journal* **101(3)** (1966) 698-706.

[4] D. H. Hutson, E. C. Hoadley, M. H. Griffiths, C. Donninger*, Journal of Agricultural and Food Chemistry* **18(3)** (1970) 507-512.

[5] S. T. Murphy, H. L. Case, E. Ellsworth, S. Hagen, M. Huband, T. Joannides, C. Limberakis, K. R. Marotti, A. M. Ottolini, M. Rauckhorst, J. Starr, M. Stier, C. Taylor, T. Zhu, A. Blaser, W. A. Denny, G. L. Lu, J. B. Smaill, F. Rivault, *Bioorganic and Medicinal Chemistry Letters* **17(8)** (2007) 2150-2155.

[6] F. F. Fleming, L. Yao, P. C. Ravikumar, L. Funk, B. C. Shook, *Journal of Medicinal Chemistry* **53(22)** (2010) 7902-7917.

[7] J-Y. Le Questel, M. Berthelot, C. Laurence, *Journal of Physical Organic Chemistry* **13(6)** (2000) 347-358.

[8] C. Laurence, K. A. Brameld, J. Graton, J. Y. Le Questel, E. Renault, *Journal of Medicinal Chemistry* **52(14)** (2009) 4073-4086.

[9] A. Allerhand, P. von Rague Schleyer, *Journal of the American Chemical Society* **85(7)** (1963) 866-870.

[10] Y. Wang, Y. Du, N. Huang, *Future Medicinal Chemistry* **10(23)** (2018) 2713-2728.
[11] L. Xue, F. Zou, Y. Zhao, X. Huang, Y. Qu, *Spectrochimica Acta - Part A: Molecular and Biomolecular Spectroscopy* **97** (2012) 858-863.
[12] R. E. Royer, M. Kibirige, C. R. Tafoya, D. L. Vander Jagt, L. M. Deck, *Journal of Pharmaceutical Sciences* **77(3)** (1988) 237-240.
[13] J. T. First, J. D. Slocum, L. J. Webb, *Journal of Physical Chemistry B* **122(26)** (2018) 6733-6743.
[14] T. Peters Jr., *All about albumin: biochemistry, genetics, and medical applications*, Academic Press Inc., San Diego, California, 1996, p. 382.
[15] M. Fasano, S. Curry, E. Terreno, M. Galliano, G. Fanali, P. Narciso, S. Notari, P. Ascenzi, *IUBMB Life* **57(12)** (2005) 787-796.
[16] P. Lee, X. Wu, *Current Pharmaceutical Design* **21(14)** (2015) 1862-1865.
[17] T. Topală, A. Bodoki, L. Oprean, R. Oprean, *Clujul Medical* **87(4)** (2014) 215-219.
[18] L. Zhang, Q. Y. Cai, Z. X. Cai, Y. Fang, C. S. Zheng, L. L. Wang, S. Lin, D. X. Chen, J. Peng, *Molecules* **21(12)** (2016) 1706. https://doi.org/10.3390/molecules21121706.
[19] Q. Zhang, Y. Ni, *RSC Advances* **7(63)** (2017) 39833-39841.
[20] D. Sood, N. Kumar, G. Rathee, A. Singh, V. Tomar, R. Chandra, *Scientific Reports* **8** (2018) 16964. doi.org/10.1038/s41598-018-35384-6.
[21] J. Yu, J.-Y. Liu, W.-M. Xiong, X.-Y. Zhang, Y. Zheng, *BMC Chemistry* **13** (2019). 95. https://doi.org/-10.1186/s13065-019-0615-6.
[22] D. Sleep, *Expert Opinion on Drug Delivery* **12** (2015) 793–812.
[23] G. L. Francis, *Cytotechnology* **62(1)** (2010) 1-16.
[24] A. M. Bagoji, J. I. Gowda, N. M. Gokavi, S.T. Nandibewoor, *Journal of Biomolecular Structure and Dynamics* **35(11)** (2017) 2395-2406.
[25] F. A. Larik, A. Saeed, T. A. Fattah, U. Muqadar, P. A. Channar, *Applied Organometallic Chemistry* **31(8)** (2016), doi.org/10.1002/aoc.3664.
[26] M. Patra, G. Gasser, *Nature Reviews Chemistry* **1(9)** (2017) 0066. https://doi.org/10.1038/s41570-017-0066.
[27] M. Patra, G. Gasser, M. Wenzel, K. Merz, J. E. Bandow, N. Metzler-Nolte, *Organometallics* **29(19)** (2010) 4312-4319.
[28] M. Görmen, P. Pigeon, S. Top, E. A. Hillard, M. Huché, C. G. Hartinger, F. de Montigny, M. A. Plamont, A. Vessières, G. Jaouen, *ChemMedChem* **5** (2010) 2039-2050.
[29] W. I. Pérez, Y. Soto, C. Ortíz, J. Matta, E. Meléndez, *Bioorganic and Medicinal Chemistry* **23(3)** (2015) 471-479.
[30] J. Yong, X. Wang, X. Wu, C. Lu, *Journal of Infectious Diseases & Therapy* **5(1)** (2017) 1000311. https://doi.org/10.4172/2332-0877.1000311.
[31] A. S. Hassan, T. S. Hafez, *Journal of Applied Pharmaceutical Science* **8(5)** (2018) 156-165.
[32] S. Li, Z. Wang, Y. Wei, C. Wu, S. Gao, H. Jiang, X. Zhao, H. Yan, X. Wang, *Biomaterials* **34(4)** (2013) 902-911.
[33] H. Benamara, T. Lanez, *Journal of Fundamental and Applied Sciences* **11(3)** (2019) 1267-1278.
[34] A. Adaika, T. Lanez, E. Lanez, *Journal of Fundamental and Applied Sciences* **11(2)** (2019) 748-768.
[35] E. Lanez, L. Bechki, T. Lanez, *Chemistry and Chemical Technology* **13(1)** (2019) 11-17.
[36] X. Gao, G. Gong, Z. Zhang, G. Du, Y. Cao, G. Zhao, *Journal of Molecular Structure* **1200** (2020) 127077. https://doi.org/10.1016/j.molstruc.2019.127077
[37] S. Sansook, E. Lineham, S. Hassell-Hart, G. J. Tizzard, S. J. Coles, J. Spencer, S. J. Morley, *Molecules* **23(9)** (2018) 2126. https://doi.org/10.3390/molecules23092126.
[38] S. Realista, S. Quintal, P. N. Martinho, A. I. Melato, A. Gil, T. Esteves, M. de Deus Carvalho, L. P. Ferreira, P. D. Vaz, M. J. Calhorda, *Journal of Coordination Chemistry* **70(2)** (2017) 314-327.
[39] T. Lanez, P. L. Pauson, *Journal of the Chemical Society, Perkin Transactions* **1** (1990) 2437-2442.
[40] A. Ray, B. Koley Seth, U. Pal, S. Basu, *Spectrochimica Acta - Part A: Molecular and Biomolecular Spectroscopy* **92** (2012) 164-174.
[41] M. Frisch, G. Trucks, H. Schlegel, G. E. Scuseria…, *Gaussian 09,* Gaussian Inc., Wallingford, 2009.
[42] B. Miehlich, A. Savin, H. Stoll, H. Preuss, *Chemical Physics Letters* **157(3)** (1989) 200-206.
[43] A. D. Becke, *The Journal of Chemical Physics* **98(7)** (1993) 5648-5652.

[44] G. M. Morris, H. Ruth, W. Lindstrom, M. F. Sanner, R. K. Belew, D. S. Goodsell, A. J. Olson, *Journal of Computational Chemistry* **30(16)** (2009) 2785-2791.
[45] O. Trott, A. J. Olson, *Journal of Computational Chemistry* **31(2)** (2009) 455-461.
[46] S. Bi, L. Yan, B. Wang, J. Bian, Y. Sun, *Journal of Luminescence* **131(5)** (2011) 866-873.
[47] M. Mahanthappa, B. G. Gowda, J. I. Gowda, R. Rengaswamy, *Journal of Electrochemical Science and Engineering* **6(2)** (2016) 155-164.
[48] J. B. M. Leuna, S. K. Sop, S. Makota, E. Njanja, T. C. Ebelle, A. G. Azebaze, E. Ngameni, A. Nassi, *Bioelectrochemistry* **119** (2018) 20–25.
[49] S. Pramanik, R. Chakraborty, *International Journal of Biosensors & Bioelectronics* **2(3)** (2017) 96-98.
[50] J. Wu, S. Y. Bi, X. Y. Sun, R. Zhao, J. H. Wang, H. F. Zhou, *Journal of Biomolecular Structure and Dynamics* **37(13)** (2019) 3496–3505.
[51] J. R. Flores, R. O'Kennedy, M. R. Smyth, *Analytica Chimica Acta* **212** (1988) 355–358.
[52] A. E. M. Radi, S. H. Eissa, *Eurasian Journal of Analytical Chemistry* **6(1)** (2011) 13-21.
[53] X. Chu, G. L. Shen, J. H. Jiang, T. F. Kang, B. Xiong, R. Q. Yu, *Analytica Chimica Acta* **373(1)** (1998) 29-38.
[54] M. Aslanoglu, G. Ayne, *Analytical and Bioanalytical Chemistry* **380** (2004) 658-663.
[55] C. M. A. Brett, A. N. A. Maria, O. Brett, *Electrochemistry: Principles, Methods, and Applications*, Oxford University Press, Oxford, UK, 1993, p. 444.
[56] M. Nie, Y. Wang, H. L. Li: *Polish Journal of Chemistry* **71(6)** *(*1997) 816-822.

Abstract

The main goal of this work is the preparation of potentially biologically active compounds and evaluating their antioxidant and anticancer activities. In this context, a series of 2, 3, and 4-benzonitrilferrocene were prepared by the coupling reaction between ferrocene and the diazonium salts of the corresponding cyanoaniline. Cyclic voltammetry and electronic spectroscopy techniques were used to characterize and evaluate the antioxidant and anticancer potencies of the ligands ferrocenyl nitrobenzenes (NPF) and ferrocenyl benzonitriles (FBN). Moreover, CV method has been concerned for studying the behaviours of both series with the targets in free and bound form for determining which form (NPF / FBN) or (NPF^+ / FBN^+) are more active through the redox equilibrium process with DNA and BSA by calculation the K_{ox}/K_{red} values. The voltammetric response of the studied compounds before and after the increasing addition of DNA and BSA shows that all the electrochemical reactions are kinetically controlled by the diffusion step and showed that diffusion coefficients values of the compounds NPF and FBN are higher than that of the ligand-DNA and ligand-BSA complexes, which can be summarized in the order $D_{ligand} > D_{complex}$. Furthermore, the magnitude and the sign of ΔG for all the studied compounds confirm the spontaneity of the reaction via non-covalent bonds. All obtained k_b values are much greater than 1 which confirm the formation of the adducts ligand-DNA and ligand-BSA. The obtained data of the electrochemical and spectroscopic assays of the ligands NPF and FBN also allowed the determination of their binding affinities towards $O_2^{-\cdot}$ and DPPH$^{\cdot}$ which were by electrostatic forces through a spontaneous reaction. In order to validate the obtained experimental results and visualize the ligand-receptor interactions, molecular docking study was carried out between the optimized structures of the ligands NPF and FBN with the treated crystal structures of DNA and BSA using AutoDock 4.2 software. The docking results showed high compatibility between the studied ligands and the target binding pockets of either DNA or BSA. Finally, ligands NFP and FBN represent strong candidates as antioxidant and anticancer agents.

Keywords:

Benzonitrilferrocene, Diazotization reaction, DNA, BSA, binding parameters.